University of Sassari
Ph.D. School in Natural Sciences
Via Muroni 25, I-07100 Sassari, Italy

Dissertation for the Degree of Doctor of Philosophy in Science and technology of mineral and rocks of industrial interest presented at Sassari University in 2013

XXVI cycle

Reconstruction of the Sardinia the north-west coast evolution: a chronologic and sedimentologic approach

PH.D. CANDIDATE: ***Dr. Daniele Sechi*** DIRECTOR OF THE SCHOOL: ***Prof. Marco Curini Galletti***

SUPERVISOR: ***Prof. Vincenzo Pascucci***

CO-SUPERVISOR: ***Dr. Stefano Andreucci***

University of Sassari
Ph.D. School in Natural Sciences
Via Muroni 25, I-07100 Sassari, Italy

Dissertation for the Degree of Doctor of Philosophy in Science and technology of mineral and rocks of industrial interest presented at Sassari University in 2013

XXVI cycle

RECONSTRUCTION OF THE SARDINIA NORTH-WEST COAST EVOLUTION:

A CRONOLOGICAL AND SEDIMENTOLOGIC APPROCH

PH.D. CANDIDATE: ***Dr. Daniele Sechi***

DIRECTOR OF THE SCHOOL: ***Prof. Marco Curini Galletti***

SUPERVISOR: ***Prof. Vincenzo Pascucci***

CO-SUPERVISOR: ***Dr. Stefano Andreucci***

INDEX

University of Sassari
Ph.D. School in Natural Sciences
Via Muroni 25, I-07100 Sassari, Italy

Abstract

The Middle-Upper Pleistocene Sardinian stratigraphy is analysed to identify the role played by sea and climate changes, in controlling sedimentation. The studied deposits crop out along the NW Sardinia coast were dated with Optically Stimulated Luminescence on both quartz and k-feldspar grains. The Quaternary successions were grouped in four major stratigraphic units mainly represented by shallow marine coastal dunes and alluvial systems, spanning from MIS 6 to MIS4. Stratigraphic and chronologic data allow some considerations on climate changes occurred within the last interglacial (MIS 5) to the early glacial phase (MIS4, post 80 ka). The last interglacial MIS 5 (130-80 ka) is subdivided in five substages (e-a) and MIS 5e (Eemian) is considered the climatic optimum. During the MIS 5e sea level was +4-6 m higher than today and climate conditions were warmer and more humid. The NW Sardinia coast paleogeography was dominated by wave cut platforms colonized by carbonate intertidal deposits (algal rim) and small gravelly to mixed sandy-gravelly pocket beaches which developed at the base of the cliff-wall. Occasionally, in the wider embayment well developed sandy barrier-lagoon systems occurred. During MIS 5b sea level drop of 15 m and the Mediterranean region was characterized by alternated dry and wet condition. At the end of MIS 5b temperature increased, most of the ice formed melted and a new interglacial phase (MIS 5c) took place. During MIS 5c (100-95 ka) the sea level rose up to ~2 m above the present and the North-west coast of Sardinia was dominated by prograding sandy-mixed pocket beaches. At the end of MIS 5c a climate deterioration led to a progressively cooler condition and sea level drop again of about -20m and alluvial plain and regressive coastal dunes developed.

KEY WORDS: *Sea level changes, MIS 5*, coastal deposits, Sardinia NW coast, OSL dating, Quaternary

RIASSUNTO

I depositi tardo quaternari affioranti lungo la costa nord occidentale della Sardegna sono stati studiati al fine di ricostruire gli eventi climatici e glacio-eustatici che hanno caratterizzato il Mediterraneo negli ultimi 200 mila anni. Attraverso i metodi classici della sedimentologia e della stratigrafia supportati da datazioni OSL (Optically Stimulated luminescence), le successioni studiate sono state divise in 4 unità litostratigrafiche principali, interpretate come depositi marini, dunali e alluvionali costieri riferibili dal MIS 6 al MIS 4.

In particolare oggetto di questa tesi è stato l'ultimo interglaciale (MIS 5).

Il MIS 5 è stato caratterizzato da ampie fluttuazioni eustatiche e climatiche e per tale motivo è stato diviso in 5 principali periodi (e-a). Il MIS 5e è considerato essere l'optimum climatico dell'ultimo interglaciale e fu caratterizzato da temperature (+2°c) e da un livello del mare (+4-6m) più alto dell'attuale. Lo studio ha permesso di ricostruire l'asseto della costa nord occidentale della Sardegna a partire da 150 mila anni fa. Durante il MIS 5e il livello del mare superò quello attuale di 4-6 m e la costa era prevalentemente rocciosa, caratterizzata da piccole spiagge ghiaiose che si sviluppavano alla base delle falesie. Il MIS 5e fu caratterizzato, per questo lato della costa, dalla proliferazione di comunità intertidali che sviluppavano spessi ed estesi trottoir al piede delle falesie. Nelle baie più protette ed ampie occasionalmente si potevano sviluppare sistemi di spiagge sabbiose o di spiaggia-laguna. Il MIS 5e terminò con brusco cambio del clima che porto condizioni simili ad un glaciale (MIS 5b). Il livello del mare calò velocemente raggiungendo almeno i -15 m. Al termine del MIS 5b il clima inizio a riscaldarsi e molti dei ghiacciai formatisi durante il MIS 5b arretrarono velocemente innescando una rapida risalita del livello del mare che raggiunse il suo picco massimo durante il MIS 5c ad almeno 2 m sul livello attuale. Durante il MIS 5c le coste della Sardegna nord occidentale furono caratterizzate da numerosi sistemi di spiaggia sabbiosa tipo pocket beach. Alla fine dal MIS 5c il clima cambio raffreddandosi velocemente e con la formazione di nuovi ghiacciai il mare si ritiro velocemente raggiungendo almeno i -20 m per Il Mediterraneo durante il MIS 5b.

PAROLE CHIAVE: *Variazioni eustatiche*, MIS 5, depositi costieri, Sardegna costa NW, datazioni OSL.

Introduction

In the last ten years Quaternary studies were forced to use new age dating methodologies to define a more precise chronology of the events occurred during the last 200 ka (Tuccimei et al., 2012; Orrứ et al., 2011; Coltorti et al., 2009; Thiel et al., 2009). This because climate change studies have been addressed to a better and detailed comprehension of what has occurred during the past interglacial-glacial cycles. Understanding the past will allow us to forecast the future climate changes of the present interglacial. Therefore, distinguishing relatively small/short sedimentary events has become an issue toward which the new dating methodologies are addressed.

Hundred-meter scale fluctuation of the global sea level occurred throughout the last interglacial/glacial cycle (ca 130-18 ka), but the precise magnitude of some of these high-frequency fluctuations are still debated by the scientific community.

The stratigraphic scale based on the marine oxygen ratio (O18/O16) (the Marine Isotopic Stage (MIS; Emiliani, 1957) is worldwide adopted, and is very helpful for correlation between events occurred at the world scale. For instance the past interglacial previously called the "Tyrrhenian" in the Mediterranean region is substituted by the MIS 5 stage (ca 130-75 ka) and further subdivided in five interstadials (e to a) to better define the different high frequency climatic and sea level fluctuations. Unlike for MIS 5e (130-125 ka) which is worldwide accepted as an interglacial characterized by an high-stand of sea level (± 6m above present sea level), new data performed along the coast of Mediterranean sea show a large fluctuation within the MIS 5 substages (Dorale et al. 2010). Recent studies have therefore focused on the MIS 5c and MIS 5a, possible interglacial substages more similar to the present one (Pascucci et al., in press – QI).

Given the limit of the "Carbon C14" radiometric method to date sedimentary events older than ~ 40 ka, several different dating methods were developed (Tuccimei et al., 2012; Murray et al 2003). One of this is the Optically Stimulated Luminescence (OSL) (Thiel et al., 2009). The OSL has revolutionized the age dating of late Quaternary/Holocene sedimentary deposits (Murray and Clemmensen, 2001). In the

last five years this method has been applied to date late Quaternary strata cropping out in the western and north western coast of Sardinia Island (Italy) (Andreucci et al., 2009, 2010; 2011; 2012; 2013, Thiel et al 2009Pascucci et al, in press,).

The new chronological data have allowed revisiting the Sardinia late Quaternary stratigraphy although a debate on the validity of these ages is ongoing (Coltorti et al., 2009)

The aim of this thesis is to better define the stratigraphy of the late Quaternary deposits cropping out along the western and north-western coast of Sardinia using a sedimentological and chronological approach. Data will also allow us to reconstruct the coastal evolution of this part of the Mediterranean during the last 200 ka under sea level and climate changes.

Principles of luminescence dating

In last ten years, the Optical Stimulated Luminescence (OSL) dating method has become an important tool for studying Earth surface process. It is a widely applicable age dating method, which can be used to determine the time that has elapsed since sediment grains (such as quartz and feldspars) were last exposed to daylight (Aitken., 1998). During burial, quartz and feldspar grains absorb and store in meta-stable traps energy (as charges) from ionizing radiation due to the natural radiation flux (alpha, beta, gamma). When grains are exposed to daylight, e.g. during erosion and/or transport some of trapped energy is released, this phenomena is called resetting or bleaching of luminescence signal. During the subsequent burial trapping of charges, as function of the natural radiation dose, start again. (Fig.1)

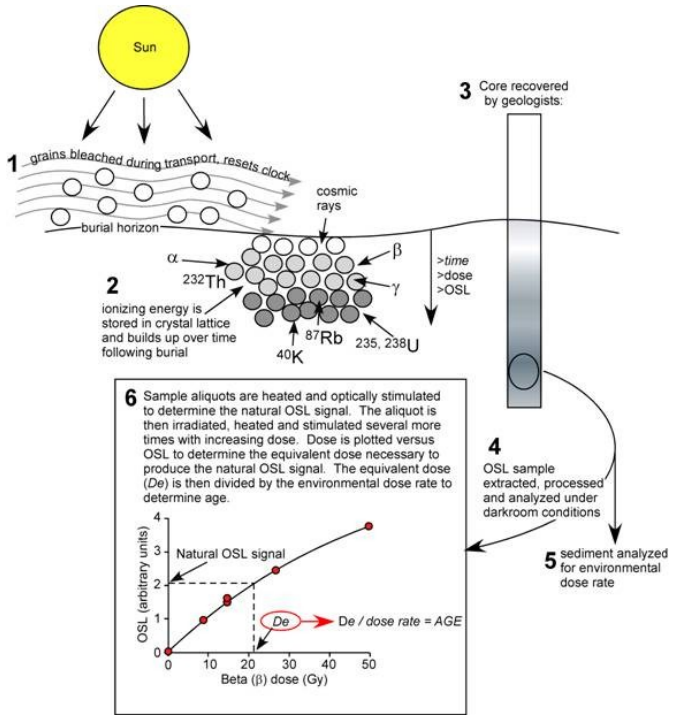

Fig. 1: Generalized processes that produce the luminescence signal (steps 1 and 2), sampling and analytical procedure to determine the age of deposition (steps 3 through 6)

Three principal components are required for luminescence age estimation: (a) the natural luminescence signal, (b) an assessment of sensitivity (luminescence signal response to applied radiation dose), and (c) determination of the burial dose rate (natural radiation flux) experienced by each sample.

The natural trapped charge can be released also inducing thermal or optical stimulation and the respectively method are called Thermoluminescence (TL) and Optically Stimulated Luminescence (OSL). By means of a dose response curve (growth curve), the natural luminescence signal can be compared to luminescence signals induced artificially using a radiation source; interpolation of the natural luminescence onto the dose response curve gives the equivalent dose (De) also called burial dose or paleodose (Fig2). The equivalent dose (De) is expressed in Gray (Gy). The natural radiation flux mostly based on the radionuclide concentrations present in the sediment is called dose rate (Dr) and expressed in Gy/ka. The burial age (i.e the time since last daylight exposure) is obtained by dividing the burial dose or paleodose (De) by the dose rate (Dr) (eq. 1)

(eq. 1)
$$Age\ (ka) = \frac{Equivalent\ dose\ (Gy)}{Dose\ rate\ (Gy/ka)}$$

In general, the most commonly used procedure to built-up a growth curve is the Single-Aliquot Regenerative (SAR) dose protocol (Murray and Wintle., 2000), in which the natural luminescence signal is first measured (and thus zeroed) prior to repeat different increasing steps of induced irradiation and measurement on a single aliquot of sample (Fig2).

Several factors influence the accuracy of De estimation: (i) complete bleaching of any trapped charge prior to burial, an incomplete removal will cause De overestimation; (ii) The cumulative charge is trapped at stable sites during burial, conversely charges stored in instable traps can be naturally released causing an age underestimation. (Mallinson., 2008; Buylaert et al., 2013).

Luminescence sensitivity changes are monitored and are corrected for using a known test dose. A general overview on approaches for De determination was given in Wintle

(2008). One criterion for an accurate measurement of the dose using quartz OSL and SAR protocol is the presence of a dominant fast component luminescence signal. The fast component represents the large part of luminescence signal that is bleached in the first second of stimulation (Wintle and Murray, 2006) (Fig.3).

Hence, the majority of conventional luminescence ages are based on the fast-component-dominated quartz OSL signal measured using (SAR) protocol. The Quartz signal is known to be rapidly bleachable by day light to very low levels and is considered stable at the timescales (e.g. Murray and Wintle, 1999, Madsen and Murray, 2009). The limit of dating range with Quartz is due to the its meta-stable traps that can be saturated at a relatively low given dose. This limit is called saturation point and depend on the Quartz grain geological history and deposits characteristics. Usually the saturation occur at ~200 Gy. This limits the application to sediments not much older than ~100 ka. However, this limit mostly depend on the level of dose rate of the deposit.

The D0 value is considered the dose saturation level which controls the maximum age limit that one sample can reach for luminescence dating (Singarayer and Bailey, 2003). In theory the Quartz maximum achievable trapped charges correspond to the double time of the D0 (Wintle, 2008b). However, reliable ages can be obtained only by quartz grains with the natural signal (Ln/Tn) and the final De lower than the 85% of 2 D0 (Fig2). Instead, for samples with De values higher than the 85% of or beyond the 2D0 the reliability of the quartz dose estimate is not proven and the resultant age should be taken with caution.(Murray and Wintle 2006).

Most of one case was encountered in the present study, for example in samples BOSBIO and BOSFOR recovered from S'abba Drucche bay, Tro4 from the Alghero area and Bom1 from Le Bombarde beach. Samples showing the majority of the measured aliquots with a De value greater than the 2D0 signal are considered unsuitable for OSL dating with the quartz grains. However, the Do value in Gy can be used to estimate the minimum age of burial time. In the case that only few aliquots of the total measured display a De value higher than the 85% of 2D0, the saturated aliquots can be omitted and a meaningful and reliable age can be calculated.

A

Step	Treatment	Observed
1	Give dose[a], D_i	—
2	Preheat[b] (160–300 °C for 10 s)	—
3	Stimulate[c] for 40 s at 125 °C	L_i[d]
4	Give test dose, D_T	—
5	Heat[b] (160–300 °C)	—
6	Stimulate[c] for 40 s at 125 °C	T_i[d]
7	Stimulate[c] for 40 s at 280 °C	—
8	Return to 1	

B

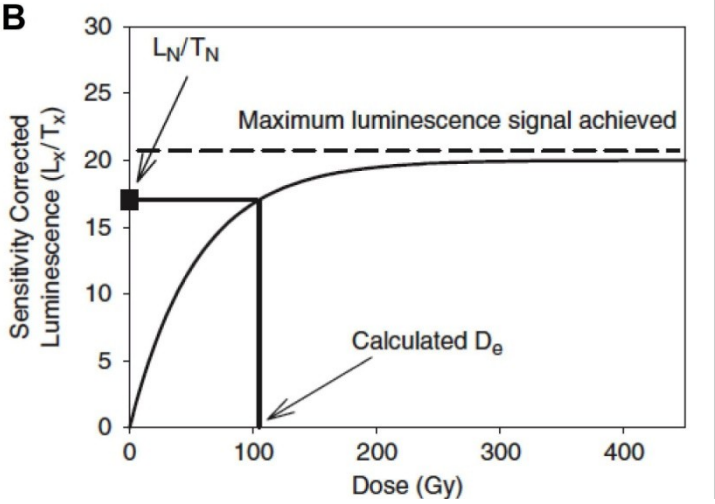

Fig. 2: General quartz Single Aliquot Regenarative dose (SAR) after (Murray and Wintle, 2000, 2003) B)Exemple of sensitivity-corrected dose-response curves with plotteed the naural signal (LN/TN) used to calculate De. Lx/Tx regenrative points increase towards the saturation level, (Lx/Tx=20), i.e. the maximum achievable value I0, according to the equation I(D)=I0 (1-expD/D0), where D0 is 55 Gy. B. Lx/Tx growth obtained as the sum of two signals, one saturating exponential with parameters as in (A) and the other a linearly growing signal.

Fig. 3: Comparison of quartz and potassium rich feldspar decay curves. A) quartz steep decay curve dominated by fast component. B) slower decay typical of k-feldspar signal. (Thiel et al 2011)

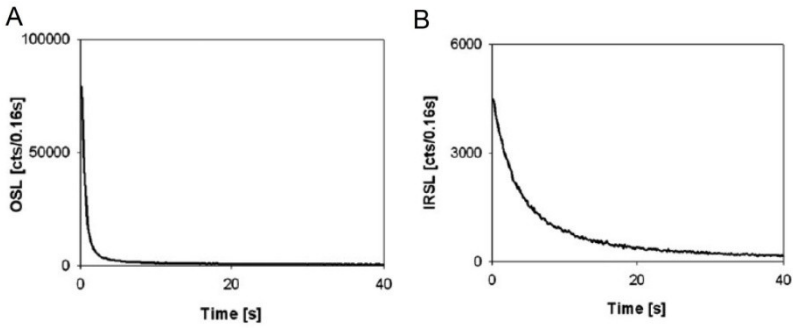

In the last decade the attention of luminescence dating has been shifted on potassium rich-feldspar grain. The k- feldspar luminescence signals bleached slower than Quartz, it is sensitive only to the IRSL (infrared stimulatated luminescence) and its dose response curves saturate at much higher dose (~1.5-2 kGy) allowing an extension of the age range of luminescence dating. Nevertheless, feldspar IRSL signals measured at ambient temperature are affected by anomalous fading. This consists of a decrease of the IRSL signal with time faster than expected from thermal stability measurements which causes age underestimations unless a (usually large) correction is made (Huntley and Lamothe, 2001). Corrections models have been proposed (Huntley and Lamothe, 2001; Buylaert et al., 2011a), however, these corrections are usually large (typically 30-40%) and are based on untestable assumptions (Morthekai et al., 2008). In addition Huntley and Lamothe (2001) argue that this correction method should not be applied to samples older than 20-50 ka, well within the quartz age range (quartz does not require any correction). This characteristic has been the limit of feldspar use for dating on the last thirty years.

Thomsen et al. (2008) have identified an IRSL signals measured in the blue wavelength part of the spectrum (Buylaert et al., 2007, 2011a) showing a lower laboratory fading rate compared to that normally used (typically stimulated at 50° C, IR50). Thus they proposed the use of a post-IR IRSL signal stimulated at elevated temperature.

Buylaert et al. (2009) tested this suggestion. Using the base of SAR protocol, after a preheat 250°C for 60 s, stimulated feldspar grain with a first IR stimulation at 50°C and with a second IR stimulation at 225° C, and observed a smaller pIRIR225 fading rates correlated with larger apparent burial doses. Residual doses after daylight bleaching remained below 2 Gy for pIRIR225 and the signal displayed markedly less fading than the IRSL50, although some fading correction was still necessary. Thiel et al. (2011) used a higher preheat temperature of 320°C for 60 s increasing the second stimulation temperature up to 290°C (pIRIR290). Using these parameters feldspar signal did not fade significantly over the burial lifetime of the sample. Finally, Buylaert et al. (2012) tested the accuracy ages based on this method against independent age control. They demonstrated that it was inappropriate to make any fading correction to the new

protocol Post-IR IRSL at 290 and known as pIRIR290. (Tab.1) This new protocol is able to date very old samples up to 500 ka.

A

Step	Treatment	Observed
1	Give dose[a], D_i	—
2	Preheat[b] (160–300 °C for 10 s)	—
3	Stimulate[c] for 40 s at 125 °C	L_i[d]
4	Give test dose, D_T	—
5	Heat[b] (160–300 °C)	—
6	Stimulate[c] for 40 s at 125 °C	T_i[d]
7	Stimulate[c] for 40 s at 280 °C	—
8	Return to 1	

B

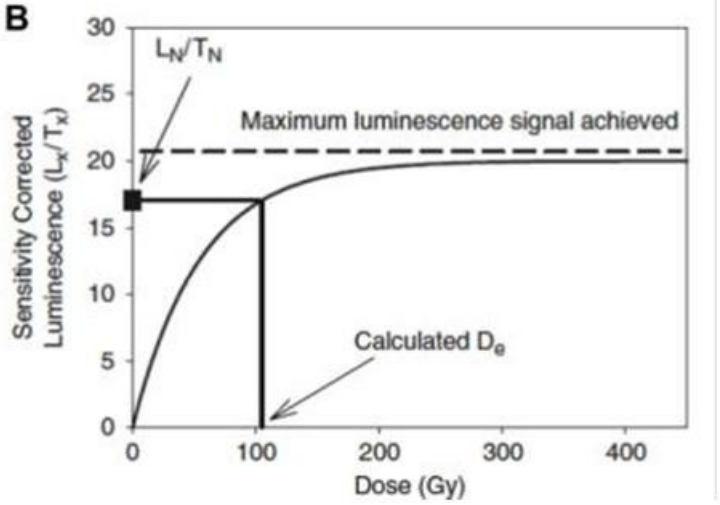

Tab. 1: Post-IR IRSL at high temperature (pIRIR290) protocol suggested by Buylaert et al. (2012). Lx (luminescence signal) Tx test dose signal.

Geological setting of Sardinia

The island of Sardinia is located in the centre-western part of Mediterranean Sea. During Oligocene-Miocene the island was involved in a rifting process and into an anti-clockwise rotation toward east, at end of Miocene it reached its actual position (Fig4-A-B). Associate with this rotation important volcanic episodes occurred and several half-graben basins developed, later filled by a thick mixed carbonate-siliciclastic sedimentary succession (Carmignani et al 2011). A second large volcanism associated with the opening of the Tyrrhenian back-arc basin (Sardinia east-side) interested the west part of the Island during Middle-Miocene early Quaternary period. The tectonic and volcanism activity related to this opening (last rifting phases) ended at the beginning of Pliocene involving also most of the East part of the island. However, a part from minor but consistent patterns of vertical motions recognizable in local stable areas, since the late Pliocene Sardinia has been generally considered tectonically stable and affected by a regional subsidence rate of -0.01 mm/a (Ferranti et al., 2006).

Quaternary deposits crop out quasi-continuously along the island coast. They mainly conist of shallow marine to alluvial/colluvial (paleosol) and coastal dune resting unconformable on bedrock of various ages (Carmignani et al 2001).

This thesis is focused on the Quaternary deposits cropping along the north-west coast of the island (Fig1-C). The present Sardinia NW coast is characterized by high promontories often facing the sea forming very high cliffs. Often these latter bound small coves where pocket beaches can develop. The cliff foots are often characterized by marine terraces or submerged shallow wave cut platforms. However, where the coast is less steep and the landscape is dominated by large plain, wide sandy beaches or barred-lagoon system develop. Presently, the north-west Sardinia coast is affected by anticyclone mesoscale eddies which are responsible for most of the southward directed longshore current. (Robison et al 2001).

Dominant winds are from the fourth quadrant. North west wind (Mistral, 300° N) is the most common. It is the source of the strongest marine winter storms (Istituto Idrografico della Marina; Rete Ondametrica Nazionale, APAT; www.idromare.com) (Fig 5).

The annual largest significant wave heights range from 4 to 6m with maximum values of 8m and significant wave periods of 12 s (Gaillard et al 2004). Tidal range does not exceed 50 cm in average.. The shallow coast from the average depth of -4 m to -30 m is very often dominated by sandy plain where extensive seagrass meadows occur. Seagrass is the main source of bioclastic sand. This is deposited along the coast during the major storm and re-distributed by waves and longshore current during the fair-weather (Donda et al. 2008). Siliciclastic sand and gravel are transported on the coast by a wide net of ephemeral streams mostly active during winter season; a relative small amount derives from the cliffs erosion.

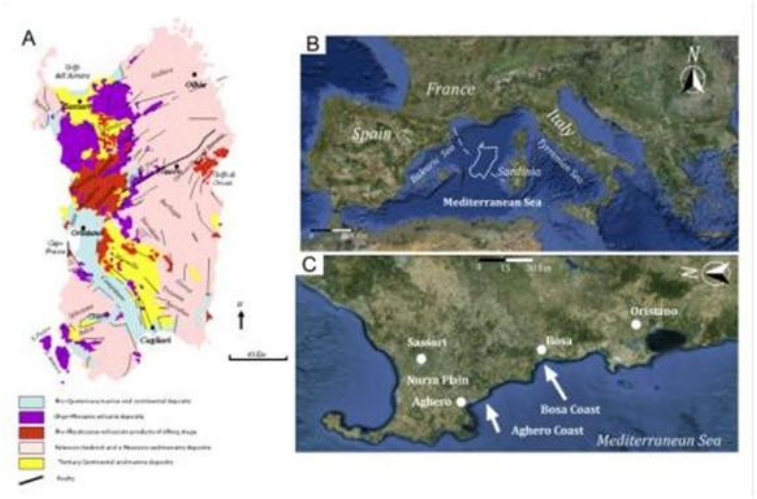

Fig. 4: Location map of Sardinia. A) Main geological features of Sardinia. B) Satellite view of Mediterranean sea C) Satellite view of North-West coast of Sardinia, arrows indicate the location of the main areas studied for this thesis.

Fig. 5: Rose plot of waves and wind directions. A) Main waves direction on the NW coast B) Mainly winds direction

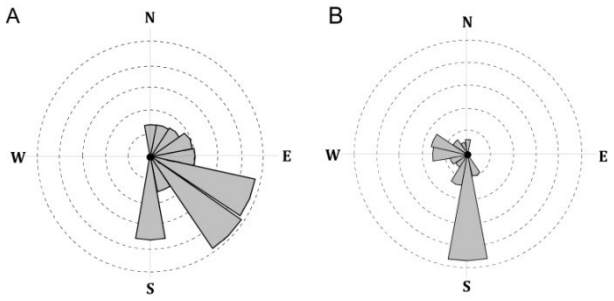

Methods:

Luminescence laboratory analysis

Luminescence analysis were mostly conducted at the Risø Nordic Laboratory for Luminescence dating (Denmark); others at the CUDaM laboratory, University of Milano-Bicocca (Italy) and at the SCIRD (Sheffield centre for international Dryland research, Univerisity of Sheffiled, UK).

In the present study the widely accepted protocol, Single Aliquot Regenerative dose (SAR) (Murray and Wintle, 2000) has been used for the measurement of quartz minerals.

Some internal checks are tested in each sample to evaluate the validity of the SAR protocol and the reliability of the derived ages. Firstly the preheat has been chosen. This step is setted before each luminescence stimulation and is an indispensable part of SAR cycle because it helps to empty the light sensitive shallow and instable traps particularly filled during laboratory irradiations (Wintle and Murray, 2006) (Fig.1-2).

The preheat conditions can be chosen performing the preheat plateau test. The value of De has been analysed under different preheat temperatures in order to test if the sample behaves differently to the preheat treatments, and thus if the temperature causes sensitivity changes leading unwanted charges transferred to the light sensitive traps. If sample is not or poorly affected by any sensitivity temperature changes the resulting plotting of the De against the temperature is a plateau. The SAR protocol is also characterized by and additional step named test dose; this let to monitor the sensitivity change per unit of the given dose. (Fig 1-2).

The robustness of the SAR method to date accurately samples is tested by a recycling point. This consists to repeat a measurement (usually the first) at the end of all procedure to check whether samples behave differently during the procedure. Usually the ratio of the measure of two identical steps of regenerative dose should be equal to 1±0.1. This ratio is used as rejecting criteria, an aliquot with a recycling ratio below 0.9 or above 1.1 is rejected.

The SAR protocol is also characterized by a step where the given dose is at zero point (zero regeneration dose), this step usually is set before the recycling test. This test is also known as recuperation test and each non- zero sensitivity corrected signal obtained from the zero regeneration dose may be expressed in percentage of the natural signal. High value of recuperation derives as result of the charge transfer from deeper traps due to previous irradiation, optical stimulation and preheats (Wintle and Murray, 2006). SAR protocol provides high precision estimates of De, commonly with overall uncertainties of <5% of recuperation (Bailey, 2000b; Wintle and Murray, 2006). Finally the dose recovery test has been performed as a routine test for all samples to ensure the accuracy of De values estimated and the efficiency of the protocol to recover a given dose (Roberts et al., 1999; Murray and Wintle, 2003). The test requires the resetting of the natural signal to zero by artificial stimulation and subsequently to give a known laboratory dose to the sample. For ideal measurement conditions the SAR protocol should be able to recover the given dose close to unity (known dose/dose measured ratio of ~1.00±0.1). If the known dose is not well recovered within acceptable ratio, the measurement used for the De estimation is considered unsuitable. Conversely, if the measured dose is indistinguishable from the known dose, it is usually assumed that the protocol is applicable to the measurement of whatever unknown natural doses within a reliable ranges of uncertainty. Often the preheat plateau and dose recovery test have been performed at the same time.

For this thesis quartz grains were mounted on stainless-steel discs using silicon oil as adhesive, whereas for the potassium feldspar grains stainless-steel cups (0.1 mm thick) were used. Standard size aliquots, 6 mm in diameter (i.e. hundreds of grains), were used for all quartz measurements unless otherwise specified. Luminescence measurements were made with an automated Risø TL/OSL reader (DA-20 and DA-15; Bøtter-Jensen et al., 2003) using a calibrated 90Sr/90Y beta source (~0.15 Gy/s and ~0.08 Gy/s, respectively). For the standard quartz measurements blue light emitting diodes (LEDs) were used. The quartz signal was detected in UV through a 7.5 mm Hoya U-340 filter. The potassium feldspar was stimulated with infrared LEDs, and the luminescence was detected in the blue-violet region through a Schott BG39/Corning 7–59 filter combination.

For each study area one representative sample of quartz was analysed following the standard procedure described above in order to estimate the main luminescence characteristics and the reliability of the SAR protocol.

Firstly, the absence of any feldspar infrared signal contamination (the purity of the quartz) was checked using IR depletion procedure (Duller et al 2003). Passed this test best temperature for the preheat was measured using preheat plateau test performed on 24 aliquots for each sample. The temperature for the preheat ranges from 180 to 280°C, whereas the cutheat was set always 20°C lower than preheat temperature; that is, between 160°-260°C.

The dose recovery test was performed in combination with the preheat plateau test in order to estimate the best preheat and cut-heat temperatures and whether samples were affected by any temperature sensitivity changes. If this standard procedure is passed each sample is analysed in order to estimate the De (paleodose). Each SAR growth curve performed was also characterized by the recuperation and recycling points. Any aliquot showing a low recycling ratio 0.9>R<1.1 was rejected.

Firstly the saturation of the signal was tested applying a growth saturation dose response curve based on increasing of given doses to reach the probably saturation point.

Finally, the standard SAR procedure was applied to estimate the average De for each sample. For samples showing a quartz saturated signal or suffering a partial bleaching the pIRIR290 mentioned above was applied. The K-feldspar SAR post (post-IR IRSL) at elevated temperature (290°C) protocol consists of a preheat at 320 °C for 60 sec, the samples were bleached with IR diodes at first at 50 °C for 200 sec and then at 290 °C for 200 sec. The same preheat conditions were used for regenerative and test doses. An IR illumination at 325 °C for 100 sec was inserted at the end of each cycle (Thiel et al., 2011, Buylaert et al., 2012). (Table 1)

The early background time interval subtracting procedure was used for the integration time of quartz decay curve. The very fast portion of the quartz curve was integrated at 1-2s for calculation of equivalent dose, whereas the part of the signal laying around 5-10s was used for the background subtracting. Instead of for k-feldspar,

which are characterized by a low decay curve, the usual late background subtracting procedure was applied (Cunningham et al., 2010; Buylaert et al., 2009).

Samples collection

Most of the collected samples consisted of ~2 kg of material carved as a block (50X50X40 cm) from the outcrop in daylight, then wrapped in opaque plastic and sealed. All sample treatments were conducted at the University of Sassari laboratory under controlled red light conditions. The outer part of the block (~5 cm) was removed prior of any treatment cause the potentially exposition to daylight during sampling and kept for the dose rate estimation. Only the inner part was considered and weighted before any chemical treatment. Following the conventional procedure, each sample was treated with 40% HCl and H2O2 in order to remove all the carbonate and organic components. At the end of each chemic step samples were dried in the oven at the temperature of about 50° C and weighted. The resulting siliciclastic fraction was sieved and the fraction ranging from 90 to 250 µm grain size was taken for the luminescence purposes. Using different density of heavy liquid solution of polytungstate Quartz and Potassium feldspar were separated. (Stokes, 1992; Mejdahl & Christiansen, 1994; Lang et al., 1996; Mauz et al., 2002). Finally the resulting fraction of Quartz grains were etched whit 40% hydrofluoric acid (HF) for at least 1 h to remove any remaining feldspar grains and the alpha-irradiated outer layer. The feldspar grains were instead etched with weaker hydrofluoric acid (10% concentration) for 40 min to remove the alpha-irradiated outer layer. (Lang et al., 1996).

Dosimetry

The Dose rate (Dr) is normally considered as constant throughout the burial. The natural dose rate in sediments is expressed in Gray per thousand years (Gy/ka-1).

Radionuclides emit energy releasing 3 different rays/particles: α, β, γ. The α particles have a penetration depth in sandy siliciclastic-rich deposits of the order of ~20 µm, β particles of ~2 mm and γ rays- of ~ 50 cm (Aitken, 1985; Brennan 1997). The total α

dose was omitted in the final Dr calculation because the outermost part of the crystal, affected by the alpha radiation, was completely removed during the HF treatment. Thus, the total dose rate of a sandy (250-90 μm) sample includes the β and γ doses contribution. Given the μm-scale penetration of the β-particles , the final β dose rate was corrected for the dose attenuation factor based on the crystal grainssize (Bell, 1979). The radiation flux mainly derives from the decay of naturally radionuclides such as 235U, 238U and 232Th and their daughter nuclides as well as 40K and 87Rb (~1% of annual dose rate) present in the deposits.. It is worth noting that for k-feldspar grains an extra source of dose is represented by the internal decay of 40K and 87Rb that have to be taken in account for dose rate calculation for the k-feldspar final dose rate. The 40K internal radioactivity contribution of k-feldspar, was included in the final total dose rate as described by Buylaert et al 2012, assuming a K content of 12.0 ± 0.5% (Huntley & Baril, 1997) and a Rb abundance of 400 ± 100 ppm (Huntley and Hancock, 2001) .

Finally, the dose rate was corrected for the cosmic dose contribution in the sample burial depth, altitude and geographical location (Prescott and Stephan, 1982; Prescott and Hutton, 1994).

For this work different methods were used to calculate the isotope concentration:

1) An high-resolution gamma spectrometry (Murray et al., 1987) with appropriate conversion factors (Olley et., al 1996). For the gamma spectrometry analysis part of the additional sediment associated with the OSL sample was dried at 50°C. A subsample of ~250 g was pulverized and homogenized, and then heated to 450°C for 24 h to remove any organic matter. The material was then cast in wax to prevent radon loss and to provide a reproducible counting geometry. Samples were stored for at least three weeks to allow 222Rn to reach equilibrium with its parent 226Ra before being measured on a high-purity Germanium detector for at least 24 h. Details of the gamma spectrometry calibration are given in Murray et al. (1987).

2) A total alpha counting using ZnS scintillator discs (Aitken, 1985), where assumed a concentration ratio Th/U equal to 3 while the 40K activity was deduced from the total concentration of K measured with flame photometry.

3) Using inductively coupled plasma mass spectrometry (ICP-MS; for U and Th) and inductively coupled plasma atomic emission spectroscopy (ICP-AES, for K) on 10-g of

sub-samples (obtained by riffling). The resulting dose rate is carried out through conversion factors following Guérin et al., 2011).

The water circulations through sediments can affect the concentration of soluble isotopes and can cause the disequilibrium of the U and Th isotopes decay chains. The saturation of the sediment pores also causes the attenuation of radiation flux; moreover, fluctuation of the water table may produce the dissolution and re-precipitation of calcium carbonate (CaCO3) around the sediment grains, acting as a shield attenuating the natural radiation flux (Aitken, 1985). Thus, for each sample, the water content (dry and saturated values) as well as the amount of CaCO3 re-precipitated in the pores as cement was estimated. Influence on the Dr by sediment cementation was modeled following Andreucci et al. (2012). A weighted average between the present-day and saturation values was selected as lifetime water content since time of deposition for each sample.

Finally, the reliability of the measured Dr is based on the assumption that the analyzed samples were collected in homogenous deposits with a minimum thickness of 60 cm. This is based on the evidence that the γ particles have a penetration depth of ~100 cm in a sandy siliciclastic-rich deposits. Thus, an extra dose coming from the overlaying and/or underlying sedimentary units has to be considered for samples collected in deposits thinner than 60 cm (Aitken, 1985; 1995). Therefore, some samples underwent to a correction of the final Dr rate on the base of the stratigraphical relationships of the considered deposits.

Facies analysis and stratigraphic correlations

In order to define the stratigraphy of late Quaternary deposits of the north-western coast of Sardinia two different areas have been selected Bosa (S'Abba Druche cove) on the west coast, and the Alghero and on the northwest coast; five sub-areas were selected on base of their different characteristics (Fig. 4c).

In all areas, sedimentological analysis was performed. The sedimentary succession has been described on the base of different facies, according to their sedimentary (lithology, grain size, sedimentary structure) and macrofossil characteristics. Facies

have been labelled considering the main lithology (G = Conglomerate, S =Sandstone , W = silt matrix, C=carbonate), grain size (d = cobbles and pebbles, e = medium to very coarse-grained sand), sedimentary structures (l = laminated, p = planar-cross bedded, t = trough cross-bedded u = low-angle cross bedded, m = massive i = imbricated) and biogenic features (f = highly-fossiliferous, r =root traces). Therefore, facies labelled Gem stands for massive (m) conglomerate (G) with medium-coarse sand (e). For each area the main identified facies have been grouped in facies associations. In all areas, several logs were measured and then correlated on the base of the presence of unconformities, defining unconformity bounded units (Unit).

The Quaternary deposits outcropping along the north-west Sardinia coast are characterized by different sedimentary environments ranging from shallow marine to alluvial and aeolic. Generally, facies and facies associations identified along the Sardinia coast are very similar. However, facies often show small differences related to sedimentary structures mainly due to site characteristics (fig.7). Thus, in the following the main representative sedimentary structures and characteristics of the recurrent facies and facies association are summarized. The small differences, instead, will be reported area by area to better understand and constrain the strathigraphic facies relationships, their correlations and the paleogeographic evolution of any single area.

Gravel beach facies association (Bg):

The facies association Bg is present in almost all the studied areas. It ranges in thickness from 0.5 to 2 m and it is characterized by different marine clast-supported conglomerates. Clasts vary from well-rounded to sub-angular granules to megaboulders. Conglomerate clasts very often are made of rocks deriving from the close cliff-wall. In most of the cases facies association Bg rests unconformable on the bedrock forming a wave cut platform. (Fig.6 and 7B-C)

Facies Gem was identify in almost all the studied areas. it is composed of massive basal conglomerates (50 cm thick) ranging in size from large pebbles to mega boulders reflecting the local bedrock composition. A coarse matrix fills most of spaces among clasts and is composed of fine pebbles and rounded granules, medium to coarse sand

and marine shells fragments may occur as well. Often this deposit rests unconformable on the bedrock forming a wave cut platform (Fig.6, 7b, 12b-d).

Facies Gem has been interpreted as the submerged shallow and proximal part of a cliff toe/shallow rocky coast deposit, mainly developed on a submerged part of very shallow wave cut platform. Most of the biggest clasts are interpreted as rock-fall deposits, whereas the medium-sized clasts may derive from the erosion of the cliff/platform or carried by the marine long-shore current and waves.

Facies Gem is often covered by facies Cef.

Facies Cef consists of up to 1 m thick organic carbonate bodies, built up by vermetides, barnacles and red encrusting calcareous algae, mostly Lithophyllum byssoides (Fig.6,7a,12,16,23D-e). Dispersed abundant pebbles, granules, poorly sorted medium to coarse sand and marine shells (whole or in fragments) of Gastropods (C. cfr. testudinarius, Arca noae, Bolma Rugosa), bivalves, and molluscs (Patella ferruginea, Cardita senegalensis, Glycymeris glycymeris, Ostrea spp,) occur. (Fig 12A, 16E)

These carbonate bodies drape discontinuously the basal conglomerate (Gem) reflecting a mound shape geometry. The large amount of barnacles spp found in life position, encrusting serpulides, and the abundance marine shells in fragments and encrusted suggests that this carbonates deposited in a shallow marine intertidal environment. They (Cef) have been interpreted as the fossil equivalent of the living bioherms (sensu Kershaw 1994), prevalently characterized by intertidal red algae associated with barnacles and serpulides, which formed an intertidal rim at the base cliffs (Loberel et al., 1994; Cossu et al., 1997, Ministero dell'Ambiente 2009) mostly on a basal gravelly lag deposits (Gem) (sensu Massari and Parea 1981) (Figs.7).

As well as Gem, the second recurrent facies basically consist of a conglomerate deposits characterized by angular to well rounded cobbles and pebbles and often scattered boulders (facies Gd). In most of cases, boulders lye at the base of the cliff/toe, from where they derive. These can be reworked and redeposited elsewehere giving rise to a wide variability of sedimentary structures. For instance, facies Gdm is characterized by 50 cm thick of massive clast-supported pebbles to cobbles, poorly stratified conglomerate beds, gently dipping seaward and with landward clast-imbrications. This facies for example at S'Abba Drucche bay and El tro bay is interlayerd

with trough-cross bedded sandstone. This association has been related to the shoreface part of sandy beach system influenced by sporadically gravel input due to the dismantling of the surrounding cliffs and promontories (Fig. 10A). Otherwise facies Gdm(i) is characterized by massive clast-supported conglomerate strata slightly dipping sea-ward. Clasts range in size from pebbles to cobbles; they are sub-angular to rounded often with a blade shape. Scattered boulder may be found. Cobbles and boulders are often imbricate landward dipping toward the sea. Matrix consists of a very coarse sand reach in marine shells fragments. Facies Gdm(i) has been identify at El Tro bay and lays unconformable on lower conglomeratic facies (Gem/Gef (see above) (Fig6, 7c, 23).Facies Gdm(i) has been interpreted as the proximal part (outerframe) of a pocket gravel beach strongly influenced by the wash and backwash of waves action (Pascucci et al 2009) (Fig 7c). The small pocket gravel beaches are recurrent along Sardinia rocky coast and often developed on the wave cut platform between rockfalls. This particular pocket beaches show a simple structure is characterized by a fining upward trend moving from the submerged part to the emerged one. Layers of openwork well rounded granules and pebbles imbricate landward commonly characterize the emerged part (beach face). Faint of fair-weather berms may be found. This deposit is described as facies Gde. (Fig.6, 7c-d) Commonly these small pocket beach are very ephemeral and they form in a very narrow space within the low tide level and the maximum storm level so their structure may be not fully developed or partially preserved and thus difficult to be discerned. . However, modern analogues are helpful for facies interpretation of the relict deposits.

Instead, when more space is available gravel beache systems can develop more complex system structure. For instance, Gdoi facies (1.5 m thick well exposed at El tro bay) consists of clast-supported conglomerates made of clasts ranging from well-rounded blades cobbles to well rounded spherical granules. This facies is characterized by alternating dipping seaward layers of cobbles and pebbles (imbricate landward), granules (openwork feature), and well sorted coarse-grained sandstone (parallel or low angle laminated). Cobbles are often bored and occasionally encrusted by serpulides. Granules layers often rest on or in between cobbles. In places they form clouds around the bigger clasts. Sandy layers may in places occur between conglomerates. Broken or

complete marine shells are widespread throughout conglomerates (Fig.6, 7F-G,24D-E). Gdoi have been interpreted as the well-developed beachface of mature gravel beach where different generation of berms can be identified ranging between the fair weather (granules and sand layer) and storm berms (Fig78F-G).

Sandy beach Facies association (Bs)

Facies association Bs crops out in all the studied areas and shows high variable lateral discontinuity and thickness (1 to 5 m thick). Facies association Bs often rests conformably on facies associations Bg or directly on the bedrock. This facies is mostly characterized by the alternation of sandy body and locally at the top is transitional with reddish sandy or clast-supported silt deposits interpreted as colluviums/incipient paleaosol or with high angle cross bedded sandstone interpreted as aeolian deposits (see facies association A and E) (Fig.10B-C-D and 30A-C).

The facies association Bs is characterized by a shallowing upward trend changing from shoreface to the backshore environment (Fig. 10A-C and 12). The main facies that characterize the association Bs are listed in figure 6. The lower mostis often facies Set. It is composed of medium to coarse grained trough-cross bedded sandstones. Dispersed or aligned in layers several marine shell fragments may be found. Upward trough-bars often pass to very small cross-lamination sandstones. The small cross-bedding is characterized by asymmetric and symmetric ripples marks which suggest they formed under the influence of both uni and bidirectional flows (Fig.10A-B-C and 31). In only in one case (at El Tro bay) facies Set is not the basal facies. In this case the succession starts with well sorted coarse to medium parallel laminated (less evident on the bottom) strongly bioturbated sandstone (facies Seml) (Fig.6 and 24E-Ff). A thin clast-supported conglomerate (50 cm-thick) lays on facies Seml and separates it from facies Set that closes the succession. The conglomerate clasts range in size from cobble to granules, in shape from sub-rounded to well rounded. Cobbles are often borrowed or in part encrusted by serpulides. Clasts normally slightly dip toward the sea showing a good imbrication landward. Matrix is made of granules and coarse sand. Granules and coarse sand in places occur in lenses where faint trough cross stratification may be

observed. This conglomerate facies is similar to the facies described above Gdm for the Bg succession. The two gravel deposits differ for the clast- imbrications that suggest a different regime flow. This facies is referred as Gdi (Fig.7H-I and 24 F).

Facies Set is followed by the facies Seu. This ranges in thickness from 50 to 3 m and is composed of medium to coarse, low angle plane stratified, seaward dipping sandstones. Scattered pebbles may be found and black laminas made of heavy minerals are recurrent into this facies. Lamina dip-direction is mainly oriented toward the sea with an average of 5° and for rare exceptions up to 17°. The association continues with well sorted medium to coarse-grained, horizontal low angle cross laminated sandstones where laminas of granules and scattered pebbles may be experienced (facies Sep). The limit in the vertical succession between facies Seu and Sep is hard to be identified. Commonly that limit has been highlighted by the decrease up ward of the recurrent black lamina (Fig.21c)

Facies association Bs is normally in vertical continuity with facies association E which has a variable thickness (0.5-1 m) and is made of medium to coarse grained, massive sandstones with roots bioturbation (increasing toward the top) close the succession (facies Sem/Semr). Facies Semr can be associated or replaced by medium to fine (even coarse) well sorted parallel laminated high angle cross stratified sandstone, trough cross bedding can occur as well (Facies Sept) (Fig.6, 30A-C)

Facies association Bs is interpreted to represent a well developed wave dominated prograding beach system where both submerged (shoreface) and emerged (foreshore and backshore/dune) parts are preserved. In most of the areas, the shallow shoreface portion may be subdivided in two main zones: 1) the breaker zone where megaripples and bars occurr 2) the surf zone dominated by symmetrical ripples formed during the fair weather and asymmetrical ripples formed during storm events. Commonly beaches were influenced by external conglomerate input may be due to seasonal stream flooding or cliff dismantling. These coarse materials were than reworked in the shoreface-zone and deposited in part on the beach face during the major storm.

The beach systems were characterized by a wide flat backshore flooded during major storm and incipient dune systems. The present beach of Porto Alabe (figure 14) may be a good modern analogue of the above described sandy beach system.

Aeolian facies association (E):

Facies association E is characterized by brown- yellowish well stratified sandstones (facies Sept) or massive sandstone (facies Sem/r) (Fig.6, 16 and 30A-B).

Facies Sem/r is characterized by brown-yellowish, well sorted, medium to coarse grained, poorly laminated to strongly bioturbated by root sandstone. Widespread granules, pebbles and fragment of shells occur. This facies range in thickness from 50 cm to up to 2-m thick, common the bioturbation increases toward the top of the strata whereas at the bottom sandstones are massive-poorly laminated.

Facies Sep(t) is characterized by planar-cross or locally trough-cross bedded, medium to fine-grained (even coarse) sandstone in set from 1 up to 10 m thick. Foresets dip 10-20°generally toward the land or parallel to the coast.

Facies Sem/r is interpreted as the inland backshore part of a sandy beach system influenced by the major storms, strongly vegetated by pioneer coastal plants and where incipient dunes developed. Sept is interpreted as a well developed coastal dune system migrating inland or parallel to the coast. Dunes are the most representative deposits of the Alghero southern.

Alluvial facies association (A)

Facies Gwc is characterized by layers (0.5 to 2 m thick) of matrix or clast-supported poorly sorted angular pebbles and cobbles conglomerate. Beds are massive with occasional horizontal pebble alignments. Matrix consists of medium to fine-grained sandy-reddish siltstone. Occasionally Gwc drapes the lower deposits gently dipping toward the sea. Lower deposits (mostly marine) are strongly reworked at the contact with Gwc (Fig.7 and 18).

Only at le Bombarde bay were indentified recurrent lenses of sandy coarse matrix-supported conglomerate. Clasts varies from well-rounded to sub rounded granule to pebbles and diffuse marine shells (broken or whole). Matrix is formed by a well-sorted medium to coarse-grained sand. The lenses of conglomerate show a fining upward

trend and a poorly cross-bedding with recurrent cut and fill structure, diffuse small pebbles are scattered or aligned at the base of the cross bedding. This facies is referred as Ged(t).

Facies Wed is widely diffuse. It is a massive (poorly consolidated) plane laminated medium to fine-grained reddish or gray siltstone, angular to sub angular clasts (mostly pebbles) in layers or scattered occur. This facies, common show an incipient pedogenesis (Fig 16D and 31B).

Facies Gwc has been interpreted to represent the alluvial fans formed close to the valley flanks. They are dominated by cohesive debris flows triggered and affected by variable amounts of water. The conglomerate fraction is exclusively composed of clasts derived from local, inland bedrock, whereas the sandy fraction is predominantly of eolic origin. Most likely the eolic sand was initially blown inland from the coast, and then reworked by stream processes or debris flow process. The alluvial plain than can be characterized by facies Ged(t) which has been interpreted as a wide braided fluvial system deposit most likely the proximal part of an alluvial fan system.

On the contrary, facies Wed is interpreted as various ranges of mature soil developed and then weathered in-situ (paleosol sensu strictu). This facies characterizes a context of non deposition that associated with a suitable climate condition and time can trigger the pedogenesis of previous deposits such as reddish siltstone colluvial deposits.

Facies	Description	Interpretation	Figures
Gem	Massive conglomerate layer whit basal erosive surface. Clasts are pebbels to boulders.	**Gravelly lag deposit**	
Gdm	Conglomerate strata deeping slightly seaward. Faint of clast imbrication.	**Shoreface deposit**	
Gdm(f)	Massive very fossilifeorus conglomerate with sporadic lens of laminated openwork granules. Scattered boulder	**Submerged part of shalow gravel beach developed at the cliff base**	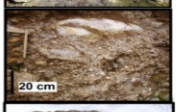
Gdm(i)	Massive conglomerate. Calsts, sligltly imbricated landward, range in size from angular to blade cobbles a well rounded pebbles. Rounded granules and fragment of marine shells occur .	**Outerframe-toe of beachface of ephemeral pocket beach**	
Gdi	Clast supported conglometate. Clast are pebbles and cobbles well rounded imbricated land ward. Lens of coarse sand and granules often cross-bedded	**Shoreface of mixed beach where gravelly bars occur**	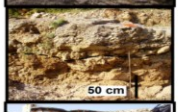
Gdoi	Clast supported conglometate. Clast are pebbles and cobbles well rounded imbricated land ward. Layers of coarse sand low angle stratified and openwork granules deposit occur.	**Beachface of gravel beach where well developed storm berms occur.**	
Ged	Clast supported pebbly-granules conglomerate. Fragments of shells occur in layer. Deposit strongly reworked at the top.	**Reworked gravel marine deposit.**	
Cef	Highly fossiliberous deposit built by intertidal invertebrates and red algea, which incorporate a medium to coarse sand and a basal conglomerate deposit.	**Intertidal red algal rim**	
Seml	Medium to coarse laminated sandstone strongly bioturbated up ward.	**Lower shoreface of sandy beach system.**	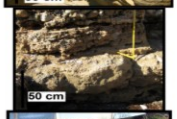
Set	Coarse-grained trough cross bedded sandstone. Scattered fragments of marine shells and granules occur.	**Upper shoreface. Ripples, mega ripples and bars occur**	
Seu	Medium to coarse low angle stratified deeping sea-ward sandstone. Laminas of black heavy mineral reccurent.	**Sandy beachface**	
Sep	Parrel laminatate corase grained sandstone, strongly bioturbated upward.	**Backshore/Aeolian sand sheet dep.**	
Sem/r	Massive well sorted medium to coarse sandstone. Faint of parallel lamination may be found. Bioturbated upward	**Backshore deposits**	
Sep(t)	Well sorted medium planar high angle cross-bedded or trough cross-bedded coarse to medium grained sandstone	**Aeolian dune deposit**	
Ged(t)	Corse sandy matrix supported conglomerate. Lens of granules cross bedded occur reccurent	**Braided stream system of alluvian plain**	
Wed	Reddish siltstone layers with dispered or aligned angular poorly sorted pebbles	**Paleaosol dep.**	
Gwc	Reddish silty matrix supported angular poourly sorted cobbly-pebbly layers	**Cobbly-pebbly debris flow deposits**	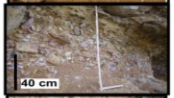
Cem	Massive carbonate deposit large fine sandy component and dispersed shell of brackish fauna	**shallow incipent lagoon**	

Fig. 6: Simplified description of the observed sedimentary facies of the study areas.

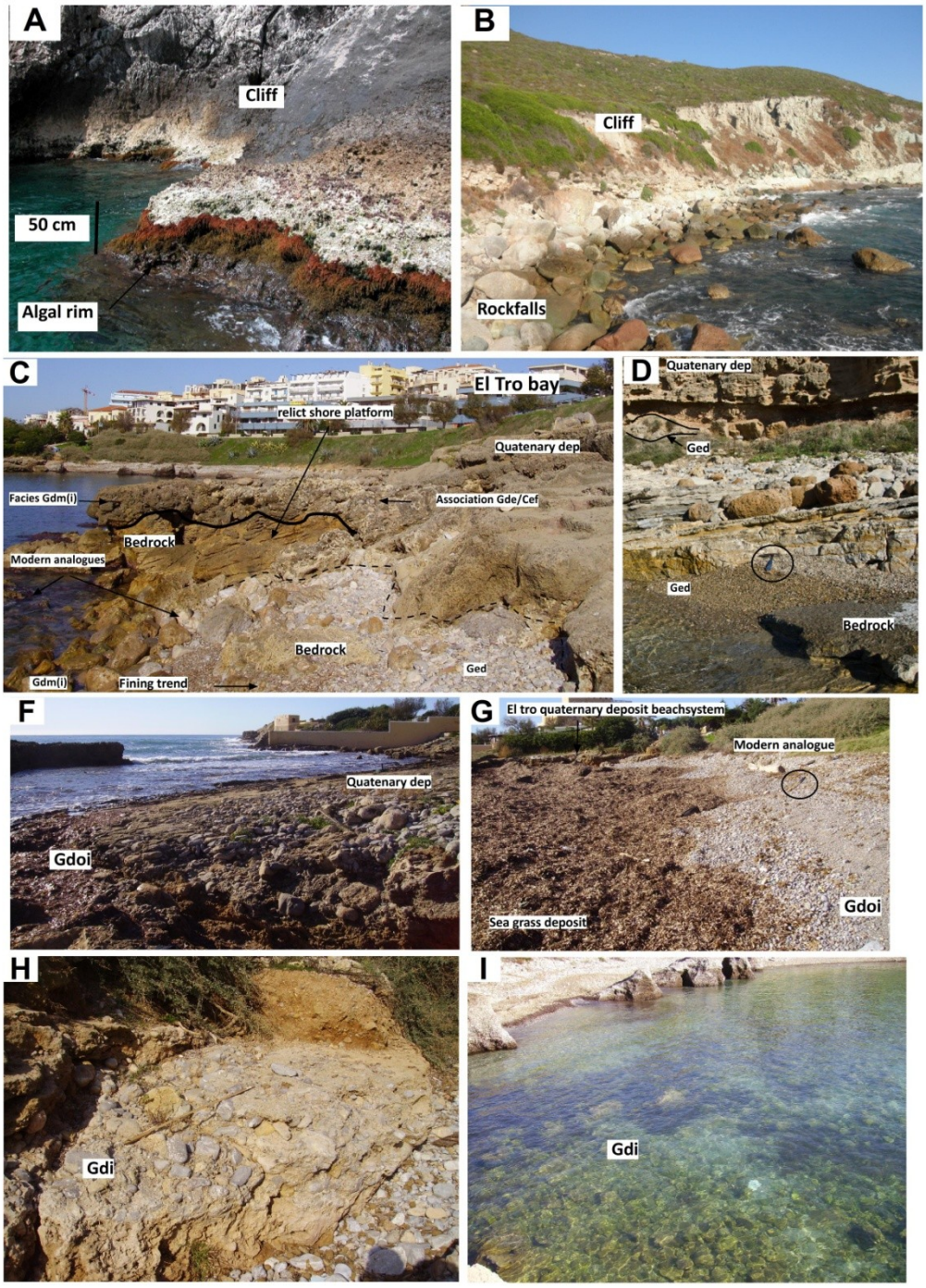

Fig. 7: Modern and relict facies comparision. A) The living algal rim B) Dismantling cliff with the wave cut platform and rocksfalls C) Example of very small pocket beach formed at the base of cliff, characterized by the outerframe (Gdmi) and the emerged part (not well developed beach face) (Ged) D) Modern example of gravel deposit on wave cut platform F-G)Relict and modern gravel beachface cropping out at EL Trò bay H-I) Relict (H) and analogues modern deposit of the very shallow mixed-shoreface, relict deposits are exposed at 1.5 m above the modern one. .

Study Areas

Study areas:

S'Abba Drucche bay (Bosa coast) west Sardinia

Geological setting of study area

The study area is located on the west coast of Sardinia island close to the city of Bosa and it is commonly known as S'Abba Drucche bay (fresh water bay) cause the presence of many fresh water springs. The area consists of a small embayment open westward and bounded by two promontories composed of Oligo-Miocene volcanic rocks. The central part of the bay is dominated by a relatively large plain where a wide gravelly beach develops. The gravel beach is fed by an ephemeral local stream mostly active during wet season. The central part of the bay is characterized by several coves, mostly carved into the quaternary rocks, where sandy pocket beaches develop. At the base of the volcanic cliffs well developed wave cut platforms may often occur. (Fig.8)

Fig. 8: Satellite view of S'Abba Drucche study area and main characteristics

Stratigraphy

Quaternary deposits crop out quasi-continuously along the bay for about 1 km. Facies analysis allows identifying four main facies associations Bg, Bs, E and A. Seventeen logs were measured on the field and correlated on the presence of different well developed unconformity surfaces. Three unconformity bounded units U3a, U3b and U4 have been defined and OSL dated. (Fig.11)

OSL Analysis and luminescence characteristics.

Two samples were collected along S'Abba Drucche bay. Sample BOSBIO was collected from the carbonate deposit (algal rim) and BOSFOR from the sandy foreshore (facies association Bg) deposit at ~1 m above the present sea level.

OSL analysis were conducted on both quartz and k-feldspar grains. Firstly, quartz grains were tested to check the luminescence characteristics. The purity of quartz samples were tested applying a IR depletion test. The analysis provide positive and thus samples were re-etched whit hydro-fluoridric acid. After a second purity check quartz samples pass the IR-depletion test. The suitability of SAR protocol were tested by means of dose recovery preheat plateau on twelve aliquots of Bosfor. About 62 Gy of dose were given to the aliquots, the mean of dose recovered was 64±5 Gy and the recycling ratio 0.98±0.07 confirming the reproducibility of the SAR protocol. (Fig.8b-d). In addition there was no significant dependency of the measured to given dose ratio on the preheat temperature. A preheat of 240 °C and a cut heat of 220 °C were chosen. Despite the good luminescence characteristics of the signal (fast dominated) quartz samples resulted saturated with a De > 85% of 2Do (Fig.8a).

The pIRIR290 protocol was conducted on 12 aliquots for each sample in order to estimate a reliable De. The k-feldspar grains show a good luminescence proprieties and any saturated signal (Fig.8b). Given that the pIRIR290 protocol has been not or less affected by the fading issue any test for this has been performed on samples. The dose rate estimation was conducted as mentioned in the method chapter using high resolution gamma spectrometer. The resulted pIRIR290 ages respectively for sample

BOSBIO is 125±8 ka and for BOSFOR 96±7 ka. The results are summarized in Table 2 and 3.

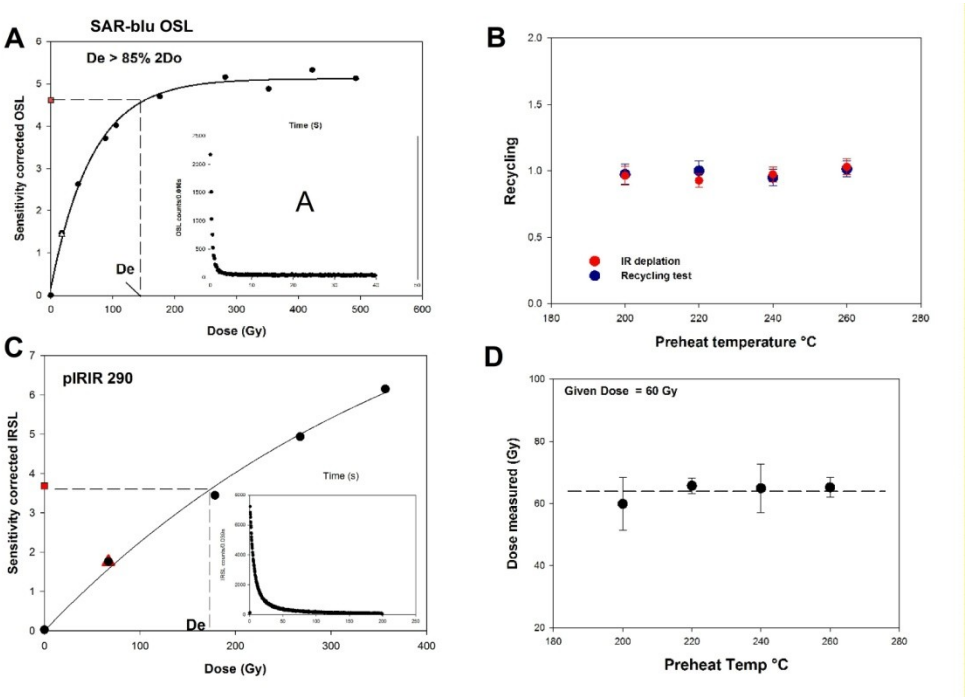

Fig. 9: OSL test performed on Sample BOSFOR and its luminescence characteristics. A) Dose response curve and natural decay curve for SAR protocol performed on quartz sample BOSFOR. Quartz show a fast dominated decay signal (inset) but a saturated signal (De > 85% of 2D0). B/D) Result of the dose recovery preheat plateau test with IR depletion. C) Dose response curve for the post-IR IRSL 290 measurements at 290° on sample Bosfor. The inset shows the pIRIR290 intensity against 200 s and the typical slow decay of k-feldspar signal

Sample	Moisture Avg (%)	Depth* (m)	Grainsize µm Avg	^{238}U (Bq/Kg)	^{226}Ra (Bq/Kg)	^{232}Th (Bq/Kg)	^{40}K (Bq/Kg)	Dr Qtz[1] Gy Ka^{-1}	Dr k-feld[2] Gy Ka^{-1}
Bosbio	7.2	3	90-120	7.6 ± 3.2	9.3 ± 3.4	7.3 ± 0.4	123 ± 4	0.595 ± 0.03	1.2 ± 0.03
Bosfor	3.4	0.5	90-250	2.7 ± 4.3	8.2 ± 0.4	9.9 ± 0.4	203 ± 6	1.18 ± 0.03	1.8 ± 0.03

[1]Dr corrected for the % of Moisture and $CaCo_3$
[2]Dr corrected for K-feldspar Internal decay
* Distance of the samples from the top of the outcrop.

Tab. 2 Summary of quartz and K-feldspar optically stimulated luminescence dosimetry data including concentrations of major radioactive elements.

Sample	Deposit	Unit	a.s.l m	De Qtz Gy	De K-feld Gy	Age Qz Ka	Age K-feld Ka	Stage
Bosbio	Algal rim	Unit 3a	3.5	Sat	150 ± 3		125 ± 8	Mis 5e
Bosfor	Foreshore	Unit 3b	3	Sat	174 ± 13	60[b]	96 ± 7	Mis 5c

[b] Minimum age (calculated average of D0)

Tab. 3: Summary of quartz and K-feldspar dose equivalent (De) measurements and luminescence ages.

Stratigraphy and chronological framework.

The quaternary deposits cropping out at S'Abba Drucche bay are interpreted as a trasgressive-regressive-tragressive sequence, bounded at the base by a ravinement surface and at the top by terrestrial deposit. Seventeen logs were correlated and the facies description suggested the presence of four facies associations (Bg, Bs, E and A) and three unconformity bounded units that, following the strathigraphic subdivision proposed by Pascucci et al. (in press), were classified in Unit 3 divided in two subunits U3a and U3b and Unit 4 (U4) (Fig.11).

The lower subunit U3a rests unconformably on the volcanic bedrock and consists of facies association Bg. It is characterized by 50 cm thick clast-supported conglomerate interpreted as transgressive gravelly lag deposits (Sensu Massari 1994) that marks the transgression surface T2. The basal conglomerate is covered and encrusted by a ~1 m thick mound shape organic carbonate deposit interpreted as intertidal rim (Fig.7,10D and 12)). Based on the characteristics of the deposits and the maximum elevation above the present sea level (+3.5 m) U3a is referred to the Marine isotope substage 5e (MIS 5e). Luminescence age dating confirms this hypothesis, referring U3a at 125±8 ka (Table 3).

The top of U3a is marked by an erosive surface probably developed during a sea level fall and, therefore, a regressive stage (R2). During a second minor sea level rise (T3) the space among the relict rim mounds was filled by clasts derived from the erosion of the rim itself and by sandy deposits. This new highstand probably reached its maximum

(still-stand) of about 2 m above the present sea level triggering the development of U3b unconformable deposited on U3a (R2/T3).

U3b is mostly characterized by the facies association Bs interpreted as a well-developed high energy wave dominated prograding reflective pocket beach system where both the submerged (shoreface) and the emerged (foreshore and backshore/ incipient dune system) parts are preserved. (Fig.10)

The shallow shoreface (2.5 m thick) is mostly characterized by two observable zone: the first dominated by trough-cross bedded sandstones, where the trough-cross bedds (concave-upward and ~30 cm thick) show a main orientation (NE-WS) almost parallel to the present coast line. Trough bases are characterized by aligned layers of granules or by a sharp cutting surface. The second zone is dominated by waves ripples marks (~10-15 cm thick) that show bi or unidirectional direction mainly parallel to the coast. Thus, the first zone is interpreted as the breaker-zone where megaripples and bars occurred whit a main direction of migration parallel to the paleo-coastline (that is NW-SE). The second is interpreted as the surfzone dominated by symmetrical waves ripples formed during the fair-weather and asymmetrical during storm events (Fig.10 and 13ea-b).

Close to the present gravelly beach the characteristic trough-cross bedding of the shoreface is interlayered with clast-supported poorly imbricated dipping seaward conglomerate lensing beds. This conglomerate deposits most likely deposited during seasonal floodings of the close stream (Fig.11a).

The shoreface deposits are overlapped by a well-developed beachface (2.5 m thick maximum) characterized by low-angle cross bedded sandstones. The cross-beds often dip toward the sea with an angle >10°. This suggests that the system experiences the character of a reflective beach. The beachface was dominated by alternation of black (heavy mineral) and white laminas, due to the swash and back swash of the waves . The Black layers became sporadic toward the top of the succession. This most likely marks the limit between the beachface (winnowing zone) and the backshore (influenced only by storms events). The backshore is maximum 2m-thick and is characterized by parallel- poorly low angle cross laminate sandstones where scattered pebbles and marine shells may be found. The succession is closed by a massive poorly

parallel laminate and strongly bioturbated sandstones. Faint of high-cross or trough cross-bedding are present. This part of the succession has been interpreted as the inland part of the backshore where incipient dunes developed and pioneer coastal plants start to grow. These deposits are referred to facies association E (Fig.10cc and 11). The sandy beach system has been OSL dated at 96±7 ka, and thus related to the MIS 5c.

Finally,U3a is overlain by U4, which is characterized by the facies association A that in this area only consists of by up to 10m thick poorly consolidated parallel laminate sandy brownish siltstone (facies Wed). Widespread cobbles and boulder may be scattered found. This deposit has been interpreted as a debris flow deposit associated with colluvia developed during the sea-ward progradation of the coast. This unit has not been OSL dated, however it is related to the end of MIS 5c and the beginning of MIS 5b (Fig.11d and 12).

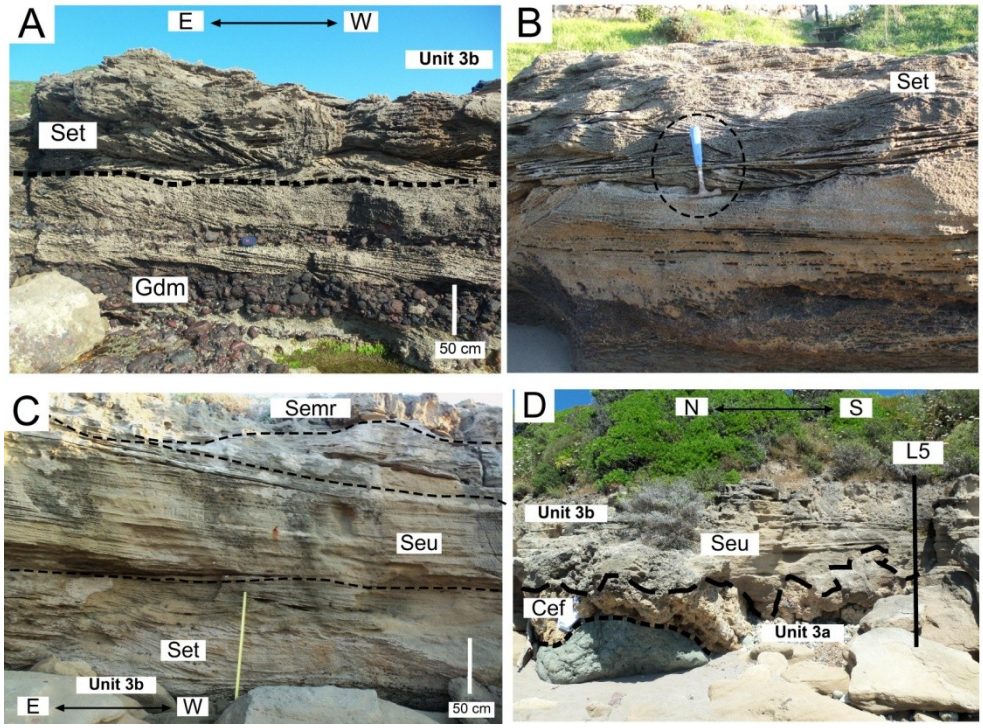

Fig. 10: Details of the main facies exposed at S'Abba Drucche bay A) Shoreface deposit (trough_cross bed and conglomerated layers, facies Set and Gdm). B) Detail of trough and ripples cross stratification (facies Set). C) Facies association Bs (sandy beach system) from the bottom: the shoreface deposit (facies Set), the foreshore (low angle cross laminated dipping sea-ward, Seu) and at the top the backshore deposit with faint of incipient dunes (massive sandstone Semr). D) Detail of stratigraphyc log 5, s detail of the unconformity between Unit3a (facies association Bg, facies Gdm and Cef) and Unit 3b (facies association Bs).

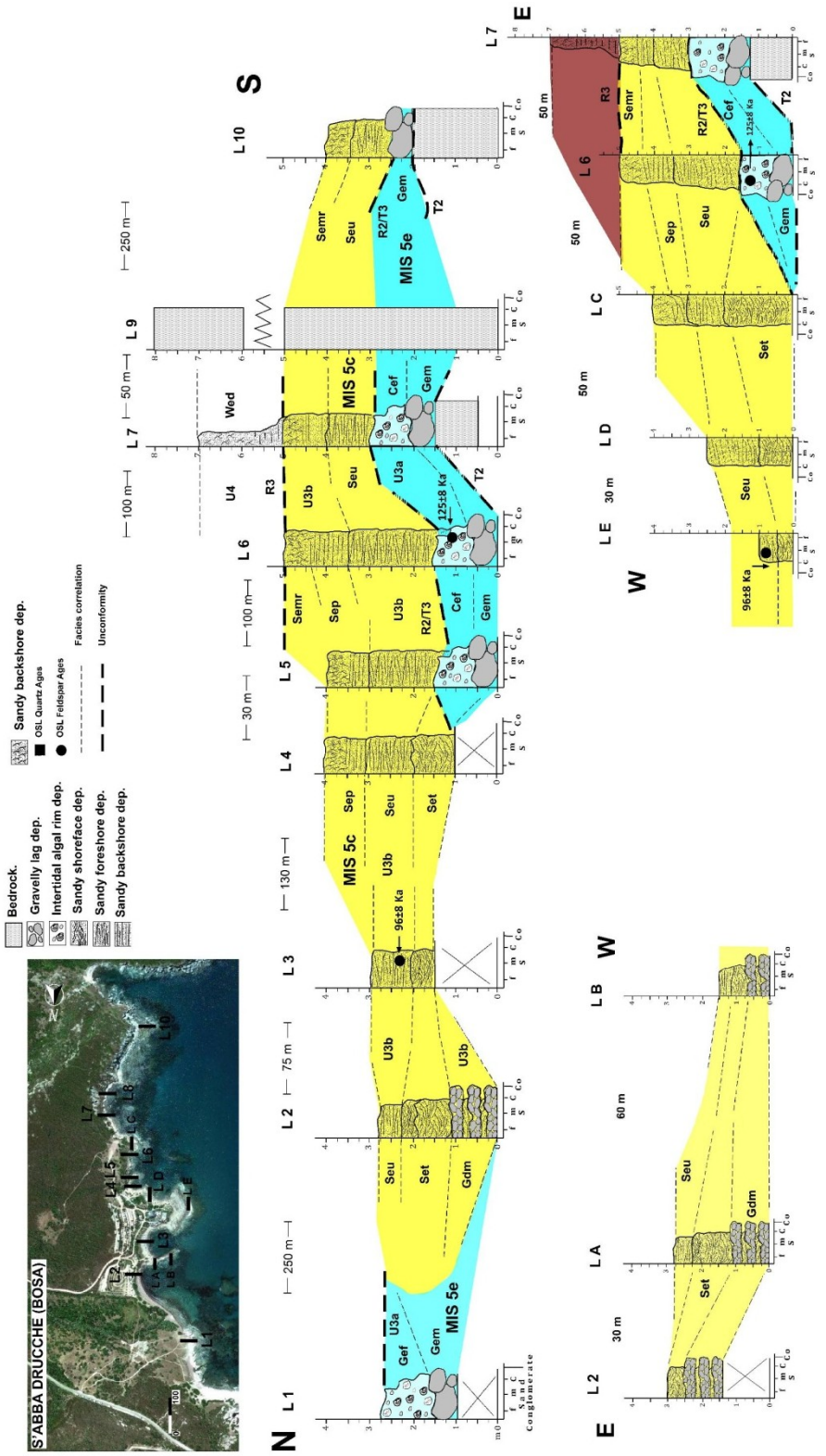

Fig. 11: Stratigraphic sections measured for S'Abba Drucche Quaternary deposits (see inset for log location). L1 = Log 1. U =unconformity bounded unit. Labels such as Seu indicate facies described in the text and in Fig.5.

Fig. 12: Field details of different stratigraphyc logs analysed along S'Abba Drucche bay, to better compression see also the text and figure 5 and 11. A) Log 1 isolated mounds of algal rim (facies Cef) well exposed on the present beach on the northern part of the bay. Inset A1) shows a colony of intertidal barnacles in life position mostly encrusted by lythophillum algae . Secondary coarse sand fill spaces. A2) Detail of encrusting crustose marine carbonate red algae, mostly *Lythophyllum byssoides*. B) View from the sea of stratigraphyc log 5, in detail the unconformity surface between Unit 3a (facies association Bg) and Unit 3b (facies association Bs). U3a characterized by volcanic megaboulders (facies Gem) encrusted by 50 cm-thick of algal rim (facies Cef). Facies association Bs rests unconformable on Bg, from the bottom: the shoreface (facies Set), the beachface (facies Seu) and the flat backshore (facies Sep and Semr). C) Detail of prograding sandy beach system (E to W view of log 6). D) Field view of stratigraphyc log 7, the gravelly lag lays on the bedrock and it is drape by the incipient algal rim covered by thick strata of facies Sep. Alluvial debris flows caps the succession (Wed).

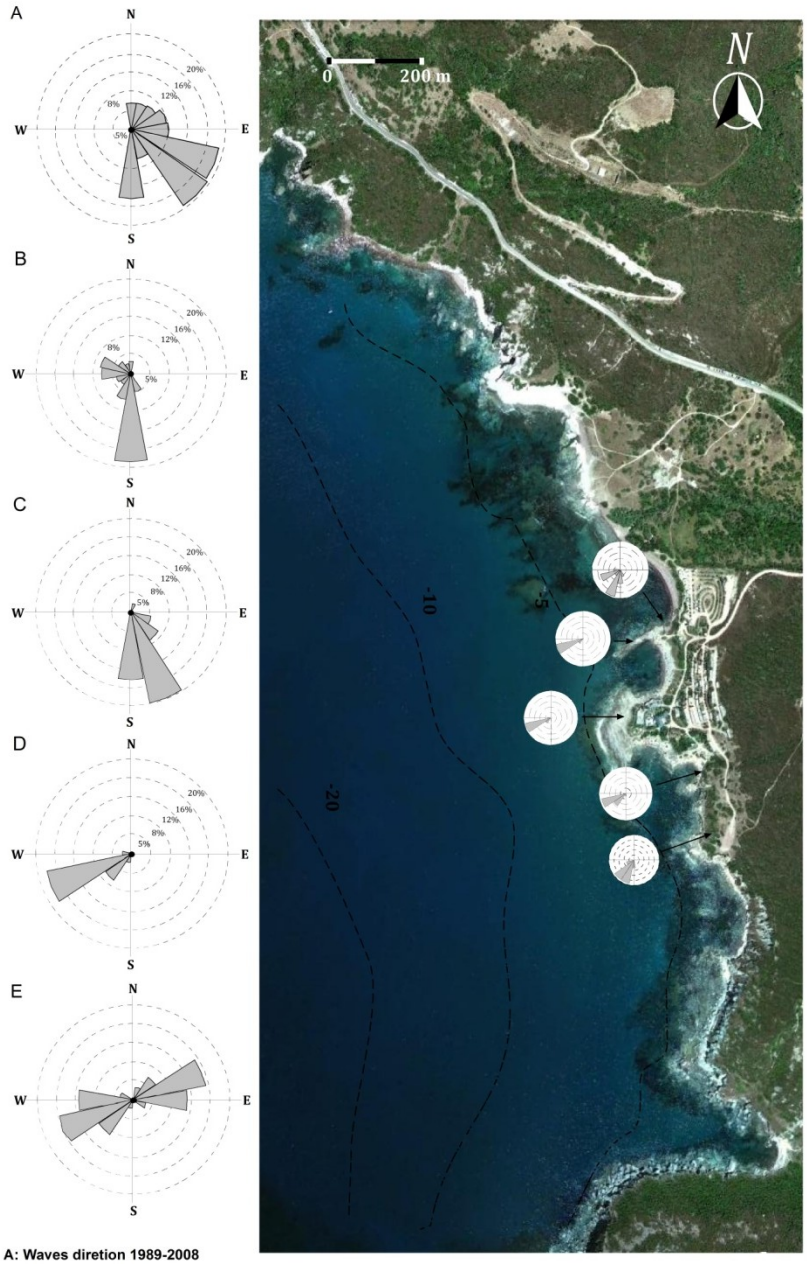

Fig. 13: Satellite view of S'Abba Drucche cove. A) Radial plot of the main waves direction of alongNW coast of Sardinia, data spanning from 1989-2008 B) Main winds direction on the NW coast (Rete Ondametrica Italiana, Ispra). C) Paleo directions of longshore current along the bay during MIS 5c D) Mean of foreshore paleo dip-direction, small plots show the foreshore paleodirection for each part of the relict beachface. E) Paleodirection of waves along the bay during MIS 5c, directions are based on the bars and ripples marks dip direction.

S'Abba Drucche bay evolution

After the penultimate interglacial (MIS 6) sea level rose reaching its maximum during the MIS 5e. S'Abba Drucche Bay was characterized by high cliffs facing the sea The rising of sea level started to erode the base of the cliffs and developed a wide wave cut platform on which rock fallen due to cliff retracting. During MIS 5e the sea reached the maximum high of about 5±1 m above the present. During this climate optimum conditions, in the most protected zones and mainly among the megaboulders, a very thick intertidal community of marine invertebrates and red algae developed (Fig.12).

During the following MIS 5d climate deteriorated and sea level started to fall (up to -15 below the present, Dorale et al 2010) shifting the all system sea-ward. The mouth of the all the river systems were forced to erode the relict marine deposits to reach a new equilibrium point and a large amount of sediments were carried seaward nourishing the new shoreline system. During the sea level dropping, the intertidal community were exposed and consequently eroded. In the following substage MIS 5c sea was marked by a new sea level rose reaching the maximum of ~2 m above the present sea level flooding again the all the bay. Part of the relict algal rim and the previous gravel deposit were reworked by waves action and most of the sand available into the system allowed the formation of a wide pocket beach system. The amount of suitable sand was due to a different climate condition occurred during MIS 5c than MIS 5e. The MIS 5c most likely was cooler and wetter than MIS 5e with more intense and abundant rainfalls. These conditions were probably responsible for a large amount of sand carried to the coast by rivers. This sand was than reworked and deposited onshore by major storm forming the beach.

The sandy beach system had its maximum evolution during all the MIS 5c high stand. A good example on how the MIS 5c beach system looked like during its maximum evolution is shown in figure 12b.

At the end of MIS 5c the level of the sea started to fall again due to the abruptly climate change turning toward glacial condition. The system shifted seaward and debris flow and colluvial deposit covered the bay. The sea level during the peak of

interglacial MIS 4/3 reached about -80 m below the present sea level. (Cutler et al 2003).

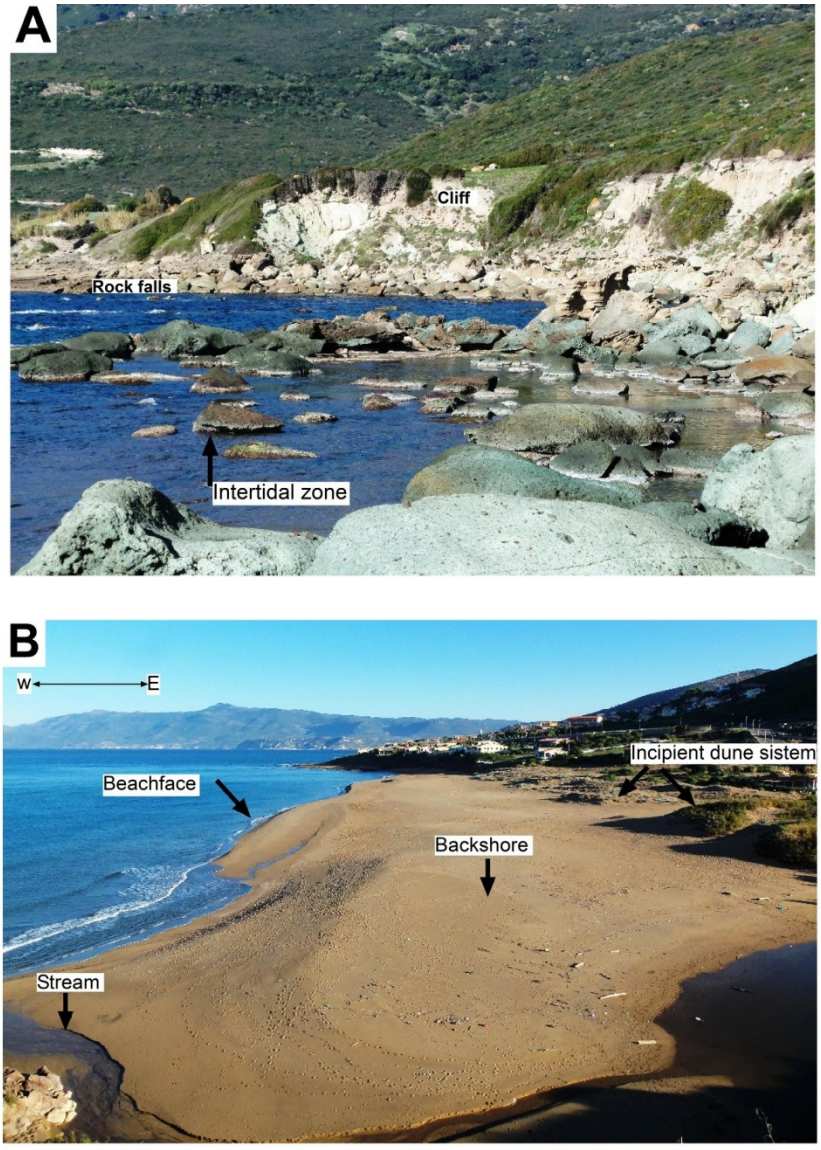

Fig. 14: A) Modern analogue of the MIS 5e paleogeography of S'Abba Drucche bay B) General view of Porto Alabe beach. Porto Alabe is a city located ~ 8 km southern from the study area. The present beachrapresents the modern analogue of S'abba Drucche sandy pocked beach formed during MIS 5c. To be noted the steepness of the beach face, and the large flat bachshore. The incipient dune system is not wide and is already strongly vegetated. On the bottom of the picture is observable the seasonal stream mostly active during winter

Alghero coast (NW Sardinia)

Alghero is one of the most important cities of northwest Sardinia. It is characterized by a wide bay where one of the few barrier lagoon beach systems of the island is still active. This is backed by one of largest plain of Sardinia, the Nurra plain. The embayment is laterally bounded by high Triassic carbonates and sandstones and/or Oligocene magmatic promontories which often face the sea as high cliff. As described for S'Abba Drucche the base of rocky cliff is often characterized by wave cut platforms. In places well developed tidal notch are visible as well. Several ephemeral streams entrance the rocky cliff often feed sandy or gravelly pocket beaches. (Fig.15).

The late Quaternary succession cropping along the Alghero coast is well exposed along the city southern side and forms a quasi-continuous 5 km long rocky cliff. This succession has been largely described in the last years by Andreucci et al (2010a, 2010b, 2011). On the contrary along the north side of the city the succession occurs in isolated outcrops and has been poorly studied.

The aim of this part of the thesis is to complete and improve our knowledge on the paleogeographic evolution of this part of the North-West Sardinia (Alghero coast) during the last 200 ka. In particular, our attention has been specifically addressed on climate and sea level changes occurred within the Last Interglacial (MIS 5). The coast has been subdivided in five sub areas, sedimentlogical and chronologic analyses have been performed (Fig. 15)

Fig. 15: Satellite view of Alghero coast, white arrows indicated the five sub-area studied, Burantino bay (Bur), Punta Padre bellu Bay (PPB), El Trò-Carlos V bay (Trò-CV) the Calich lagoon and the Le Bombarde bay (Bom).

1) Burantino and Padre Bellu coves

The Burantino and Padre Bellu coves are located on the southern coast of Alghero along a high rocky volcanic cliff. These are two small coves dominated by small sandy and gravel pocket beaches.

The sedimentology (facies analysis) and stratigraphy of this part of the coast have been well defined by Andreucci et al. (2010,2012). Two shallow marine and three coastal-continental facies associations and four unconformity bounded units were identify. Moreover several OSL ages are available for this part of the coast and allowed referring the quaternary deposits from the Marine Isotopic Stage 6 (MIS 6) 150 Ka to MIS 3, 40 ka

MIS 6 crops out only at the Burantino cove and is characterized by 2 m thick, well sorted, high angle laminated parallel or trough cross bedded coarse grained sandstones interpreted as coastal dunes deposit and OSL dated at 150±10 ka (MIS6). Thus, these deposits are referred as U2 (Pascucci et al in press) (Fig.16).

U2 is separated by the overlain U3a by a sharp erosive surface (T2). U3a is characterized by 50 cm thick clast-supported conglomerate. Clasts range from pebbles to boulder which reflect the volcanic composition of the inland promontories and cliffs mostly made of Oligocene ignimbrite. A coarse sandy matrix abbundant in fragments of

marine shells occur and filled the space between clast. This deposit is cover and encrusted by ~ 1m thick organic carbonates build up mostly made by red algae, serpulides and barnacles found in life position. A very coarse clastic matrix occurs; this is encrusted and amalgamate in the carbonate body as well. This facies association has been referred as Bg and interpreted as a gravelly lag deposit that lays unconformable on a wave cut platform on which an intertidal community (algal rim) developed (Fig.14b).

This facies association lays at ~3.5m above the present sea level. Given the stratigraphyc and sedimentologic characteristics this association was referred to the MIS 5e and is correlated with the same facies association described for S'Abba Drucche bay which has been OSL dated at the MIS 5e.

As well indentified at S'Abba Drucche the top of the U3a is strongly eroded at the top by an evident erosive surface (R2), most likely due to the drop of the sea and the emersion of the deposits. In places, the lower part of U3a is strongly reworked and mixed with a pebble-cobble conglomerate rich in sandy matrix and fragment of marine shells. Diffuse reworked clasts of the algal rim are observable. This deposit has been interpreted as a trasgressive gravelly lag (facies association Bg) developed during a second seal level transgression (T3).

Facies association Bg is overlain by 3 m thick low angle cross stratified gently dipping sea-ward coarse grained sandstone. Widespread or aligned in layers imbricate pebbles and granules occur. Sandstone land-ward and up-ward is strongly root-bioturbated and massive. This association has been referred as facies association Bs and interpreted as a well developed pocket beach characterized by a wide beachface and backshore (Fig.16c). The system developed during a secondary sea level high-stand during which sea reached about ~±1.5 m apsl. This succession is related to U3a and is OSL dated at ~98±8 ka, thus to MIS 5c (Fig.16c).

During MIS 5c highstand this part of the coast was dominated by prograding sandy pocket beaches characterized by wide backshore and incipient dune system. Most of this relict deposits crop out along the coast from 0 to 4 m apsl. In places the backshore deposits rest unconformable on the facies U3a.

The Punta Padre Bellu cove is not far from Burantino and present almost the same stratigraphyc framework, although little differences occur (Fig.14d-e).

U3b rests directly unconformable on the volcanic bedrock and it is capped by U3a that is characterized by thick carbonate algal rim deposits. U3a consists of ~70 cm of poorly laminated medium sorted coarse sandstones. Widespread or alighted pebbles and granules are observable whereas roots bioturbation may be found at the top. This unit has been interpreted to represent part of a sandy backshore.

U3a along the all coast is bounded at the top by layers or lenses (0.5 to 2 m thick) of matrix or clast-supported cobbles conglomerate or by reddish siltstone. Conglomerate deposits are characterized by angular pebbles and cobbles occasionally supported by a sandy-silty reddish matrix. Reddish siltstone deposits are rich of coarse-grained sandy component with scattered angular pebbles. These deposits have been associated to the facies association A and interpreted as debris flow and colluviums characterized by different rates of incipient pedogenesis (Fig14d). These deposits are referred to unit U4 and range in age from MIS 5d to MIS3. During the maximum glacial all the coasst was dominated by huge costal dune system, now preserved as high rocky cliff (Fig.16).

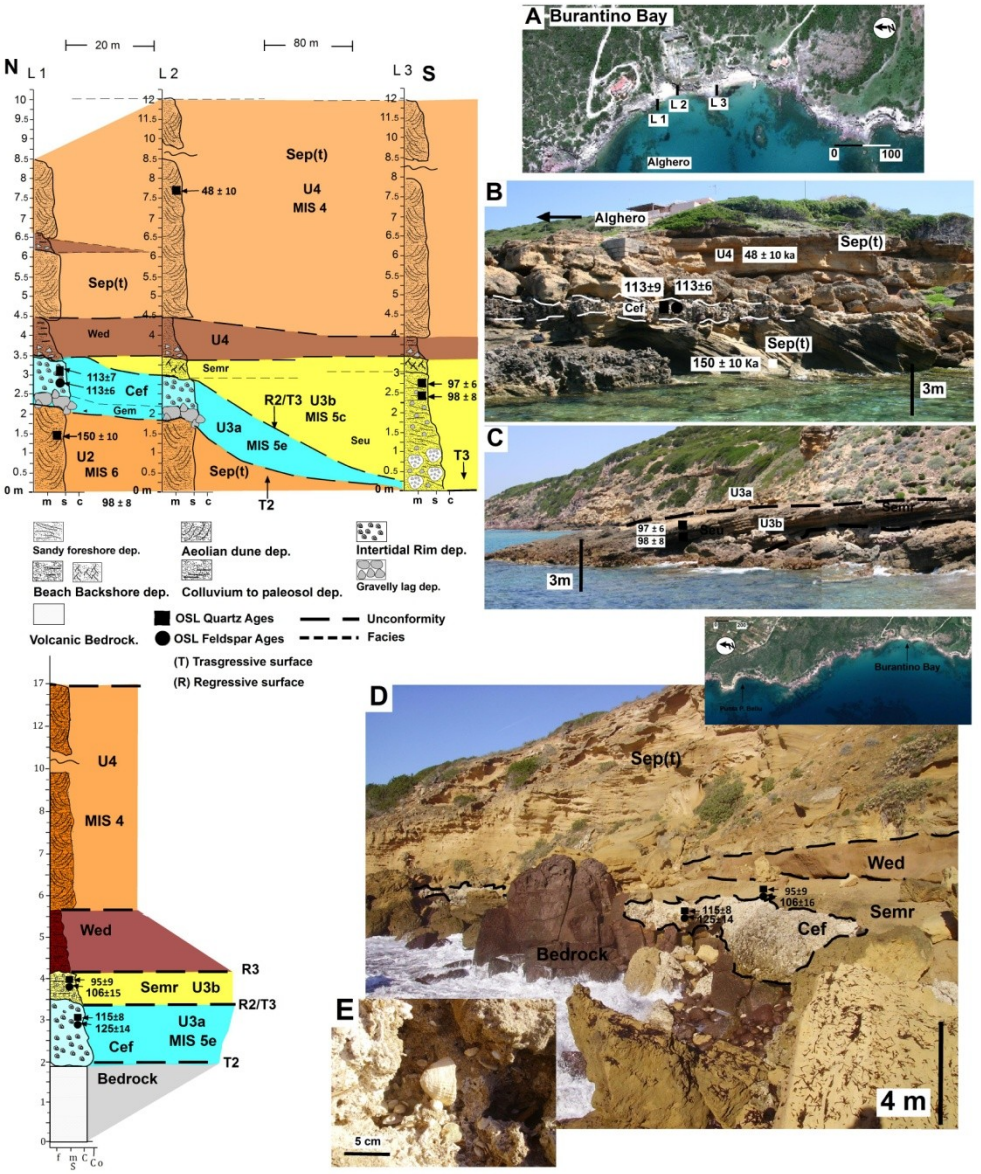

Fig. 16: Summary of the southern Alghero coast stratigraphy. On the top part Burantino cove and on the bottom Punta Padre Bellu cove. A) Logs position of Burantino bay B) View from the sea of the algal rim , USBU units and related ages. C) Lateral view of the sandy beach system cropping out at the Burantino bay. D) View of Punta Padre Bellu and related stratigraphy and OSL ages E) Detail of the algal rim cropping out at Punta Padre Bellu (fossil is a shell of *Patella Ferruginea*)

ALGHERO AREA

This part of the thesis is focused on:

I) Testing the luminescence dating method to date a heterogeneous carbonate deposits;

II)Testing the reproducibility of the luminescence (PostIR IRSL 290) method on different outcrops of carbonate deposits;

III) Complete the chronological framework of the Alghero coast.

IV) Confirm the strathigraphic correlation and improve the knowledge of MIS 5e

2) Carlos V/El Tro' and Bombarde bay

Unlike for the southern coast of Alghero, the quaternary outcrops are exposed along the city coast are not well preserved. Since the Roman time the Alghero area was highly anthropized and during Spanish domination (XIII-XVII Centuries) many quarries were carved into the Quaternary deposits, mainly sandstone, in order to collect dimension stones to build the city of Alghero. However, some spots of Quaternary deposits are still well preserved and exposed. Along the city coast we have focused our attention on a small (1 km wide) area named by Spanish El Tro'. This is a small embayment delimited by Triassic mudstone cliffs. The central part of the bay is characterized by a small cove where a small gravel beach occur. Most of the area is dominated by a wide wave cut platform on which part of the quaternary deposits lay unconformable (Fig.22A).

The Bombarde bay is located few kilometers north from the city of Alghero. It is a large bay Est-West orientated and dominated by a sandy pocket beach. The Quaternary deposits are not well preserved because continuously eroded by intense waves action.

Luminescence analysis

Along the Alghero city coast 16 samples were collected to complete the stratigraphy of this area. Samples were treated in the laboratory using the method explained in the Methods Chapter. For all the samples analyzed the 90-250 µm size fraction was used.

On the southern coast of city three samples were collected: one from the algal rim cropping out at Burantino bay (Sample BUR), and two at Punta Padre Bellu cove from both the algal rim and the overlying sandstone (samples PPB1,PPB3) (Table4-5) (Fig.15).

In the laboratory sample BUR was split in two sub-samples BUR1 and BUR2, individually treated and analyzed. This replica has allowed testing the reproducibility of OSL dating protocols on sandy-rich organic carbonate deposits. The luminescence characteristics of quartz and k-feldspar grains were firstly tested. The purity of the quartz was checked and all samples resulted contaminated. Feldspar contamination were cleaned out with a second HF re-etch and then a second purity check was applied. Samples PPB1 and PPB3 resulted clean whereas sample BUR1 and BUR2 still slightly contaminated. Hence, samples BUR1 and BUR2 were analyzed with a Post-IR blue stimulation protocol. The Post-IR SAR (Double SAR) procedure consists of a normal SAR protocol with an extra step, an IR stimulation at 50°C for 100 s, before each blue stimulations for the luminescence analysis. The temperature of this step was left low (50°C) to avoid sensitivity problem due to the temperature. This accessory step might allow cleaning out quartz signal from the k-feldspar contamination. Commonly the final De value in presence of feldspar contamination might be considerably underestimated (Banerjee et al., 2000; Thiel et al., 2010).

The preheat plateau dose-recovery test was performed on twelve aliquots using the post-IR SAR on BUR1 and BUR2. The test showed that samples were not affected by sensitivity change during the analysis (Fig.17G) resulting fast dominated natural signals suggested also the reliability of Double SAR protocol to erase feldspar contamination. Hence, Double-SAR was applied for the De estimation on samples still slightly contaminated. Otherwise, the standard (SAR) protocol was used on pure ones (Murray and Wintle, 2000) (Fig2). By means of preheat plateau dose recovery the temperature

were set at 240°C and 220°C respectively for the preheat and the cutheat (Fig17E-G). Samples analysed (BUR and PPB) showed a good luminescence characteristics, fast dominated (not saturated) signals and good recyclings (mean 1.00±0.05) (Fig 22). The early background subtraction was applied to get the most reliable De (Cunningham et al 2010). Each aliquot with a bad recycling and a saturated signal was rejected. Along the El Tro-CarloV area, 11 samples (label CV and TRO) were collected and listed in Table 4.

On twelve aliquots of sample TRO6 and TRO5 the preheat plateau dose recovery test was tested. Samples did not show sensitivity change and a good dose recovery resulted with a ratio of 0.99 ±0.03. Quartz samples were considered suitable for applying the SAR and Post-IR SAR protocol to De estimation. Preheat and cutheat temperature were set at 240°C and 220°C respectively. The average of the recycling ratio for samples is 1.00±0.04, most of all characterized by fast dominated signal resulted saturated for six. (Table4).

On most of all samples, (strathigraphic key samples and saturated ones) the pIRIR290 protocol was performed on k-feldspar grains. This protocol as well as SAR protocol was applied for the first time on sandy-rich carbonate deposits sampled (facies Cef) in order to test the method on deposits unusual for luminescence dating (Table).

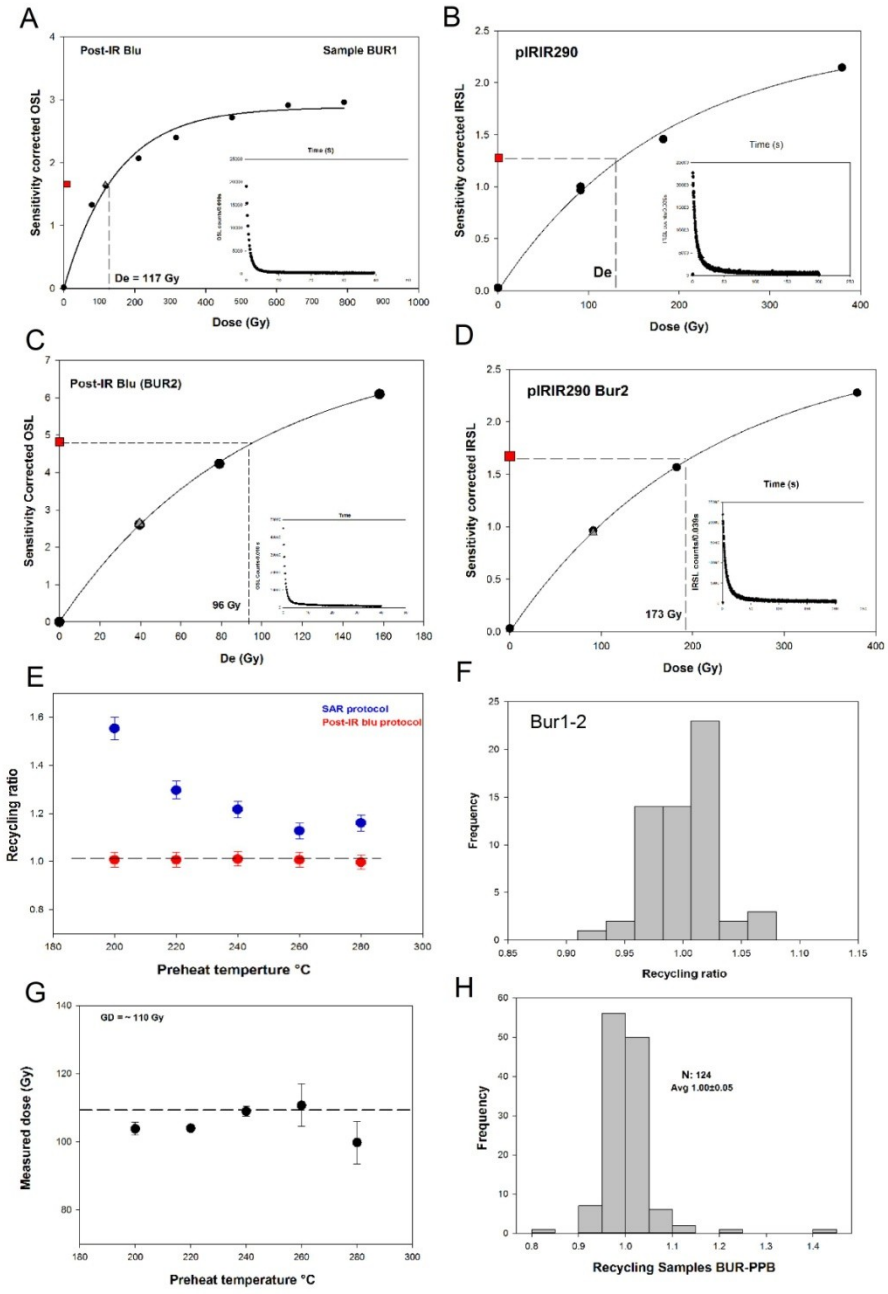

Fig. 17: OSL tests performed on Sample BUR1 and BUR2 and their quartz and feldspar luminescence characteristics. A,C) Dose response curve and natural decay curve(inset) for SAR protocol performed on BUR1 and BUR2. Quartz grains show fast dominated decay signal not saturated. B/D) Results of the dose recovery preheat plateau test performed with both protocol SAR (blu dot) and Post-IR SAR (red dot), impure quartzs analysed with the SAR protocol show scattered value of dose given/measured ratio. G) doses response to the dose recovery preheat plateau testtest (given dose of 100 Gy).. F) Recycling ratio frequency distribution analysed for for both samples BUR1 and BUR 2. H) Distribution of recycling ratio of BUR and PPB samples.The resulted mean was 1±0.05 thus the SAR method were considered reliable.

Quartz Paleodose analysis: Partial bleaching, post depositional mixing and Dose rate correction

The paleodose (De) is the relative measure of the total radiation that quartz and feldspar grains received since their last exposure to daylight. The age of the deposit is determined by dividing the De by the radiation dose rate from the environment. A complete reset of the luminescence signal during the grain transportations (bleaching) before the last depositional event is a fundamental requirement of the OSL method. A sample is considered well bleached when the distribution of a De value population is close to a normal distribution of a tight Gaussian curve. However, in natural environment sedimentary deposits are vulnerable to different natural or artificial disturbance and frequently samples show a broader De distribution than expected.(e.g. Roberts et al., 1999; Jacobs et al., 2008).

Excludeding the measurement and instrument uncertainties the scattering of De values is common attributed to different environmental factors, such as the heterogeneous or/and heterogeneity in the radiation field, the possible partial bleaching or post-depositional reworking and mixing.

The partial bleaching is the most common cause of uncertainty; it consists on a not complete reset of the luminescence signal before the burial event. This phenomenon might be ascribed to a short, rapid or mass-flow transportation before the burial event that prevent the zeroing of the signal. Thus, the laboratory measured the resulting De comprises both the signal build-up after the latest daylight exposure and a variable amount of residual signals.. This often implies an overestimation of the final Age.

More difficult to evaluate is, instead, the post depositional mixing of well bleached grains with different value of De (greater or lower) This mixing can causes both an age overestimation or underestimation (Thomsen et al., 2005, Bateman et al., 2007, Jacbos 2008,)

Although Sardinian quartz samples showed good luminescence characteristics, such as fast dominates signal, recycling within the unit and a good recover of the given dose, several differences of paleodose distributions were found. Generally, using the large aliquots (~7 mm diameter) the wide scattered of De values have been attributed to the

grain-size and to the large number of grains analyzed (~10.000 grains per aliquots). In this case is common to use the unweighted mean of De value for dating calculation. (Duller et al 2008).

Sandy rich organic carbonate deposits (algal rim) cropping out along the north-west coast have been tentatively dated with the OSL. Given that is stratigraphically and OSL chronologically well constrained within the MIS 5e (130- 110 Ka) the carbonate deposits cropping out at the Burantino bay is the most indicate deposit to test the reliability of the method on this type of sedimentary deposits (Fig.16b). Sample Bur1 and Bur2 showed respectively De (mean) of 96±5 Gy and 77±4 Gy with a difference of ~20 Gy (Fig. 17, Table 5). For both samples, the resulting dose rates were 0.5±0.03 Gy/ka (Bur1) and 0.5±0.07 Gy/ka (Bur2) (Table 4). Despite the algal rim deposits show a macroscopic high heterogeneous composition the resulting dose rate seem to be overall uniform. However, the calculated ages for the deposit using uncorrected Dr and De were 177±16 ka and 138±12 ka. Thus, the OSL method seems to overestimated the expected MIS 5e (110-130 Ka) age. The heterogeneity and differences in gamma ionizing flux may have influenced the resulting age dating (Aiteken, 1985). In fact, at The Burantino bay the carbonate deposit lays on a 50 cm-thick of volcanic boulders strata (Fig 16).

The radiation flux for t boulder deposit was calculated using the ICP-MS data and the dose rate is at about (5.5±0.01 Gy/ka),, resulting significantly higher than the carbonate one (ca 0.5 Gy/ka). Unfortunately, the algal rim has a maximum thickness of 1 m and the BUR samples was collected only at 50 cm far from lower boulder deposits. Giving that gamma rays can penetrate in to the rocks for a meter is reasonable to infer that basal conglomerate due to its high DR may have somehow influenced the “total” gamma radiation flux experienced by BUR samples. Thus, the total dose rate was corrected for the gamma contribution of the volcanic-rich conglomerate proportionally to the distance between the sample position and the top of lower deposit (~ 50 cm) (Aitken, 1985; 1995, Brennan 1997)

The Dose rates corrected resulted ~0.8±0.04 Gyka-1 and new corrected ages were 113±9 ka for BUR1 and 90±7 ka for BUR2.

After the Dr Correction BUR1 age resulted in agreement with the k-feldspar age (~113±6 ka) whereas the age of Bur2 is underestimated. It is worth to notice that the De unweighted means of Bur1 (96±5 Gy) and Bur2 (77±4 Gy) show a wide and unexpected difference of ~20 Gy. Thus in order to understand the reason of this difference a statistical analysis of the De distribution has been performed (Galbraith et al 1999, Bateman et al 2007, Andreucci et al 2012). Galbraith (1999) suggested that a well bleached undisturbed sediment should have a leptokurtic and unimodal distribution (Gaussian-like) with an overdispersion lower than 20%. The all De values obtained for BUR1 and BUR2 were plotted on a radial plot based Galbraith in 1988 (Vermeesch, P., 2009) and the probability density distribution of all De were calculated. As shown in figure 18, BUR1 shows an evident bimodal distribution with a tail toward greater De values and an overdispersion (OD) of 22%; whereas BUR2 has a slightly trimodal distribution with an OD of 36%.

Commonly the reason of a multiple peaks distribution is ascribed to the the partial bleaching of grains producing a tail toward the high De value. Thus, only the aliquots with a smaller De values are considered to be well bleached and used to calculate the final paleodose useful for dating (Minimum DE method Fuchs and Lang 2001,Galbraith 2010)

However, several cases of post depositional mixing are reported (Bateman et al 2003, 2007, Arnold 2009, Jacobs 2011, Bueno et al 2012). In such cases the scattered distribution (cloud-like) or the multiple peaks are attributed to the intrusion and mixing of grains from the overlying deposit and thus, with smaller De values and younger age respect to the analyzed deposit. Using the Minimum De method, described above, the laboratory calculated age will underestimate the “true” burial one. Therefore, for samples affected by the post depositional mixing, only the De with high values has to be used to calculate the “true paleodoses” and the final ages.

Overall, sample whether affected by partial bleaching will have a younger age than the "true" whereas older if affected by depositional mixing.

Thus, in presence of multi-peak distributions is mandatory to recognize whether a sample is affected by partial bleaching or post depositional mixing. Unfortunately so far, few are the accepted produce to discriminate between the two phenomena

Murray et al 2012 suggested two ways to confirm the adequate resetting of grains (bleaching) prior the burial event:

1) test the modern analogues bleaching

2) use and compare different bleaching rates of various luminescence signals in an attempt to confirm whether the better bleached signal was completely reset at time deposition. (Wallinga et al 2002).It is well-known that the IR-stimulated signals from feldspar bleach more slowly than the blue-stimulated OSL from quartz (Godfrey-Smith et al., 1988; Thomsen et al., 2008; Buylaert et al., 2011). The pIRIR 290 signal is known to be "difficult bleachable" in nature and when samples are well bleached the resulting De is common 20% higher than quartz. Murray et al (2012) suggested that in absence of external control such as independent ages, if quartz and feldspar luminescence ages agree with each other, it is highly unlikely that the quartz signal was incompletely bleached at burial, and in some cases the pIRIR 290 De or ages may be help in understanding the true quartz De or age in presence of partial bleaching.

In principal our samples, can suffer both of partial bleaching or post depositional mixing. However, given the depositional characteristics of the deposits which developed in the intertidal zone where the sediment is persistently mixed by the wave action and well exposed to the sunlight (Fig.7a-b), we may reasonably exclude that the source of scattered De for BURr samples is the partial bleaching.

To confirm this hypothesis, we have analyzed the k-feldspar grains for both BUR1 and BUR2 with the pIRIR 290 method (see for detail the next chapter) and the resultant ages are ~113±6 ka. It is worth to notice that this age agrees with the stratigraphic order if compared with the published ones (~150 ka for lower strata and ~100 ka for the upper deposits) and with the predicted oneThus,, we infer that the pIRIR signal was well bleached at the moment of grains deposition and it is unlikely that feldspar bleached and quartz grains did not under the same sun-light exposition. Therefore we can conclude that the source of the De scattered values is the post depositional mixing.

Sample BUR1 shows the presence of a tail in the distribution with two peaks at 94±2 Gy and 71±1 Gy with two different result ages of 113±7 ka and ~80 ka respectively (Fig.18a). .

BUR22, instead shows three peaks with De values of 96±2 Gy, 71±1 Gy and 51±1 Gy, with resultant ages of 112±7 ka, 83±5 ka and ~60 ka respectively. Based on the above data the "true" ages for both samples are the older ones (113±7 ka and 112±7 ka) that are in good agreement with the k-feldspar results (~113±6 ka) and concordant with the the stratigraphic constrains. On the other hand, the younger ages (~80 ka) cleary underestimate the presumable age of deposition, but look really similar to the age of the dune capping the studied succession (Andreucci et al 2010a) (Fig.16). It is worth nothing that the algal rim deposits show evidence of several micro-and macro cavities such as karsts, related to thecalcium carbonate dissolution during a subaerial exposure.Therefore, it is possible to reconstruct a possible geological evolution of the study area based on a statistical approach on the De distribution. In particular the algal rim developped during the MIS 5e, subsequently during the MIS 5d falling stage (110 ka; see stratigraphy analysis) this deposit was exposed and underwent to a phase of weathering which produce the karsts. Moreover, during the MIS 4 (80 ka) and MIS 3 (50 ka) transgressive coastal dunes developed capping the studied succession (Andreucci et al 2010a/b) and it is possible that wind-blow coarse sands filled the algal rim cavities. Finally, a phase calcium carbonate precipation allow the sand grains to be cemented within the agal rim.

The analytic approach described above was applied to the other two collected algal rim deposits cropping at Punta Padre Bellu cove (sample PPB1) and El Trò bay (sample CV2) (Fig 16d-e and 25). This two samples show a Dr very similar to what measured for BUR, as well as the stratigraphic relationship, thus the correction of the Dr total gamma dose was applied too. (Tab.4)

Sample PPB1 shows a very platikurtic distribution, the unweighted resulted mean was 107±8 Gy whereas using the central age model for all the aliquots (n:34) analysed it was 99±6 Gy with an overdispersion of 39% (Fig.19a). The radial plot shows the presence of several, probably outliners, which displaying a very higher or very lower De. These values were not considered into the final distribution (rejected) which

showed a greatly improve on the OD (~18%) without any considerable variation on the final De mean (100±3 Gy). The resulted ages were 123±12 (all aliquots) and 115±8 ka (after rejecting), although both ages are concord with the proposes stratigraphyc interpretation(MIS 5e) and with the k-feldspar age (125±14 Ka), it is worth noting that using this rejection criteria an improvement of the standard error occurs from the 10% to the 6% on the final age. In addition, this final age fit perfectly with the Burantino ones.

On the contrary, CV2 shows a very good unimodal leptokurtic distribution. The age using the uncorrected Dr was 130±12 ka whereas 114±9 ka using the corrected one. Despite the resulted ages are in good agreement each-other and with the other deposit dated, the second one 114±9 ka is much more concordant with the k-feldspar age of 113±9 Ka (Table 5).

Unlike BUR deposit this last two did not show a post depositional mixing, most likely because after their exposure during the MIS 5d they were rapidly covered by new deposits (MIS 5c backshore deposits see stratigraphy) which protect them from the weathering action preventing the karst formation. (Fig 20e and 16d)

Sample TRO2 and CV1 were collected respectively from a sandstone (foreshore of EL TRO) and conglomerate (Gravel beach) (Fig.19, 23c, 21a). Sample Tro2 shows a very platykurtic slightly trimodal distribution with and OD of 27%. (Fig19d) The radial plot did not suggest any prevalent component. In this case, it was very problematic to apply the statistical model and, thus the resulted age of 97±8 ka was calculated on the base of the unweighted mean. However, the final age is in within the uncertainty of the age derived using k-feldspar grains (105±7 Ka).

Sample CV1 shows a platykurtic, bimodal distribution with an OD of ~26 %. Two peaks were identified pointing to a De mean value of 104±4 Gy and 67±3 Gy and ages of 125±9 ka and ~80 Ka respectively (Fig 19c). Unfortunately, for this deposit no feldspar ages have been calculated and only the stratigraphic control have been used to interpret the OSL ages.

In order to check the ability of coarse-grained deposit (conglomerate rich) to bleach the sandy fraction (such as CV1) a sample was collected from the modern analogue (Fig.7d). Quartz was analyzed with Double SAR protocol. Quartz De resulted 0.3±0.08

Gy. The distribution of De resulted trimodal with a large scattered of De, most aliquots show a negative value or no quartz signal (60% of all aliquot). The 40% of aliquots gave a good recycling in average 1.02±0.04. Thus the modern analogue of CV1 is overall well bleached, although scattered De were found.

Result and interpretation described above are preliminary and more tests should be done to investigate better the source of the De scattered of quartz grains for the Alghero area. However, we suggest that the well sedimentological interpretation of the facies and sedimentary environment and a good knowledge of the stratigraphyc relationship strongly help in refining the final age.

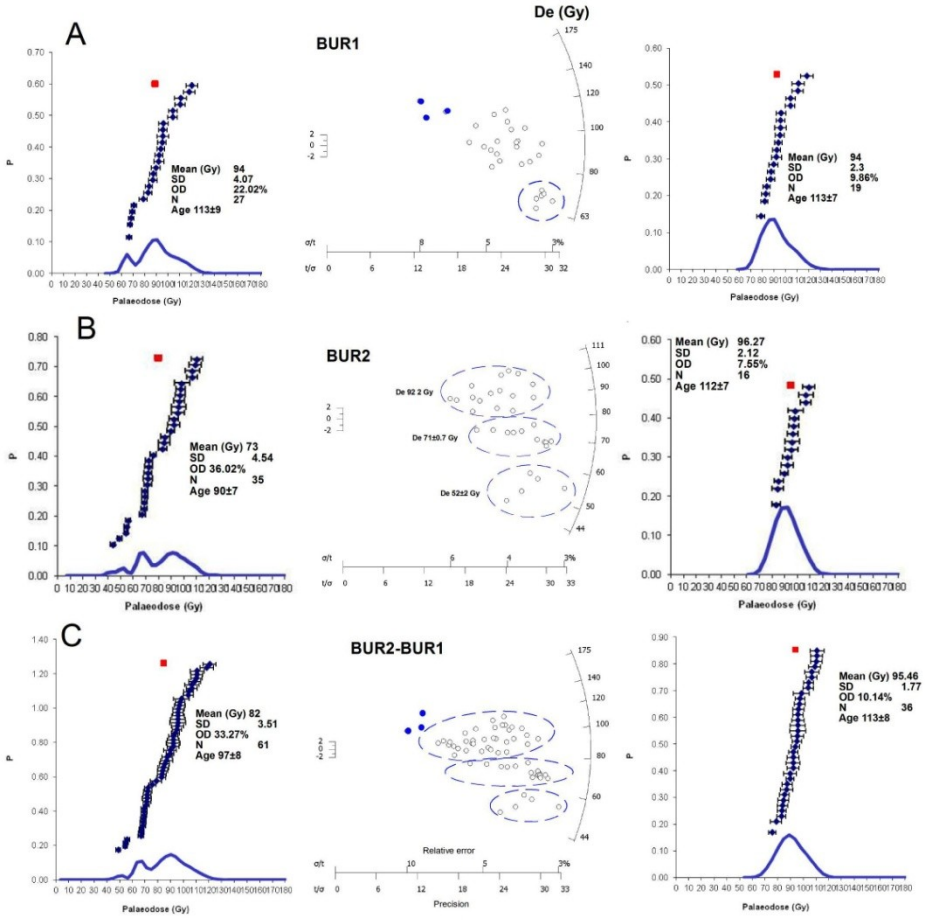

Fig. 18: Single aliquot De distribution and scatter plot of BUR samples. A) BUR1 B)BUR2 C) BUR1 and BUR2 analysed as the same samples. Graphs show: the Gaussian curve of relative probability of De values of individual aliquots, inset the unweighted mean of the distribution, the over dispersion of values in percentage (OD %), number of values used and the final Age. A) From the left the probability distribution of De of BUR1 using any rejection criteria, at the centre scatter plot of the De distribution, blu dots highlight outliners and blu circles the probably outsider family of De. On the right the probability distribution of the De after applied the rejection criterias B) Sample BUR2 shows a trimodal distribution which is highlighted by the scatter plot, the two minor families of De value were rejected, on the left the probability distribution after the rejection C) Sample BUR1 and BUR2 analyzed as to be the same sample.

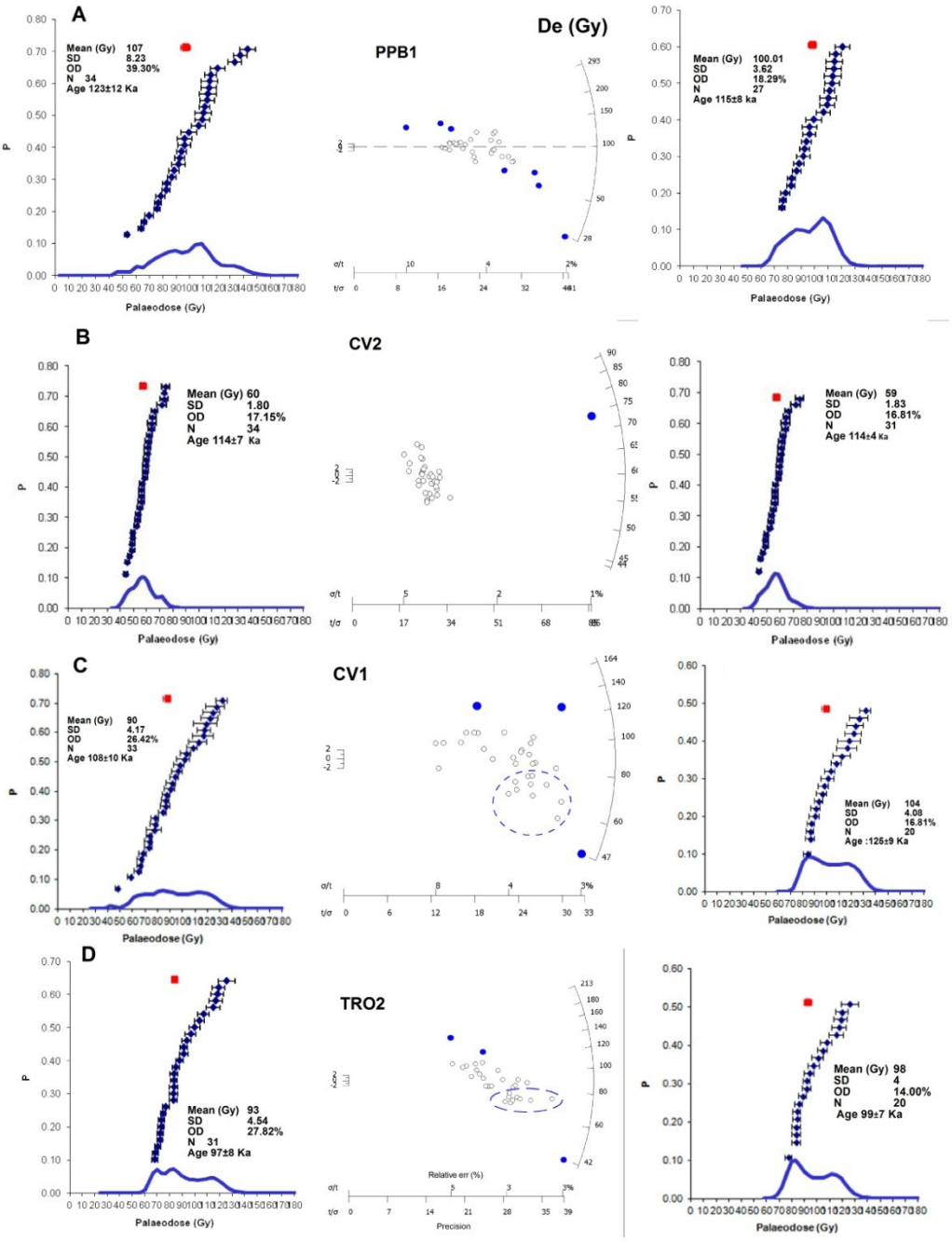

Fig. 19: Single aliquot De distribution observed for 4 samples (PPB1,CV2,CV1,TRO2). The Gaussian curve shows the relative probability distribution of De values for aliquots analysed. Inset shows the dispersion values (OD %), the mean, number of value used and the final age. A) Aliquots distribution of sample PPB1 from the left the probability distribution of De of PPB1 using any rejection criteria, on the centre the scatter plot of the De distribution, blu dots highlight outliners and blu circle the probably outsider families of De. B) Statistic analysis of CV2, sample shows a normal very tight distribution and using the statistic method any changes in the mean of De is observed. C) Statistic analysis of sample CV1, sample shows a very platikurtic dispersion of De, the scatter plot (in the centre) shows the presence of an outsider family of De. On the right the final distribution after the separation of the two families. D) Statistic analysis of sample TRO2.

	Facies	Moisture Avg (%)	Depth* (m)	Grainsize µm Avg	^{238}U (Bq/Kg)	^{226}Ra (Bq/Kg)	^{232}Th (Bq/Kg)	^{40}K (Bq/Kg)	Dr Qtz[1] Gy Ka^{-1}	Dr Qtz[2] Gy Ka^{-1}	Dr Qtz[3] Gy Ka^{-1}	Dr k-feld[4] Gy Ka^{-1}	Age Qz[1] Ka
BUR1	**Cef**	3.1	4.5	90-250	7.6 ± 3.27	8.6 ± 0.3	4 ± 0.2	49 ± 3.5	0.50 ± 0.03	0.84 ± 0.04	0.7 ± 0.04	1.19 ± 0.04	177 ± 16
BUR2	**Cef**	2.9	4.5	90-250	14 ± 3.57	8.33 ± 0.3	3.66 ± 0.3	49.6 ± 3.5	0.56 ± 0.07	0.86 ± 0.05	0.78 ± 0.05	1.21 ± 0.04	138 ± 12
PPB1	**Cef**	2.3	13.5	90-250	3.4 ± 4.15	7.8 ± 0.3	2.7 ± 0.3	51.6 ± 3.4	0.42 ± 0.08	0.87 ± 0.04	0.72 ± 0.04	1.08 ± 0.04	254 ± 32
PPB3	**Semr**	6.6	13	90-250	11 ± 4.55	11.8 ± 0.3	4.7 ± 0.4	82.5 ± 4.2	0.64 ± 0.06	0.68 ± 0.06	0.83 ± 0.04	1.27 ± 0.04	100 ± 9
AHO1	**Semr**	2.1	18	90-250	7.7 ± 3.8	8.3 ± 0.3	8 ± 4.0	82 ± 4	0.74 ± 0.05				95 ± 7
AHO4	**Sep(t)**	5.2	6.3	90-250	22 ± 3.1	13 ± 0.3	17.7 ± 3.0	97 ± 4	0.80 ± 0.04		0.96 ± 0.03		150 ± 10
AHO6	**Seur**	4.8	10.3	90-250	20 ± 3.6	13.1 ± 0.3	15.4 ± 5.0	201 ± 6	1.23 ± 0.03				97 ± 6
AHO7	**Seur**	3.4	9.8	90-250	17 ± 4.5	12.4 ± 1.6	14.4 ± 4.0	203 ± 7.5	1.14 ± 0.04				98 ± 8
CV1	**Gdmf**	6.7	7	90-250	15 ± 3.88	12.5 ± 0.3	3.5 ± 0.3	45.9 ± 3	0.87 ± 0.04	0.83 ± 0.04	1.22 ± 0.03		104 ± 8
CV2	**Cef**	5.1	2	90-250	7.1 ± 4.26	7.35 ± 0.3	2.22 ± 0.33	74.2 ± 5.6	0.46 ± 0.08	0.53 ± 0.07	0.89 ± 0.04	1.14 ± 0.04	130 ± 12
CV4	**Sem**	7.8	1	90-250	10 ± 5.6	11.4 ± 0.5	5.33 ± 0.47	74.2 ± 5.6	0.76 ± 0.06	0.53 ± 0.08	0.82 ± 0.04	1.33 ± 0.04	75 ± 5
CV5	**Ged**	10.2	5	90-250	17 ± 4.18	13.2 ± 0.4	3.31 ± 0.34	137 ± 5.4	0.90 ± 0.04		1.02 ± 0.03	1.52 ± 0.04	80[b]
CV6	**Gwc**	11.7	4.5	90-250	23 ± 6.69	23.5 ± 0.6	30.1 ± 0.66	771 ± 16	3.04 ± 0.02		3.4 ± 0.01	3.85 ± 0.02	30[b]
TRO1	**Seml**	5.4	0.8	90-250	2.1 ± 3.74	9.61 ± 0.3	4.8 ± 0.31	46 ± 3.1	0.58 ± 0.06		0.84 ± 0.04		
TRO2	**Seu**	4.6	0.5	90-250	9.8 ± 6.04	14.8 ± 0.5	23.6 ± 0.57	23.1 ± 3.9	1.00 ± 0.04		1.12 ± 0.03	1.59 ± 0.03	
TRO3	**Sem**	7.4	1	90-250	9.2 ± 5.1	9 ± 0.4	4.43 ± 0.4	55 ± 4	0.67 ± 0.06	0.68 ± 0.06	0.69 ± 0.05		112 ± 8
TRO4	**Sep(t)**	7.7	1	90-250	8.2 ± 3.6	7.45 ± 0.3	8 ± 0.3	123 ± 5.5	0.87 ± 0.04		1.01 ± 0.03		44[b]
TRO5	**Sep(t)**	9.4	1	90-250	8.2 ± 3.6	7.45 ± 0.3	8 ± 0.3	123 ± 5.5	0.81 ± 0.04		1.01 ± 0.03	1.51 ± 0.03	81[b]
TRO6	**Seml**	4.9	0.8	90-250	15 ± 5.6	8.84 ± 0.4	4.43 ± 0.43	53.6 ± 4.5	0.68 ± 0.06		0.88 ± 0.04	1.31 ± 0.04	
BOM1	**Seu**	4.2	1	90-250	14 ± 2.98	11.8 ± 0.3	1.42 ± 0.19	16.4 ± 2.6	0.54 ± 0.20		0.64 ± 0.05		135[b]
BOM2	**Gedt**	3.8	0.3	90-250	13 ± 5.3	8.45 ± 0.4	3.09 ± 0.4	31.4 ± 4	0.601 ± 0.07		0.88 ± 0.04		132 ± 11

[1]Dr corrected for the % of Moisture and carbonate content

[2]Dr corrected for the % of Moisture and carbonate content and stratigraphycal relationship

[3]Dr caludated using ICP-MS corrected after Guerin et al 2011

[b] Minimum age (calculated average of D0)

sat (saturated samples)

* De corrected following Galbraith et al 2012

Tab. 4: Summary of quartz and K-feldspar optically stimulated luminescence dosimetry data including concentrations of major radioactive elements.

Sample	Facies	De Qtz	De Qtz*	De K-feld	Age Qz[1]	Age Qz[2]	Age Qz[3]	Age Qz*	Age K-feld
		Gy	Gy	Gy	Ka	Ka	Ka	Ka	Ka
BUR1	**Cef**	95 ± 4	94 ± 2	135 ± 4.59	177 ± 16	113 ± 9	136 ± 11	113 ± 7	113 ± 6
BUR2	**Cef**	77 ± 6	96 ± 2	135 ± 6.89	138 ± 12	90 ± 7	100 ± 8	112 ± 7	112 ± 10
PPB1	**Cef**	107 ± 8	100 ± 4	134 ± 6	254 ± 32	123 ± 12	136 ± 12	115 ± 8	125 ± 14
PPB3	**Semr**	65 ± 4		134 ± 16.6	100 ± 9	95 ± 9	78 ± 7		106 ± 15
AHO1	**Semr**	70 ± 2			95 ± 7				
AHO4	**Sep(t)**	120 ± 4			150 ± 10		124 ± 8		
AHO6	**Seur**	119 ± 5			97 ± 6				
AHO7	**Seur**	112 ± 5			98 ± 8				
CV1	**Gdmf**	90 ± 5	104 ± 4		104 ± 8	108 ± 10	74 ± 5	125 ± 9	
CV2	**Cef**	61 ± 2.01	59 ± 2	119 ± 3.4	130 ± 12	114 ± 9	68 ± 4		113 ± 9
CV4	**Sem**	53 ± 2.8		133 ± 6.1	75 ± 5	98 ± 10			102 ± 6
CV5	**Ged**	sat		161 ± 12.4	80[b]				106 ± 9
CV6	**Gwc**	sat		341 ± 16	30[b]				91 ± 6
TRO1	**Seml**	sat				131[b]			
TRO2	**Seu**	93 ± 5.4	98 ± 4	168 ± 6.39		97 ± 8	84 ± 6	99 ± 7	105 ± 7
TRO3	**Sem**	72 ± 2.59			112 ± 8	106 ± 8	101 ± 7		
TRO4	**Sep(t)**	sat			44[b]				
TRO5	**Sep(t)**	sat		148 ± 7.67	81[b]				98 ± 7
TRO6	**Seml**	87 ± 3.31		175 ± 6.67		127.42 ± 3.4	100 ± 7		134 ± 8
BOM1	**Seu**	sat		241 ± 11	135[b]				203 ± 22
BOM2	**Gedt**	79 ± 3			132 ± 11		90 ± 6		

[b] Minimum age (calculated average of D0)
sat (saturated samples)
* De corrected following Galbraith et al 2012

Tab. 5: :Summary of quartz and K-feldspar dose equivalent (De) measurements and luminescence ages.

K-feldspar analysis and Ages

Presently, the research on the k-feldspar luminescence propriety is ongoing especially to better understand the bleaching, saturation and fading characteristics. It is well known that feldspar dating is complicated by the fact that IRSL signals are resetted by daylight slower than quartz and feldspars grains are much prone to partial bleaching. Nevertheless well bleached feldspars samples analyzed with the new protocol (pIRIR290) gave accurate ages (Li and Li, 2011; Reimann et al., 2011; Buylaert et al., 2012; Godfrey-Smith et al., 1988; Thomsen et al., 2008; Buylaert et al., 2012; Murray et al., 2012).

In this study we use, the pIRIR290 protocol proposed by Buylaert et al. (2012) to measure the natural dose (De) on different coastal deposits such as the fossil intertidal algal rim, shallow marine gravelly deposits and also on sandy beach deposits.

Commonly, feldspar grains show an efficient recovery of a given dose with a recycling ratio usually very close to the unit. Despite some authors observed a bad recycling ratio in their experiment, Buylaert et al. (2012) suggested that a poor dose recovery ratio is not necessarily a criteria for aliquot rejections as it is for the quartz grains. However, we decided to use as aliquot rejection criteria the recycling ratio and recuperation % of the natural together with the luminescence signal characteristics. In this thesis for each sample about 15 very small aliquots were analyzed (max 100 grains). The inset of figure 20 (b/d) shows the natural regenerated pIRIR290 luminescence decay curves for k-feldspars belong to the carbonate deposit of Burantino (Sample BUR1 and BUR2), and the resulting sensitivity-corrected pIRIR290 dose response curve is presented. The sensitivity-corrected signal is very far from the saturation point with a mean of the recycling ratio of 0.99±0.03 and a recuperation of 1.2±0.26%, thus feldspar signal has been considered stable and the resulting De reliable. The average of recycling ratio for all samples analysed is 0.98±0.03 with a recuperation always less than 3% of the sensitivity corrected natural signal (Fig.17a). All sample have shown a very bright natural signal and good dose–response curves, which were fitted using a single saturating exponential function. The resulting

equivalent doses (De(s)) for each sample were considered and listed in Table E figure 20.

Thomsen et al. (2008) and Buylaert et al. (2009; 2012) have demonstrated that the pIRIR signal is easy to bleach down to a certain residual level of 10–20 Gy, but it is necessary to verify this assumption, since bleaching characteristics are strongly dependent on the sediment type and mineralogy of the feldspars. Three aliquots for each sample were left under the sun light (June in Sheffield) for three sunny days and then analyzed with the pIRIR290 in order to identify the presence and the amount of the unbleachable compontents for each sample. Samples showed in average 9±0.4 Gy of dose residual after a long exposition to the day light, this is almost always ~5% of the De. (Fig 20a-e). In order to test if 3 days under sun light were adequate for fully reset the luminescence signal, two samples of a sandy deposit were bleached under Hönle SOL2 solar simulator for different time ratio and then the apparent dose was measured in the usual manner. The graph figure 20c shows the value of residual after different bleaching time. The main result is that three days under sun light were able to bleach the feldspar signal and it is worth noting that the some samples needed ~90 hrs (8 days) under a simulated light to get the same mean value. This is very unusual given that several authors have indicated that the time range necessary to adequate bleach feldspars is around 4 hrs of solar simulator. However, the pIRIR290 signals are almost complete bleachable by daylight exposure for Alghero samples.

Murray et al (2013) compared the bleachability of feldspar with different method. The authors observed that the same samples bleached under sun light and then analyzed with different protocol (IR50 and the pIRIR290) show different residual dose. It is known that IR50 signal is much more affected by fading than pIRIR290, however after the correction for fading they observed that the residual dose has the slight tendency to grow with the increasing of doses.

Given this uncertainty of the amount of the unbleachable residual doses and because checking literature it is not clear if these residuals should be subtracted or not, we have compared ages obtained by the subtraction and without it. (Fig.20d). In our case the corrected and the uncorrected ages are consistent each other with those obtained from quartz with slight differences, most probably dependent from the deposit

characteristics. Hence, as showed by Murray et al. (2013) the residual dose has little influence on the final age with the increasing of the De. Therefore, we have chosen do not subtract the residual value to the final ages.

The pIRIR290 obtained ages are in good agreement with the expected ages. Moreover, it is important to emphasize that pIRIR290 ages, unlike SAR and post-IR SAR ones, were obtained with a dose rate corrected only for the 40K internal contribution. On the other hand, for alkali feldspar grains a considerable portion of the total dose is derived from the decay of radioactive elements 40K and 87Rb that are present in the lattice structure. This means that k-feldspars proportionally receive a minor annual external radioactive dose from the environment than same size quartz grains

The larger the grain, the greater is the contribution of the internal dose. (Bo Li et al 2008). Thus, feldspars, as show in this thesis, are less influenced by the stratigraphic position of the sample and by the heterogeneity of the deposit a finally, the pIRIR290 can be effectively performed on carbonate heterogeneous deposits and can also be used to understand quartz bleaching.

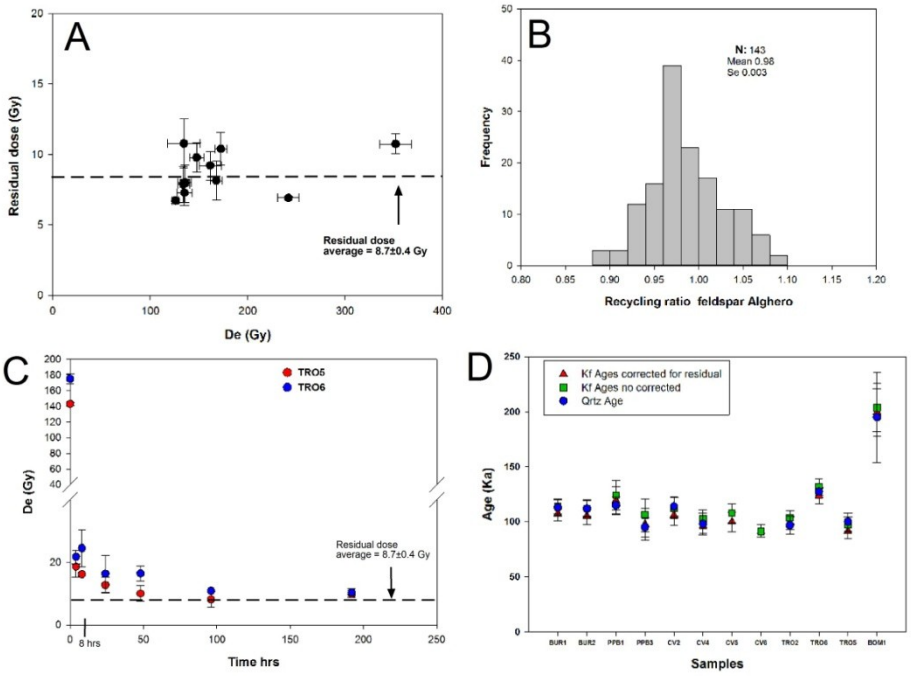

E

Samples	Residual (Gy)	De	De[1]	Age	Age[1]	Qrtz Age
BUR1	7.9 ± 1.3	135 ± 5	127 ± 5	114 ± 7	107 ± 6	113 ± 7
BUR2	8.0 ± 0.2	135 ± 7	127 ± 7	112 ± 8	105 ± 7	112 ± 7
PPB1	7.9 ± 1.3	134 ± 6	129 ± 6	124 ± 13	119 ± 13	115 ± 8
PPB3	10.8 ± 1.8	134 ± 17	124 ± 17	106 ± 15	98 ± 15	95 ± 9
CV2	6.7 ± 0.2	126 ± 3	118 ± 4	113 ± 9	106 ± 9	114 ± 9
CV4	7.3 ± 0.9	135 ± 8	126 ± 6	103 ± 8	96 ± 6	98 ± 10
CV5	9.2 ± 1.0	161 ± 11	152 ± 11	108 ± 9	100 ± 9	
CV6	10.7 ± 0.7	352 ± 16	352 ± 16	91.4 ± 6	91 ± 6	
TRO2	8.2 ± 1.4	168 ± 6	160 ± 6	104 ± 6	99 ± 6	96.7 ± 8
TRO6	10.4 ± 1.2	172 ± 6	162 ± 6	132 ± 8	124 ± 7	127 ± 3
TRO5	9.8 ± 1.1	148 ± 8	138 ± 8	97.8 ± 7	91 ± 6	100* ± 8
BOM1	6.9 ± 0.1	242 ± 11	237 ± 11	204 ± 22	199 ± 21	195* 41

[1]Corrected for redisual dose
* Age calculated using aliquot not saturated

Fig. 20: Feldspar luminescence analysis. A) Residual pIRIR290 dose measured after 3day under sunlight (Sheffield) bleaching are plotted as a function of the natural pIRIR290 dose for all samples (Tab.E). Error bars represent standard errors. The mean value is plotted as a horizontal straight line B) Histogram summarising the recycling ratios C) Post-IR IR290 bleaching curves measured for samples TRO5 and TRO6 using pIRIR290 protocol protocols. Aliquots were exposed for different lengths of time under a Hönle SOL2 solar simulator from 2hrs to 8 days simulator and then sensitivity-corrected luminescence was measured. The data are normalised to the natural sensitivity-corrected luminescence (zero exposure time). Each data-point is the average of three aliquots and error bars standard error. Straight lain is the mean of unbleachable residual observed after 3 day of exposition under sun light (Sheffield). D) Plotting uncorrected and corrected age for the residual pIRIR290 ages and Quartz ages of most of smaples. E) Summary of feldspar De, residual and Ages, and quartz ages.

Alghero coast stratigraphy

A total of 43 stratigraphic logs were correlated along the northern Alghero Coast.

Log correlation logs highlights the presence of five major unconformity-bounded units U1, U2; U3a, U3b, U4.

U1 crops out in the northern Le Bombarde bay (Fig. 21) resting unconformable on the Triassic mudstones bedrock. The Triassic mudstones are intensely bored by two generations of lithophagas burrows; the lowest occur at ~1.5 m above the present sea level, and the highest at ~3.5 m.

U1 (1.5 m-thick) consist of clast-supported fossil-rich granules to pebbles conglomerate. Granules commonly are aligned in lenses showing openwork features and dip seaward; layers of imbricate marine shells (broken or complete) occur. This deposit has been interpreted as the beachface (foreshore and berms) of pocket beach (association Bg) developed on a wave cut platform (transgressive surface T1) (Fig.21a).

U1 has been stratigraphyc related to the MIS 7(see below).

U1 is reworked and overlain at the top by recurrent lenses of sandy coarse matrix-supported conglomerates, that is U2. Clasts range from well rounded to sub rounded granule to pebbles and diffuse marine shells (broken or intact). Matrix is made by a well-sorted medium to coarse-grained sand. The lens of conglomerates show a fining upward trend and a crude cross-bed lamination with recurrents cut and fill structure; small pebbles are common scattered or aligned at the base of lens. This facies is often associated with lenses of coarse-grained cross-bedded sandstone (Fig.21b-d). U2 marks a regressive stage (R2) and has been interpreted as a braided river part of an alluvial fan system. U2 has been OSL dated at 200±22 ka and thus related to the transition between MIS7 and MIS 6. The gravelly pocket beaches have not been OSL dated and thus related to a sea level high stand occurred before the MIS 6, most likely MIS 7.

On U2 rests unconformable U3 characterized by the sub-unit 3a. U3a consists of low angle stratified gently dipping toward the sea well sorted coarse-grained sandstone (Fig.21c). U3a has a maximum elevation on the present sea level of ~2 m and has been interpreted as the foreshore of a well developed sandy pocket beach system, probably similar to the present one (Fig.21c). This deposit has been OSL dated at 130±11ka and

thus related to the MIS 5e highstand. However, the MIS 5e markers indentify for the north Alghero suggest an elevation of the MIS 5e of 3.5-5 m. (Tuccimei et al 2006, Ferranti el al 2006). Given the low elevation on the present sea level of the Le Bombarde bay MIS 5e deposits, we infer that the area has been affected by neo-tectonic activity. The bay, in fact, is located between two faults NW-SE oriented. Faults may be responsible of the relatively elevate subsidence of the area. This is more evident in the eastern part of the bay where the youngest Quaternary deposits are almost underwater (Fig.21e).

On the U3a rests unconformably on U4, this is characterized by the facies association A. In the central part of the bay U3a is cut and reworked at the top by facies similar to those described for the above U2 (Fig.21d.). At the edge of the bay U4 consists of 0.5 to 1 m-thick, matrix or clast-supported cobbles conglomerates. Conglomerates are characterized by angular pebbles and cobbles occasionally supported by a sandy-silty reddish matrix. This deposit has been interpreted has debris flow flooding the all plain. Most likely, the debris flows were triggered by the major rainfall associated tothe climate change occurred at the transition between MIS 5e and MIS 5d. The debris flows are covered by aeolian deposits. (Fig.21)

At El Tro bay four units (U3a, U3b, U4) have been recognized (Fig 25).

U3a rests unconformable on the Triassic mudstone. U3a is composed of two different marine facies associations Bg and Bs.

Facies association Bg rests unconformably on the bedrock in almost all area. (Fig.25) In the southern part of the bay Bg crops out as a single facies characterized by a scattered deposit of very fossil-rich clasts-supported conglomerates. Clasts range from well-rounded granules to sub angular boulders. Granules show openwork features with a slightly alignment and diffuse fragments of marine shells, whereas scattered boulders are experienced (Fig.22a-a1). This deposit is ~1 m-thick and lays at 3 m above the present sea level. It has been interpreted as the submerged part of a small shallow gravelly pocket beach developed at the base of the cliff on the wave cut platform (Fig.7c-d). In this zone the cliff are bored at the elevation of 5±0.5 m by Lithophaga spp burrows and sporadic serpulides in life position may be found as well (Fig.25). Thus the shallow gravelly beach formed during a period when the sea level was 5 m above the

present; that is, the MIS 5e highstand. The OSL ages obtained for the deposits confirm this hypothesis referring U3a at 125±9 ka, that is MIS 5e (Fig.22a and 25).

This part of the bay is separated from the central part by a high cliff (Fig. 25). In the central part of the bay facies association Bg is characterized at the base by 50 cm thick clast-supported conglomerate. (Fig.23) Clasts are well rounded pebbles to cobbles, a very coarse sandy matrix rich in broken marine shells fill the spaces. Upward this conglomerate is covered and encrusted by an organic carbonate deposit (similar to that described above for Burantino and S'Abba drucche bays), on which lays unconformable a second clast-supported conglomerate, which strata gently dip seaward. Clasts (cobbles and pebbles) show a slight imbrications landward and very coarse sand to granules sandy matrix fill the spaces.

This last conglomerates land-ward vary in grainsize, pass from cobbles-pebbles to pebbles-granules dominated by diffuse fragments of marine shells. Granules often are openwork (Fig.23). This succession show a maximum high above the present sea level of 3.5 m, although part of this succession is dislocated downward by faults. This succession is overlapped by 0.5 to 2 m-thick very coarse mostly root bioturbated sandstone (part of the facies association Bs following described) (Fig23 and 25).

The succession Bg has been interpreted from the bottom to the top as transgressive gravelly lag deposits (Sensu Massari 1994) that marks the transgression surface T2. The basal conglomerate is covered and encrusted by a ~ 1m thick mound shape organic carbonate deposits interpreted as algal intertidal rim (Fig.23d). The upper conglomerate has been interpreted as a second transgressive small gravelly pocket beach formed unconformable on the previous deposits marking a second possible transgression (T3) (Fig.23 and 25)

The Carbonate deposits (algal rim) are 3.5 m apsl in the higher part, its elevation is comparable with the same deposits cropping out at the Burantino and S'Abba Drucche bays. Hence there are evidences that neo-tectonic partially affected these system being active during the last 125 ka. The algal rim has been OSL dated at 114±9 ka, thus is referred to the highstand MIS 5e. The upper conglomerate is instead stratigraphycally referred to the MIS 5c (see below). (Fig.23 and 25)

Laterally toward the north, facies Bg passes to facies association Bs which is characterized by 1.5 m-thick sandstone (Fig.24 and 25). From the bottom the succession consists of medium to coarse grained parallel laminated sandstones strongly bioturbation at the top. On these lays 50 cm of cobbly-pebbly matrix-supported conglomerate; clasts are imbricate landward and lenses of poorly cross-bedded sandstones and granule conglomerates occur. Succession closes with 30cm-thick of trough-cross bedded sandstone. Facies association Bs has been interpreted as the shoreface (lower and upper) zone of pocket sandy or mixed sand and gravel beach (Fig7H and I). Clasts most probably derived from the close rocky cliff, they were reworked and transported to the shoreface during the major storms and then deposited on the beachface, similar to what is occuring today (Fig.7f-g). During the fair-weather the shoreface was characterized by small wave ripples. The base of the succession has been OSL dated at ~130±7 ka, and thus referred to the highstand MIS 5e.

Along the bay U3a rests unconformably on U3b. The facies associations are almost the same and characterized by Bg and Bs.

In the southern part of the bay U3a crops out quasi-continuously; it is characterized at the base by scattered portion of 50 cm of pebbly-cobbly fossil-rich conglomerate deposits with a coarse sandy matrix and broken shells, lens of openwork granules are present as well. This deposit crops out at an elevation of 5 m above the present sea level and has been interpreted as the foreshore part of a beach system referable to the MIS 5e However, these deposits has been partially reworked by debris flow associated to an alluvial fan system. In particular is evident a thin (30 cm thick) of transitional strata between the two facies which shows the mixing of the two deposits.

They have been OSL dated respectively at 106±9, ka and 90±6 ka and thus respectively related to the MIS 5c and the transition MIS 5c/b.

The central part of the bay is dominated by mixed sand and gravel beach system overlapping MIS 5e deposits.(Fig24 and 25). These deposits are characterized by alternating dipping seaward layers of cobbles, pebbles (imbricate landward) and granules (openwork feature). Cobbles are often bored and occasionally encrusted by serpulides. Granules layers often rest on cobbles or are among these. In places they

could form clouds around the bigger clasts. Broken or entire marine shells are widespread throughout conglomerates. Common lenses of well sorted parallel or low angle laminated coarse-grained sandstone are interlayered with conglomerate strata. These lenses show diffuse laminas of black heavy mineral and nicely preserved deer footprints (Premegaceros cazzioti, Fanelli et. al., 2007). As additional note most of the sandstones were carved for dimension stones used to build Algero buildings during 13th and 16th centuries.

Sea-ward this conglomerate succession passes to a 2 m-thick medium to coarse sandstone. The bottom (70 cm-thick) is slightly laminated and scattered pebbles and marine shells occur. This sandstone is capped by ~1 m-thick of parallel laminated high angle cross stratified sandstone. The described succession has been interpreted as the beachface of mixed- sand and gravel high energy beach system characterized by a well-developed seaward dipping storm gravelly berms and fair-whether sandy foreshore, which passes to well a developed sandy backshore and dune system (Fig.24). The beach system has been OSL dated; the beachface at 105±7 ka, the backshore at 106±8 ka and the dunes system at 98±7 ka. Thus, the system has been related to a highstand (2 m apsl) occured 100 ka ago; that is, to the MIS 5c. During MIS 5c the system onlapped the previous eroded shoreface deposits refeered to MIS 5e. During its maximum evolution almost the all the bay was dominated by a sandy beach system characterized by a wide a backshore dominating most of the inland part of the bay where dunes developed.

Fig. 21: Stratigrafic section (E-W) of Quaternary deposits cropping out at le Bombarde bay. At the top correlated logs and their position. A) View of the gravelly beach deposit to be note the layer of of granules and marine shell, rules scale is 1 m. B-D) Field view of the braided stream to be note the channels structure C) Sketch of the low angle cross bedding of sandstone (beach foreshore) E) Detail of the of parte terrestrial deposit (colluvium and dunes) within the tidal range.

Fig. 22: A)Panoramic view of the quaternary deposit part cropping out El tro bay sud. Each observed facies has been indicated , for more deatail see the text and figure 5. Inset (A1) detail of gravel deposit formed at the base of cliff. B) View of Quaternary deposits cropping out in a small cove close to the study area. it is worth to be noted the analogies, inset show the beachface of well developed small gravelly pocket beach exposed laterally at the main view

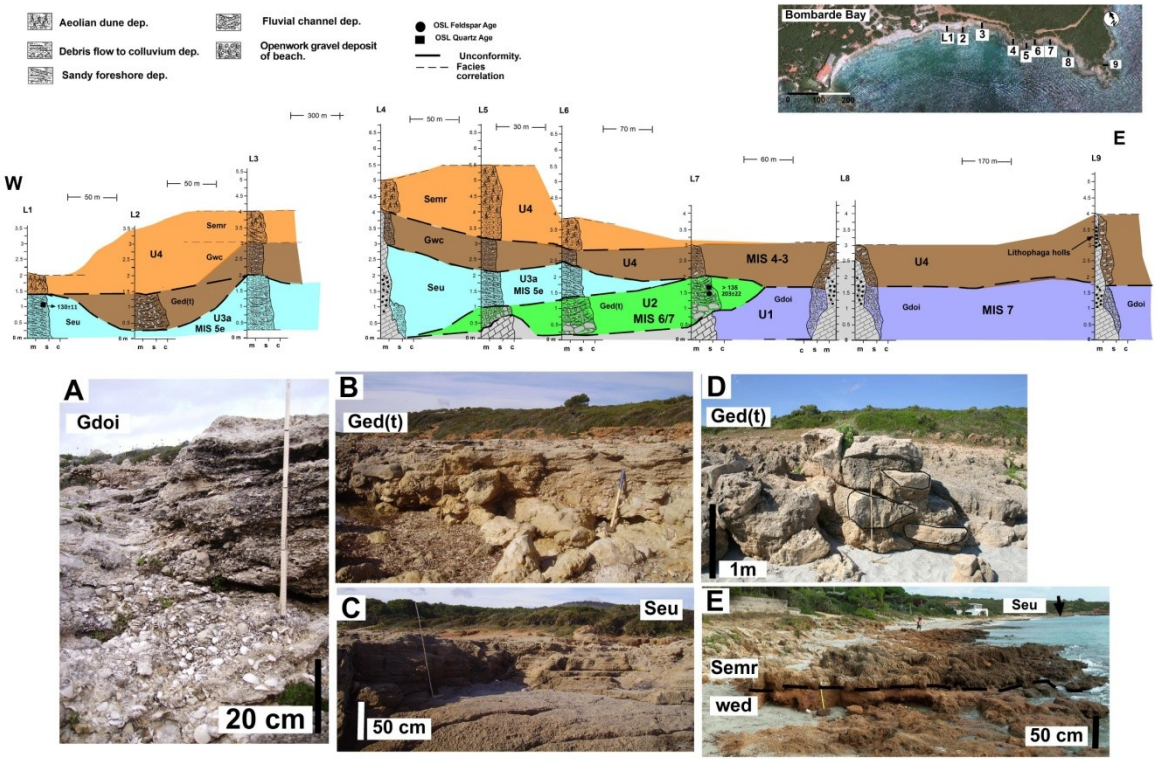
Aeolian dune dep.
Debris flow to colluvium dep.
Sandy foreshore dep.
Fluvial channel dep.
Openwork gravel deposit of beach.
OSL Feldspar Age
OSL Quartz Age
Unconformity.
Facies correlation
Bombarde Bay
W
E
Semr
U4
Gwc
Seu
Ged(t)
U3a MIS 5e
U2 MIS 6/7
MIS 4-3
U1
Gdoi
MIS 7
Lithophaga holls
A
Gdoi
20 cm
B
Ged(t)
C
Seu
50 cm
D
Ged(t)
1m
E
Seu
Semr
wed
50 cm

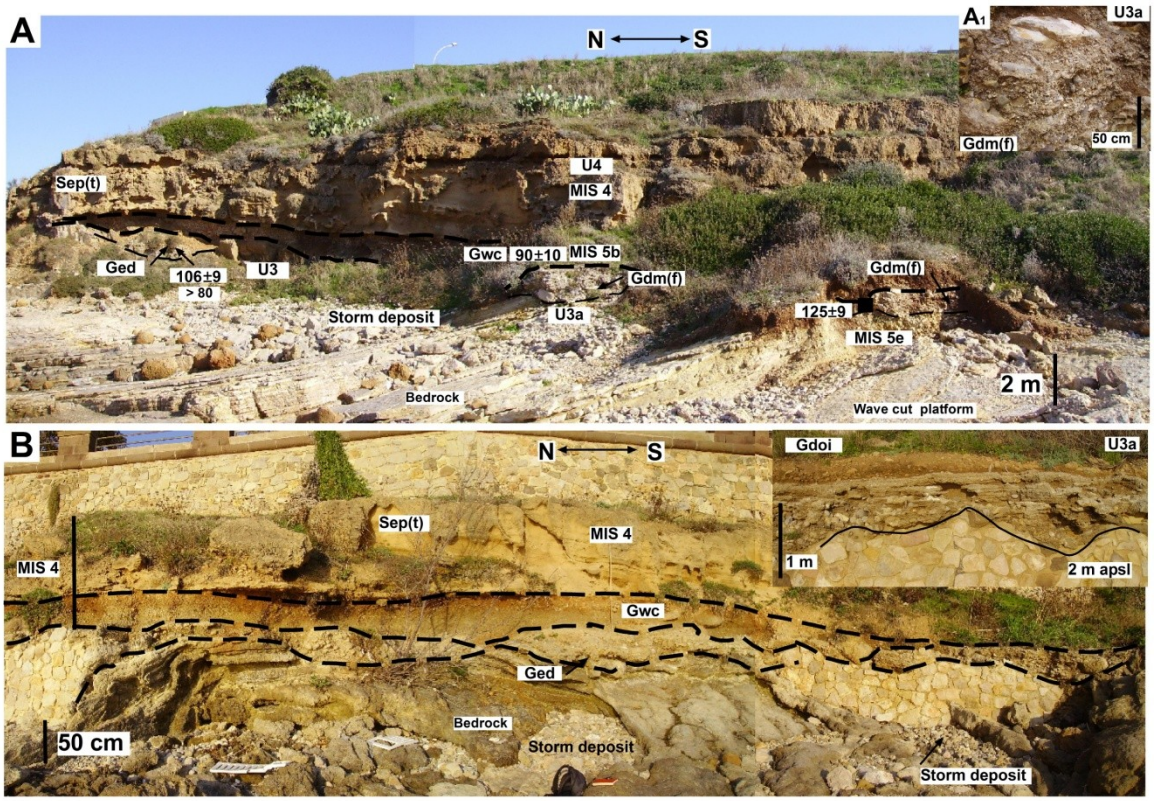
A
N
S
Sep(t)
U4
MIS 4
Ged
106±9
> 80
U3
Gwc
90±10
MIS 5b
Gdm(f)
Storm deposit
U3a
125±9
MIS 5e
Bedrock
Wave cut platform
2 m
A1
U3a
Gdm(f)
50 cm
B
N
S
Gdoi
U3a
Sep(t)
MIS 4
MIS 4
1 m
2 m apsl
Gwc
Ged
Bedrock
Storm deposit
50 cm
Storm deposit

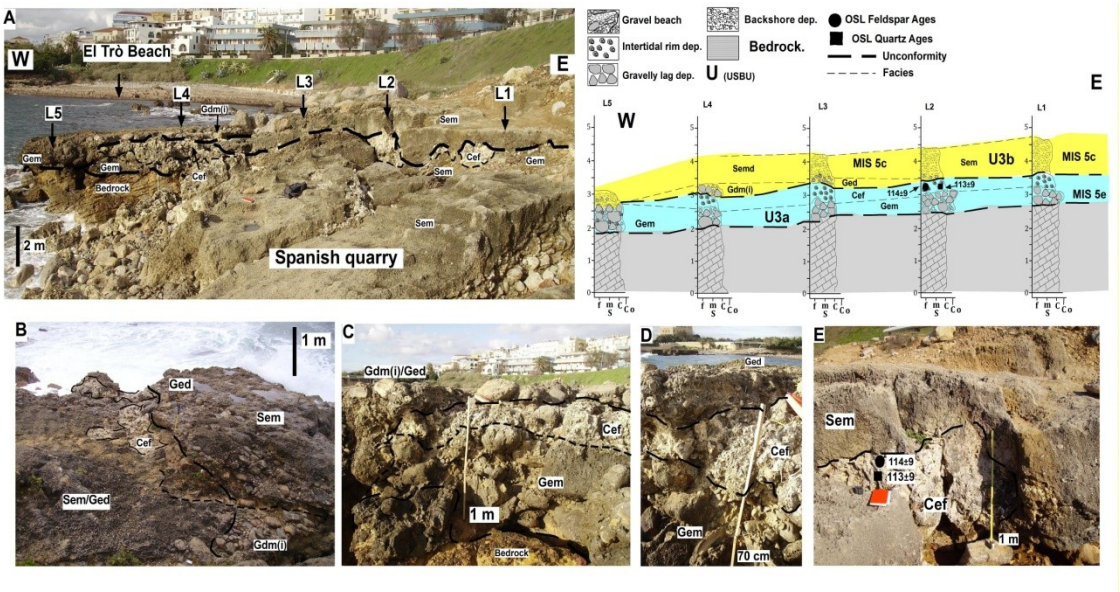

Fig. 23: A) Stratigrafic section (E-W) of cropping facies association Bg cropping out at El Trò . A) Log position and field view of the quaternary outcrop. Notice the Spanish quarry carved in to the quaternary deposits, partially dislocated. B-C) Details of the unconformity between algal rim partially reworked by the overlapping conglomerate D-E) Detail of in situ deposit of algal rim capped by sandy backshore deposits

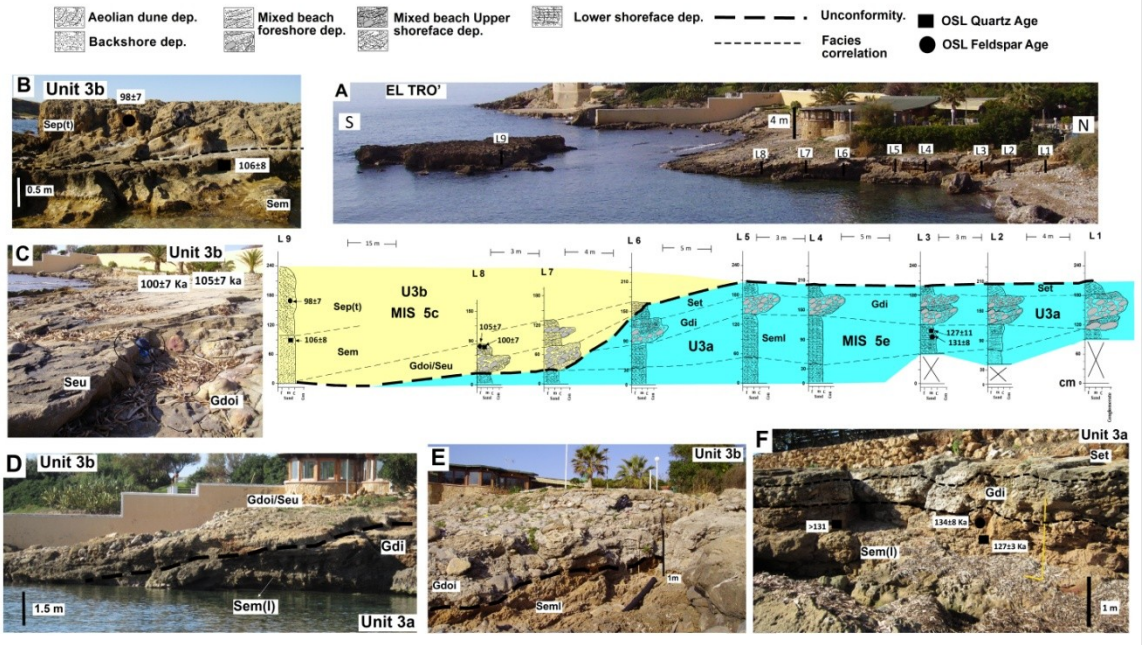

Fig. 24: Logs measured at El Trò bay for the beach system (Alghero city). Up top: A) N-S view of the relict beach system of El Trò Bay and logs location, correlation highlighting the relationships between MIS 5e (U3a) and MIS 5c (U3b) deposits. Down: B) View of log 9 see strata limit dividing the high angle cross stratified sandstone from the lower massive. C) Detail of the foreshore (low angle cross stratified sandstone layer). D) detail from the sea of the unconformity between U3a and U3b, see as U3a is overlapped on U3b. E) Detail of the gravelly beachface and the alternation of granules and cobbles strom berms. F) Detail of U3a characterized shoreface deposits.

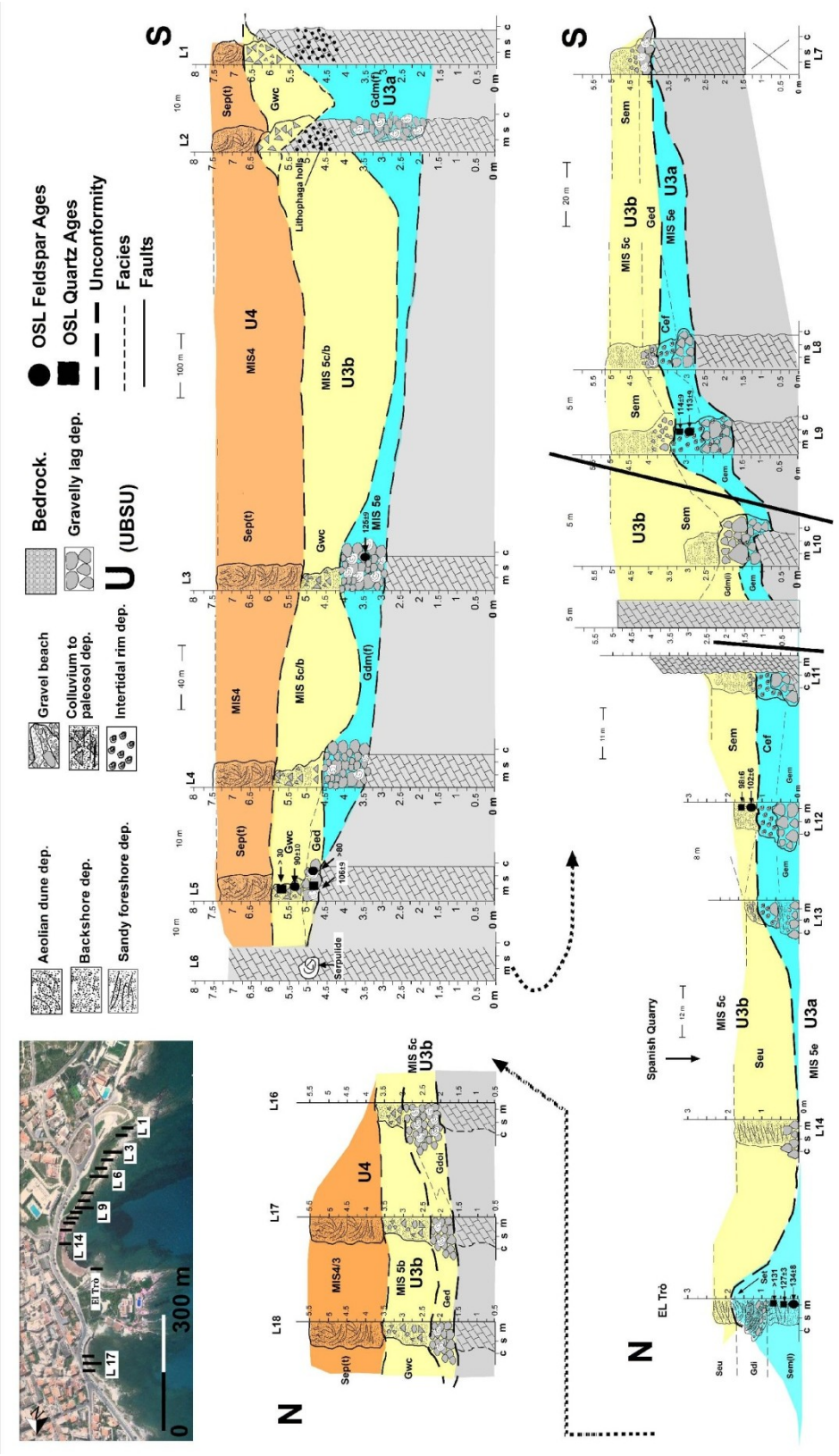

Fig. 25: General stratigraphyc section and related ages of the quaternary deposits cropping out at El-Tro Bay. Each deposit were labelled with the respective facies description and the related USBU. On the top on the left inset shows the logs position.

Alghero bay and Calich lagoon

The Alghero City is located on westward-facing bay dominated by a 5 km long sandy beach ridge-lagoon system fed by three small rivers and surrounded by Mesozoic limestone cliffs and Oligocene volcanic promontories. A relatively well developed dune system, stabilized since the 50s, separates the beach from the lagoon (Fig.26). The late Quaternary deposits crop out along the western side of the lagoon. These are generically attributed on base of their elevation above the present sea level (~5m) to the last interglacial (125 ka, MIS 5e) (Pecorini et al 1954). This part of the thesis is addressed to the reconstruction how the beach-barred lagoon system developed during the last intergalcial.

Fig. 26: Satellite view of Alghero coast, at the top on the left the Calich lagoon and the Alghero bay. White arrows indicated the different sub-area studied, Burantino (Bur), Punta Padre Bellu (PPB), El Trò-Carlos V (TRO-CV) and the Bombarde (Bom bays).

OSL analysis

A total of nine samples were collected and dated using both quartz and k-feldspar grains in order to develop the chronological framework of the Calich-lagoon system. As described above for the other areas the single regenerative dose (SAR) and the Post-IRIRSl 290 protocols were performed to estimate the equivalent dose (De) measurement. Alghero samples usually contain a range mixing of quartz and k-feldspars so different techniques to clean out the samples were used. A fraction of contaminated samples were re-etched with HF and tested for the purity. Purity check provided negative so the pure sample were analyzed with the standard SAR protocol. Another fraction of the contaminated samples underwent to the less used protocol called the post-IR pulsed blu stimulation (SAR-POSL). Derby et al, (2006) clearly show that quartz and k-feldspar luminescence signals posses different life time. Thomsen et al (2008), based on the above evidence proposed the post-IR blu pulsed stimulation protocol which use discrete light stimulation (alternate stimulation to off-period) to discriminate quartz from feldspar signals. Pulsing setting was based on the parameter used by Thiel et al. (2010) for Sardinian samples as well. The purpose of this is to test the validity of SAR-POSL for the studied deposits. (Fig.27)

For both protocol the temperatures of 260°C and 240°C respectively for preheat and cutheat were set based on preheat plateau dose recovery test (Fig. 27A-B). Despite most of the quartz samples resulted fully saturated, three samples (Cal2, 3 and 8) show few saturated aliquots (rejected) given a final reliable De. For these three samples the De and resulting ages using both methods resulted consistent with each other, thus the POSL method is a reliable method to estimate the quartz De using feldspar-rich samples (Table6).

The Post IR IRSL290 protocol were performed in order to estimate a reliable De for dating Calich deposits. Sample showed a good regenerative dose response curve, recuperation value was not more than 3% of the natural and the recycling ratio (average of 0.98 ±0.03) despite the large dispersion of value (Fig.28). For all samples the presence of unbleachable residual were estimated.wand the mean of 13±1 Gy obtained. The respective residual for each samples is displayed in Table 7. As well as for

the previous studied area the residual dose rate has not been subtracted to the final feldspar De. Feldspar ages corrected and uncorrected resulted in good agreement each other and with the quartz age (Table 6-). However, sample Cal1 underestimate the real probable burial age (MIS 5e). Although we are not sure yet about the origin of this underestimation, this is likely due to partial the bleaching of feldspars grain, thus we considered it the minimum age.

Sample collected at the quarry site, shown in figure 31B show a very variable dose rate ranging from 1.4 and 4 Gy/ka. In particular, for the carbonate deposit (Cem) and the top sandstone deposit (Sep) the first resulting ages were not in agreement with the stratigraphyc order. (Table)

In fact, the lagoon deposit as well as seen for the carbonate algal rim deposits shows a very low dose rate 1.4 Gy/ka whether compared with the lower and upper deposit, ~2 times higher (4 Gy/Ka). Thus, although potassium feldspar is less sensitive to slightly changes of burial dose rate, it is not totally independent from that. For this particular situation, a correction for the gamma contribution due to the lower and higher deposits was applied for carbonate deposit. For the sandstone deposits the correction was done taking only into account the contribution of the lower reddish colluvium. The corrected ages resulted in agreement with the stratigraphy. (Table 7)

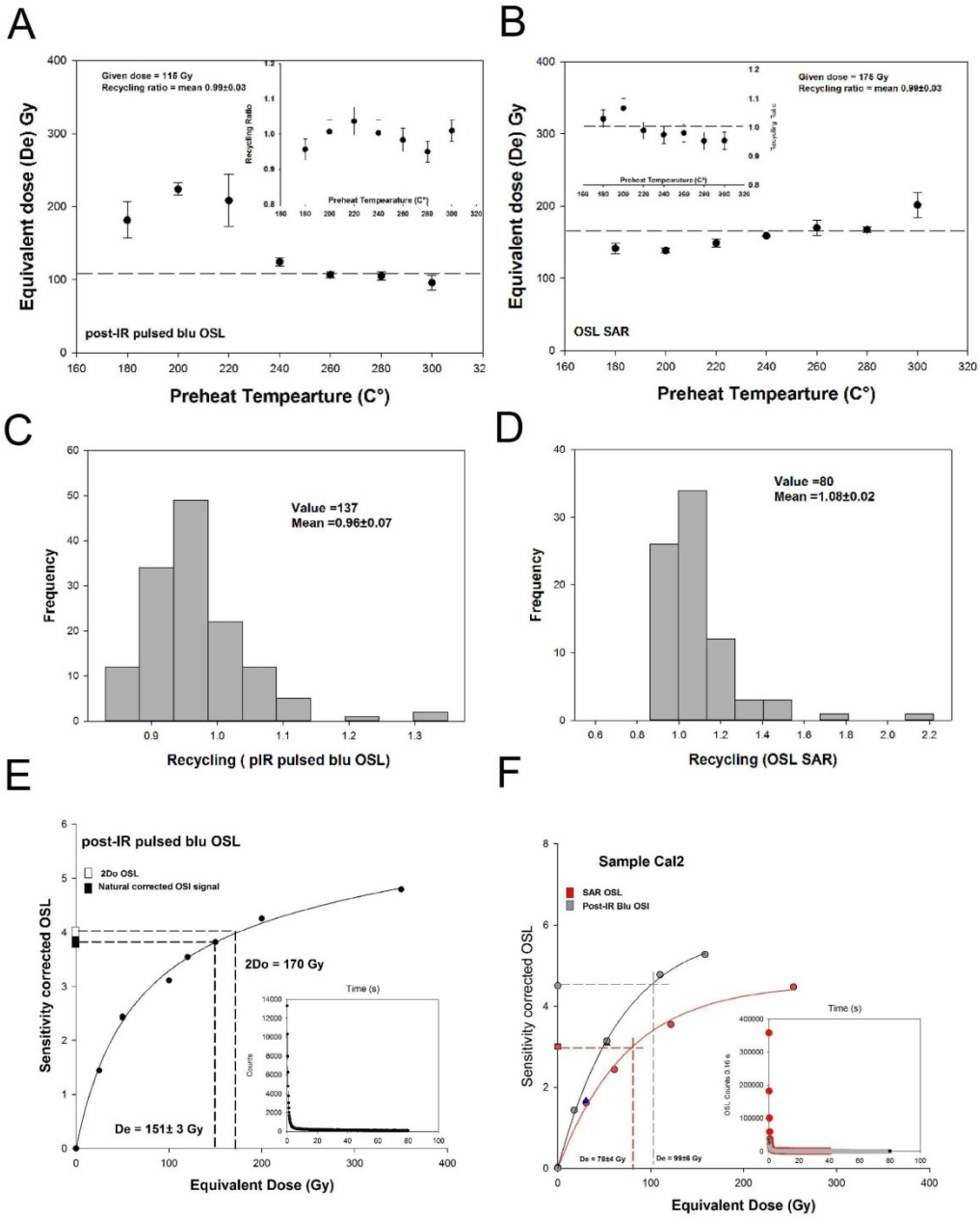

Fig. 27: A-B) Results of the dose recovery tests under different preheat temperatures performed with both protocol SAR and POSL. For all preheat temperatures the measured given dose ratio is within 10% of unity, dose recovery ratios plateau (Given De/Measured) are shown in the insets for each protocol. Temperature chosen for the preheat is 260°C. C, D) Respectively distribution of Post-IR pulsed and SAR protocol recycling ratio for all the aliquots analysed E) Example of dose response growth curve for quartz affected by saturated signal. F) Sensitivity corrected signal for each protocol used. In both cases, quartz shows fast dominated signal (inset).

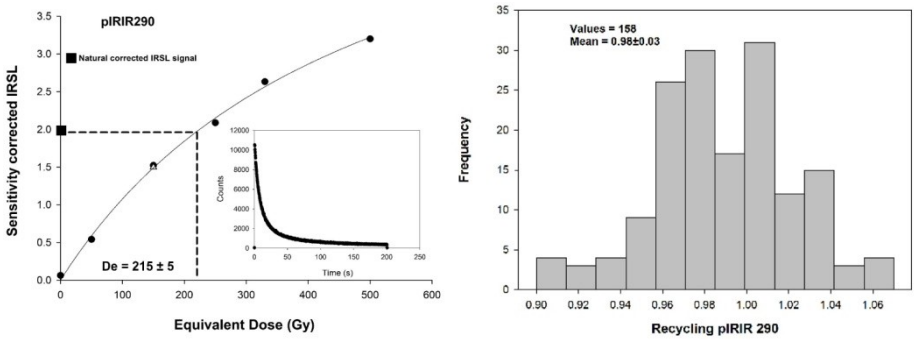

Fig. 28: pIRIR290 dose response curves and decay curves (insets) for samples Cal1. The triangle are the recycling point, and the square show the sensitivity corrected IRSL signal, and distribution of the recycling ratio for all the samples analysed.

Sample	Facies	Depth (m)	Grainsize µm Avg	238U (Bq/Kg)	226Ra (Bq/Kg)	232Th (Bq/Kg)	40K (Bq/Kg)	Dr k-feld Gy Ka-1	Dr Qtz[1] Gy Ka-1
Cal1	**Set**	4	90-250	12.8 ± 5.1	10.7 ± 0.4	10.1 ± 0.4	233.7 ± 6.9	1.8 ± 0.03	1.3 ± 0.0
CAl2	**Sep**	2	90-251	9.0 ± 3.7	8.3 ± 0.3	7.1 ± 0.3	97.9 ± 3.8	1.4 ± 0.03	0.8 ± 0.0
Cal3	**Sep**	1.5	90-252	12.0 ± 4.6	8.4 ± 0.4	6.8 ± 0.4	112.8 ± 4.8	1.3 ± 0.04	0.8 ± 0.0
Cal4	**Wed**	2	90-253	16.5 ± 5.6	19.5 ± 0.5	35.2 ± 0.7	629.8 ± 13.5	3.5 ± 0.02	2.8 ± 0.0
Cal5	**Cem**	4	90-254	4.5 ± 3.3	7.7 ± 0.3	10.9 ± 0.3	158.4 ± 5.7	2.6* ± 0.02	2.0 ± 0.0
Cal6	**Sem**	11.5	90-255	2.0 ± 3.9	7.6 ± 0.3	8.4 ± 0.3	130.3 ± 4.5	2.0 ± 0.02	1.4 ± 0.0
Cal7	**Sedf**	5	90-256	26.3 ± 6.2	24.7 ± 0.5	45.5 ± 0.8	968.1 ± 18.8	4.0 ± 0.02	3.4 ± 0.0
Cal8	**Sep**	1	90-257	6.7 ± 3.6	7.9 ± 0.3	6.6 ± 0.3	103.4 ± 3.8	1.4 ± 0.03	0.7 ± 0.0
MP1	**Seuf**	0.5	90-258	35.0 ± 7.0	/ ± /	26.0 ± 0.7	147.0 ± 4.0	2.2 ± 0.02	1.5 ± 0.0
MP2	Wed	0.5	90-259	±	±	± /	±	1.5 ± 0.02	2.1 ± 0.0

[1]Dr corrected for the % of Moisture and carbonate content
*Dr corrected for the % of Moisture and carbonate content and stratigraphycal relationship

Tab. 6: Summary of quartz and K-feldspar optically stimulated luminescence dosimetry data including concentrations of major radioactive elements

Sample	Facies	Depth (m)	POSL Ali	POSL Ali rej#	OSL Ali	OSL Ali rej#	SAR (De) Gy	POSL (De) Gy	Pul (De) Gy	Age (SAR) Ka	Age POSL Ka	Age K-feld Ka
Cal1	**Set**	4	23	10			sat	sat	sat		>120[b]	>100[b]
CAl2	**Sep**	2	34	15	27	11	96 ± 3	95 ± 2.9	95 ± 2.9	124 ± 9	125 ± 8	113 ± 8
Cal3	**Sep**	1.5	42	14	26	11	97 ± 3	88 ± 3.8	87.65 ± **3.8**	120 ± 8	110 ± 8	115 ± 7
Cal4	**Wed**	2	/	/	/	/	Sat	Sat	Sat			114 ± 8
Cal5	**Cem**	4	/	/	/	/	Sat	Sat	Sat			121 ± 9
Cal6	**Sem**	11.5	/	/	/	/	Sat	Sat	Sat			100 ± 5
Cal7	**Sedf**	5	/	/	/	/	Sat	Sat	Sat			117 ± 20
Cal8	**Sep**	1	38	11	28	11	89 ± **9**	96.96 ± 3.3	96.96 ± 3.322	123 ± 15	133 ± 12	123 ± 8
MP1	**Seuf**	0.5	/	/	/	/	Sat ±	Sat ±	Sat ±	87[b]		100 ± 8
MP2	Wed	0.5	/	/	/	/	Sat ±	Sat ±	Sat ±			75 ± 5

[b] Minimum age (calculated average of D0)
sat (saturated samples)
#De corrected pulsing

Tab. 7: Summary of quartz and K-feldspar dose equivalent (De) and ages

Stratigraphy and Chronological framework of Calich lagoon

Stratigraphiyc and sedimentological analysis performed on the Quaternary deposits cropping out Along the Alghero bay allow us to indentify three unconformity bounded units (UBSU). Based on the previous works and the possible correlation with these, UBSUs were named U3a, U3b; U4. (Fig.29).

Most of the studied Quaternary deposits crop out along the lagoon. In the southeastern zone in a well exposed quarry wall, it has been possible to clearly identify four different facies (Fig.29, Log17; Fig.30B). From the bottom the quarry succession is characterized by 50 cm of grayish very coarse grained sandstone with aligned slightly dipping landward disarticulated brackish bivalve shells (*Cardium edule*) and dispersed or aligned volcanic granules (mostly ignimbrites). Unconformable on it a 1.5 m-thick (maximum) massive clay-carbonate deposit hardly cemented up-ward rich in a well rounded medium-fine sandy component and brackish shells (*Cardium edule*) rests.

This passes to a 1 m-thick (maximum) reddish sand-rich silty deposit with dispersed small angular bedrock-derived granules and scattered pebbles. These deposits show a vertical interaction with the lower carbonate deposit and a mixed zone ~30 cm-thick is clearly observable at the contact limit. Succession is closed by 2 m-thick well sorted strongly roots-bioturbated coarse-grained sandstone. From the base to the top, the succession has been interpreted as the inland beach-backshore environment, where ephemeral streams (small volcanic pebbles) and major storm forming wash over fan (landward aligned shells) occurred. This passes to a thick deposit of incipient lagoon mostly influenced by streams and sands blows (from closer coastal dune) contribution. Given the elevation of the quarry of 5 m apsl (at the base), this deposit was referred to the MIS 5e. OSL ages confirm this period relating the basal deposit at 117±20 ka and the lagoon deposit at 121±9 ka. The lagoon deposit marks the maximum transgression (T2) of sea level for the bay at ~7 m apsl (the Sardinia general subsidence of 0.01 mm/yr was taken in account). This succession is referred to U3a whilst the following to U3b. This last has been interpreted as a reworking colluvial deposit. In addition, a recent pedological work (Zucca et al, in press) performed on the quarry succession confirmed the colluvial origin of the reddish deposits. This color is due to a post burial

conditions or inherited from reworked soil material. The authors observed an increasing of in situ-weathering downward with an incipient pedogenesis much more evident at the contact with the lower carbonate deposit which show thick cemented calcrete layer of lacustrine origin, reworked by pedogenesis and bioturbation.

The top sandstone has been interpreted as thick dunes deposit strongly bioturbated by plants. The colluvial and the dunes deposits were OSl dated respectively at 114±8 ka and 100±5 ka, thus the first is referred to the end of MIS 5e and the second to the MIS 5c. The colluvial deposit marks a regressive stage (R2) occurred at the end of MIS 5e.

Laterally toward the north-west the succession passes to 5 m-thick strongly bioturbated coarse-grained sandstone. (Fig.29 and 30C). Sandstone shows faint of parallel lamination and high angle cross-stratification (20-30°). Foresets dip manly landward and often the limit of strata marks a change of foresets dip-direction mostly to NE-E and W-NW (Fig.30C-A). This facies is related to facies association E and interpreted as coastal dunes moving landward under the influence of two mainly winds blowing from SW (Libeccio) and SSE (Levante-Scirocco). The coastal dune system has been OSL dated at 120±8 ka with quartz ad at 115±7 ka with feldspar. Laterally, the facies association E overlays and passes to facies association Bs (Fig. 30A).

Bs has a maximum range in thickness from 2 to 5 m and is characterize at the base by ~1 m-thick trough cross-bedded sandstone rich in well rounded quartz and volcanic sub rounded-angular granules (mostly ignimbrites). Layers of disarticulated or broken marine (mostly *Glycymiris Glycyimiris*) gastropods (*Bittium*) and brackish (*Cardium Edule*) shells occur. This deposit is overlain by 0.5 to 2 m-thick coarse-grained planar laminated sandstone, sporadically trough-cross bedded with waves ripples mostly orientated NW-SE. The bioclastic component often reached the 50% of the total grain composition (Fig.31). This succession is capped by low angle (5°) cross-laminated dipping seaward (SW) coarse-grained sandstones. These lay generally at ~4 m above the present lagoon water level. Facies association Bs has been interpreted as a well-developed prograding dissipative beach system, analogue to the present one (Manca et al 2013).

The beach was characterized by a large breaker zone were megaripples and bars occurred and by a very shallow wide flat surfzone where sporadically wave ripples and

bar-trough systems developed, and where the strength of the waves were almost totally dissipated before to reach the shoreline. The foreshore was almost flat dipping toward SW. The system, given the elevation on the present sea level, has been related using the backshore deposits at the base the quarry, to U3a. The OSL ages gave minimum ages ranging between 100 ka and 120ka, thus the most probable period of maximum evolution of the system was the MIS 5e highstand when the sea level was at about 5±1 m above the present. The prograding barrier-lagoon system has been considered correlatable with the MIS 5e sandy beach systems of the Le Bombarde and El Trò Bay.

A small outcrop of Quaternary deposits is exposed along the present beach (Maria Pia beach). It consists of 75 cm thick of coarse-grained low angle laminated sandstone resting on volcanic deposits. Sandstones are made of lamina set dipping 5° (maximum) toward the sea; dispersed or aligned along the lamina broken or complete shells occur (*Glycimiris Glycymiris, Cardita Senegalensis, Tapes diana, Cradium edule, Ostrea spp.*). Often the disarticulated bivalve shells (mostly *Cardium edule*) form 10 cm thick shell layers. A 50 cm thick (maximum) reddish sandy silt deposit covers and interfingers the lower deposit. This deposit shows incipient pedogenesis characteristics.

The lower sandstone has been interpreted as the beachface of a sandy beach system on which unconformable lays a reddish incipient palaeosol. The beachface marks a second transgression stage (T3) which is chronologically (OSL) related to MIS 5c (100±8 ka) whereas the palaeosol has been related to a second regressive stage (R3) occurred at end MIS 5a/begging of MIS 4.

Fig. 29: Measured stratigraphyc section performed at the Calich lagoonand Maria Pia beach: A) Logs position and satellite view of the lagoon label of each facies (eg Set) and Unit were reported B) Tomography performed with the Ground Penetrating Radar highlights the unconformity between Unit 3b and Unit 3a on the top. The thick reflector is probably the continue colluvium deposit. Label of facies

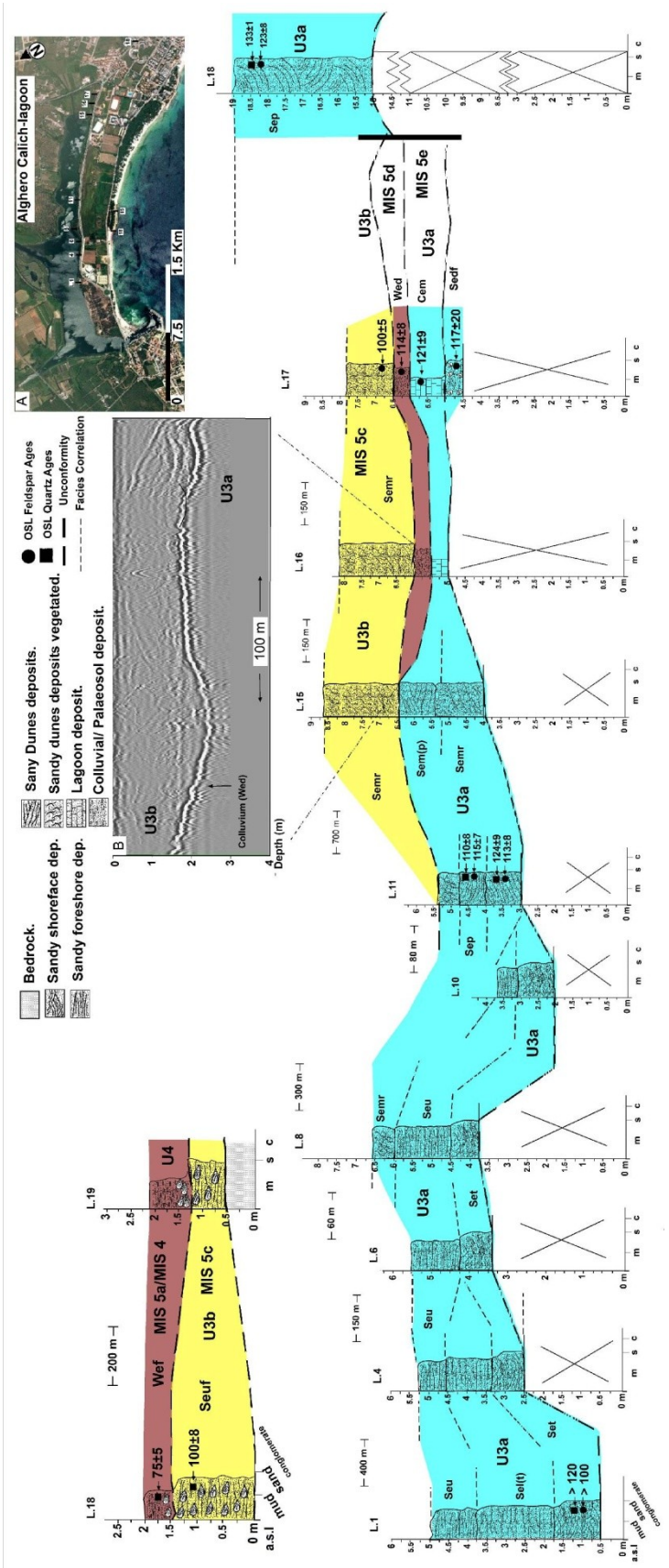
Alghero Calich-lagoon
1.5 Km
Bedrock.
Sandy shoreface dep.
Sandy foreshore dep.
Sany Dunes deposits.
Sandy dunes deposits vegetated.
Lagoon deposit.
Colluvial/ Palaeosol deposit.
OSL Feldspar Ages
OSL Quartz Ages
Unconformity
Facies Correlation
100 m
Depth (m)
Colluvium (Wed)
U3b
U3a
MIS 5e
MIS 5d
MIS 5c
MIS 5a/MIS 4
Wef
Seuf
Wed
Cem
Sedf
Semr
Sem(p)
Seu
Set
Sel(t)
Sep
U4
mud
sand
conglomerate
a.s.l
75±5
100±8
100±5
114±8
121±9
117±20
110±8
115±7
124±9
113±8
133±1
123±8
> 120
> 100
L.18
L.19
L.17
L.16
L.15
L.11
L.10
L.8
L.6
L.4
L.1
200 m
150 m
700 m
80 m
300 m
60 m
400 m

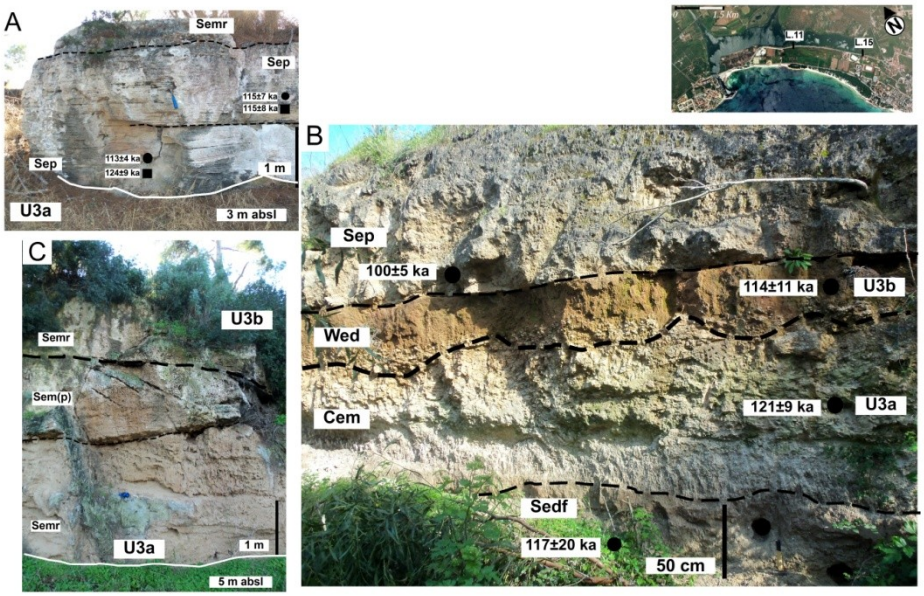

Fig. 30: Field view of succession cropping out along the lagoon. A) High angle cross stratified sandstones interpreted as coastal dune system and related feldspar (filled circles) and quartz (filled squares) ages. B) Detail of the Calich quarry succession, from the bottom the washover, incipient lagoon , colluvium and dune deposits. The thicker dashed line show the unconformity surface between U3a and U3b. C) Detail of different generations of coastal dune systems, on the bottom highly root bioturbated sandstones with faint of high angle cross stratification.

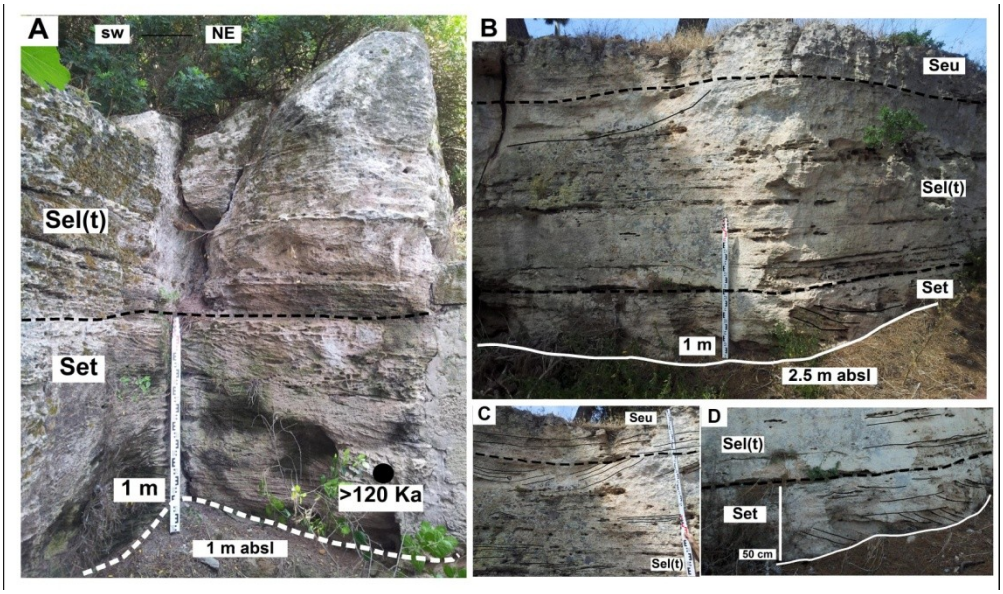

Fig. 31: Facies association Bs cropping out along the Calich lagoon. A,B) Field view of f, from the bottom Facies Set, facies Sel(t) (shoreface deposit)and facies Seu (beach face). C) Detail of large trough cross bed of facies Sel(t) D) Limit of facies between facies Set (cross bedded) and Sel(t) planar laminated.

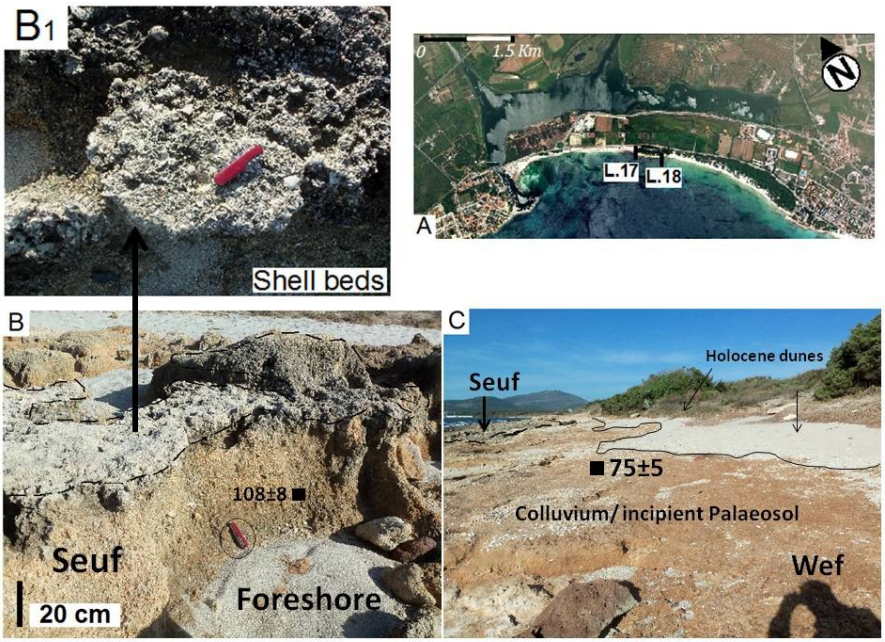

Fig. 32: Field view of deposits cropping out along the Maria Pia Beach. A) Location of logs analysed see also figure 29 B) Field detail of foreshore. B1) Detail of shells bed C) Detail of reworking colluviums and incipient reddish palaeosol.

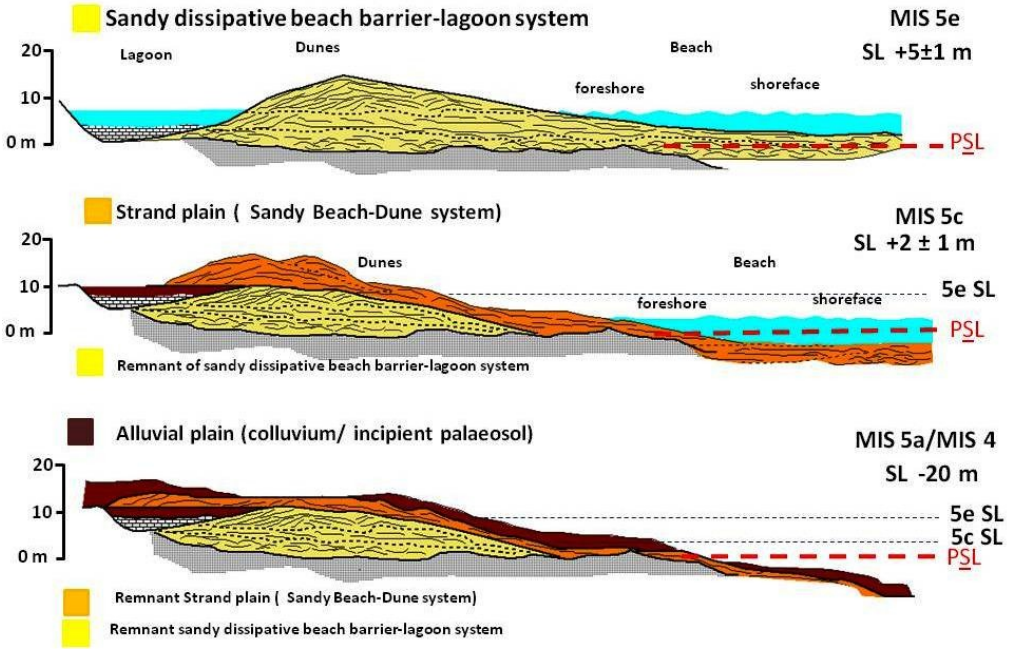

Fig. 33: Schematic evolution of Calich lagoon and the Alghero bay during interglacial MIS 5 (130-80Ka) and glacial stage MIS4 (65 ka).

Evolution of the Calich lagoon system during the MIS 5

After the glacial stage MIS 6 (150 ka) low stand (-130 m bsl) the sea level rose again reaching its optimum maximum at of 5±1 m above the present sea level during the last interglacial optimum; that is, at about 125 ka ago (MIS 5e). During the MIS 5e it is possible that the maximum sea level transgression reached 7 m apsl. During this highstandtthe beach barred-lagoon system developed and continued to prograde during almost the all MIS 5e (125 ka) (Fig.33)

Although the MIS 5e is worldwide considered a warmer and humid period, the climatic changes within this period is less investigated. Sedimentological and pedological analysis (Zucca et al in press) performed on the quarry succession highlight two major climatic pulses for the north-west Sardinia. The first pulse coincides with the maximum evolution of the lagoon under warm and humid condition that triggered an intense carbonate leaching. The second occurred under much drier conditions and is associated to the lateral switching of the coast triggered the partial drying up of the lagoon recorded by the deposition of massive calcrete layers. During the last phase of MIS 5e wetter climatic conditions restored and triggered the partial pedogenesis of the dried lagoon. A rapid sea level regression associated to the MIS 5d have as main effect the partial erosion of the barred-lagoon system on which an alluvial plain characterized by wide colluvial deposits formed. The pedogenic evolution of the colluvial material is characterized by weak in situ chemical weathering and moderate physical processes. These processes most likely occurred during wet and temperate conditions and were followed by a drier period that allowed a moderate calcification of the lagoon deposits.

A second transgression occurred during the MIS 5c. Sea level rose under warm conditions (Pascucci et al 2012; Andreucci et al 2010, Moreno et al.,2012). The paelogeography was characterized by a sandy strand plain developed at least 1.5 metres above the present sea level as recorder by the foreshore deposit outcropping at the Maria Pia Site (Fig.32). Associated to this coastline regression an a transgressive dune system developed on the colluvial deposits During the MIS 5b the sea level fall again with the restoration of the alluvial plain which was mostly characterized by

colluvial deposits. This plain continued to develop also during the MIS 5a and under wet and warm condition that triggered the incipent palaeosol formation (Fig.33).

Sea level changes during MIS 5e

Climate change during the late Quaternary was dominated by periodic large-scale oscillations between glacial and interglacial conditions.

The Last Interglacial, also known as the Eemian in Europe, corresponds to the global interglacial record of Marine Isotope Stage 5 (MIS 5) and it may be used as an analogue of present Holocene interglacial. The MIS 5 stage spanned between 130-80 ka ago and was characterized by different insolation regimes to which are related large fluctuations of climate and sea level.

Based on this characteristic the MIS 5 is divided in five interstadial sub-stages (e-a). The MIS 5e substage is worldwide considered the climate optimum of the whole interglacial; it spans from 130 to 115 ka ago, and was warmer than today with sea level 4-6 m above the present, although large variation in elevation have been measured in different studied sites (Siddall et al 2007).

At the peak of the interglacial conditions, the north Atlantic summer temperatures were 2 to 5°C warmer than today (40°N). Several authors documented two high stands during MIS 5e; one occurred at the beginning of the last interglacial period at 135 ka, and one centered around 117 ka, divided by a very short low stand occurred at ~125 ka (Hearty, 1987; Cuerda, 1989; Hillaire-Marcel et al., 1996; Zazo et al., 2003; Bardají et al., 2009, Dorale et al 2010). The MIS 5e ended around 115 ka ago and was followed by a cold period were climate condition abruptly changed toward glacial (MIS 5d). The glacial substage MIS 5d reached its maximum peak at ~110 ka and coincided with a sea level fall of about -20 m. (Dorale et al., 2010)This cold peak was followed by two others interglacial substages, the MIS 5c (100 ka) and MIS 5a (80 ka) divided by a glacial stages know as MIS 5b (90Ka) very similar to the 5d one. Although 5c and 5a stages are largely consistent with periods of high insolation (July 65°N) they were considered slightly colder than MIS 5e with an eustatic (ice equivalent) sea-level greater below the present (Martrat et al., 2004 Siddal et a.,l 2007, Dutton et al., 2012) (Fig.34).

However, during the last 20 years scattered data from different areas of the world rise the debate on the intensity of the sea level fluctuation within the MIS 5, especially for the MIS 5a and MIS 5c (Hollin et al., 1980, Potter 2004, Dorale et al., 2010). These

differences in the past sea elevation may be attributed to the particular site characteristic. In fact, the sea level does not reflect only the changes in global ice volume but also to responses of Earth to these changes; that is, surface loading, surface deformation and geoid changes and glacial isostatic adjustment. In the absence of tectonic motions, the relative sea level (RSL) reflects the combination of glacio-hydro-adjustment (GIA) and eustacy. Stable areas, far from the influence of ice-sheets and GIA are the most suitable sites to study the RSL only related to the eustatic fluctuations (Lambeck et al., 2003; Tuccimei et al., 2012).

The Mediterranean is situated at an intermediate position between ice-margin sites and sufficiently remote from centre of deglaciation to be little influenced by the effects of GIA and, therefore, RSL variation is expected to be most significantly influenced by the local water load emplaced upon the basin itself (Pierazzoli et al 2004).

In the last few years Dorale et al. (2010) increased the debate on the MIS 5 sea fluctuation for the Mediterranean sea identifying a second high-stand above the present sea level (+1.5 m) occurred during the MIS 5a (~81 ka) for the Mallorca island (Balearic Island). The author suggested that the highstand was glacio-isostatic free and only related to the eustatic variation. The authors, moreover, suggested that during the MIS 5a the north hemisphere was involved in a rapid ice melting in conformity with high insolation peak at ~84 ka ago (Fig.34). The ice melted in a very short time (about 4 ka) and triggered a fast rise of sea level (Dorale et al., 2010; Tuccimei et al., 2012).Sardinia is the second biggest island of the western Mediterranean sea and faces Mallorca (Balearic Island 450 Km far) and similarly it has been considered tectonically stable with only local slowly subsidence and small vertical motions (Antonioli et al., 2006, 2007, Ferranti et al 2006). Hence, Sardinia can be used for modeling the sea level changes occurred in the Mediterranean since the last interglacial. The two islands are however rarely compared (Tuccimei et al., 2008 , 2012).

Sedimentologic and stratigraphic studies combined with ages obtained with Optically Stimulated Luminescence (OSL) dating performed on coastal deposits of NW Sardinia coast documented two main highstands occurred above the present sea level.

The firsts one occurred at the elevation of ~5±1 m above the present sea level during a period spanning between 130 and 115 ka and thus related to the last interglacial

highstand MIS 5e. The west coast during MIS 5e was dominated by pocket gravelly small beaches mostly developed at the base of cliffs or in small embayment at the beginning of the transgression. The warmer conditions triggered the formation of thick intertidal organic carbonate rim deposits developed on ock falls deposited at the edged cliffs. The elevation of these deposits is consistent along the NW coast at +3.5 m apsl. Considering the subsidence ratio of 0.01 mm/yr for the island and the tidal range (50 cm), these deposits were formed at an elevation of +4.6 m. Resulted OSL ages are consistent for all carbonate deposits placing them around 115-120 ka, thus these deposits could be stratigraphycally and chronologically referable to the MIS 5e. Evidences of the possible MIS 5edeposits were found at El Trò, Le Bombarde and at Calich sites where are characterized by sandy pocket beaches referred to ~130 ka ago. However, the true elevation above the present sea level for deposits of El Trò and Le Bombarde bay can be only inferred. For El Trò bay the MIS 5e beach is characterized by a very shallow shoreface deposit. They are, however, surrounded by cliffs marked at the elevation of 5 m apsl by lithophaga bores and by intertidal fauna. It seems therefore most likely that beach system developed in a cliff-bounded bay where sea level was 4-5 m higher than the present. Instead, for the Le Bombarde bay the MIS 5e sandy beach has an elevation of 1-2 m apsl, thus a post MIS 5e neo-tectonic is active with the subsiding of bay. Considering the elevation of the estimated MIS 5e markers for the closer areas of Capo caccia and Porto Conte (NW Sardinia) at 4.2-5.2 m, the sandy beach system of Le Bombarde developed at almost 5±1 m apsl. Thus, we estimate for the bay a -0.032 mm/yr of tectonic subsidence (Tuccimei et al., 2006 , Pascucci et al., in press, Pinna, 2013). In addition, during MIS 5e the bay of Alghero was dominated by a well developed beach barred-lagoon system, Calich site. The maximum elevation of the system (beachface and lagoon deposit) is indentify at 6±1 m apsl, thus taking in account only the subsidence, the maximum evolution of the system might have taken place t under a sea level of ~ 7.2±1 m, this probably cone related to the peak of MIS 5e when the maximun flooding of the bay occurred. The MIS 5e data are consistent with the previous results proposed for Sardinia. (Kindler et al 1997, Tuccimei et al 2006, Ferranti et al 2006, Hearty et al 2007, Andreucci et al 2009, Thiel et al 2011) and are also consistent, within few meters of difference, proposed around the world

(Siddal et al., 2007, Waelbroeck 2002). The MIS 5d is not well preserved around the NW coast of Sardinia and thus the abrupt sea level fall can be only inferred on the base of the erosive surface that cut all the MIS 5e deposits. Only at the Calich quarry site the transition from MIS 5e to MIS 5d stage has been recorder by a reddish colluvial deposit (115±8 ka). The end of MIS 5e was marked by an abrupt deterioration of the interglacial climate shifting to an alternation of dry and very rainy cool-temperate seasons. At the end of MIS 5e the sea level fallstarted and is associated with the beginning of climate deterioration. The sea level fall gradually during all MIS 5e and continue increasing during the MIS 5d where it reached at least -15 m for the Mediterranean sea area (Dorale et al 2010).

The second highstand occured during the MIS 5c (100 ka). The sea rose up to ~2 m higher than the present; that is, in contrast with the global sea level reconstruction which indicates that sea level during the MIS 5c was lower than the present (10-20 m). Nevertheless, an active tectonic uplifting for the Sardinia island can be excluded because it is unlikely that MIS 5c deposits were uplifted of ~15 m and the MIS 5e did not. In addition, to support this the MIS 5c and MIS 5e deposits are in good stratigraphic sedimentlogical connection along all the NW coast of Sardinia.

Around world, scattered data about the high of MIS 5c sea level closer to the present were highlighted but they are contradictory and often influenced by regional tectonic.

Nowadays we do not have a true answer about the presence of this sea highstand stage although marine shallow deposits of Sardinia north-west coast highlight its presence.

Given the several analogues between MIS 5c and MIS 5a. The MIS 5c the rapid melting of ice sheet formed during MIS 5d triggered a fast rising of sea during a very short period, similarly to what hypothesized for the MIS 5a by Dorale et al. (2010).

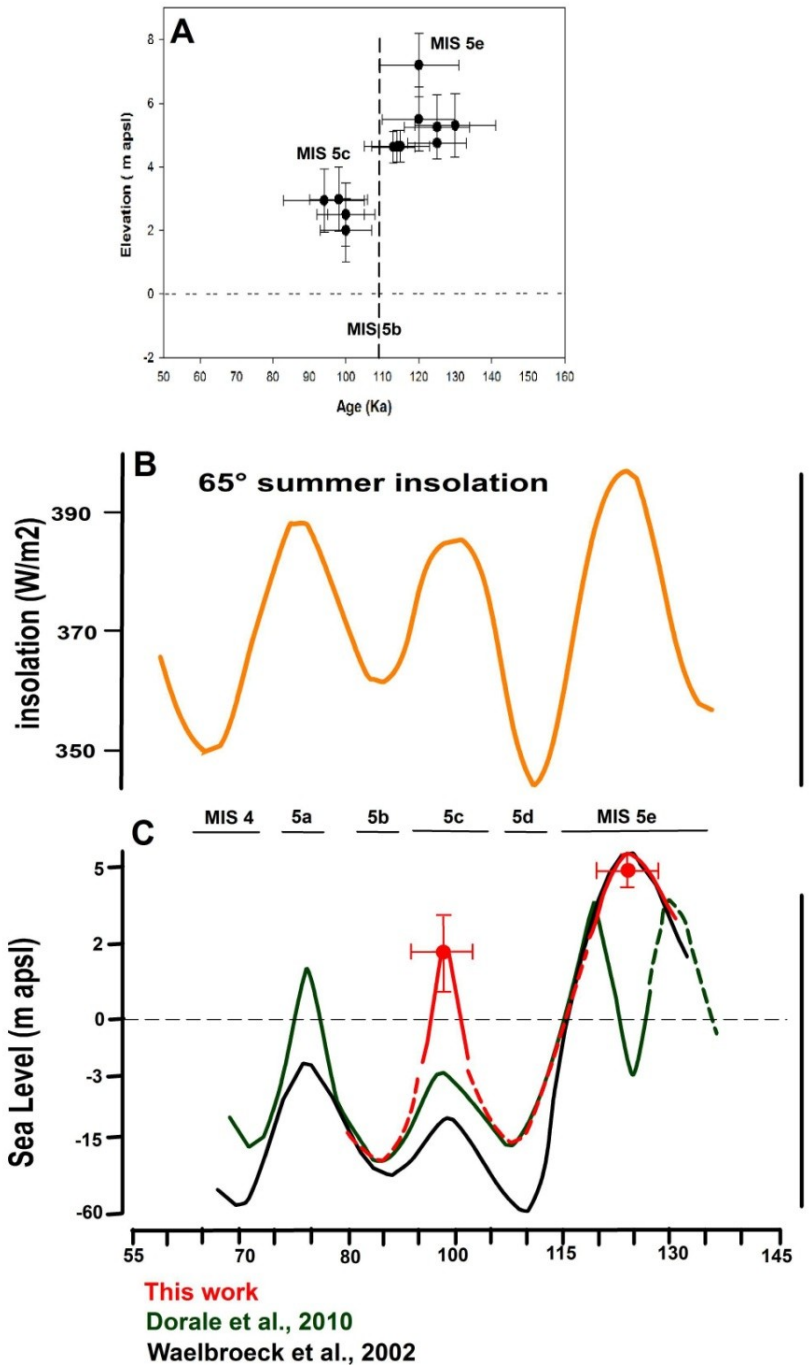

Fig. 34: A) Elevation of MIS 5e and MIS 5c of markers along NW Sardinia coast (this study) B) 65°N summer half-year insolation curve (Cutler et al 2003) C) Reconstructed MIS 5 sea level for Sardinia NW coast (Red this work), sea level curve reconstructed for Mallorca Dorale et al 2010 (Green). The reconstructed ocean water ^{18}O sea level curve Waelbroeck et al 2002.

Discussions

Late Quaternary deposition along the northwestern and west coast of Sardinia was influenced by sea level fluctuations related to the alternating stadial (glacial) and interstadial (interglacial) cycles. At least along the coastthere are no evidences of strata older than 300 ka; that is, MIS 8. This could be most probably related to the continuous erosion, recycling and cannibalization of the pre-existing deposits by the new forming ones during the following regressive and transgressive

cycles. Overall, since 300 ka, depositional environments alternated in a very similar way. During interglacial highstands beach systems developed both on a cliffed rocky coast, and on a more open embayment (coastal plain). The first were characterized by small pocket gravelly (or sand and gravel) beaches prograding over a wave cut platform; the latter were dominated by wide sandy beach or mixed beach. During the following glacial falling stages alluvial fans developed on hill slopes and exposed shelf. As soon as a truly glacial stage established wide coastal dune systems developed on the exposed shelf migrating landward toward the internal bedrock ranges, today rocky cliff. However, glacial and interglacial conditions were characterized by fluctuations that in some cases strongly modified the local paleogeography.

As ready mentioned, MIS 5 was characterized by three positive (e, c, a) and two negative (d, b) peaks. MIS 5e (130-115 ka) deposits are always present along the coast either as biogenic carbonate deposits or beach systems. Carbonate deposits normally occur at maximum of 3.5 m above the present sea level and are characterized by encrusting red algae (Lithophyllum byssoides) with intertidal invertebrate fauna (serpulides spp. and barnacles spp.). Recent works have demonstrated that the life and development of this algal rim is strongly related to particular climate conditions such as wind, waves and to substrate (Cossu et al., 1997). They therefore may provide good information on the maximum sea level reached during the MIS 5e high stand. Considering that for this part of Sardinia a constant subsidence rate of 0.01 mm per year has been estimated (Ferranti et al., 2006), it is possible to claim a sea level 5± 1 m higher than today. This also implies a temperature warmer of at least 2 °C (Rohling et al., 2008). In places, high energy mixed sand and gravel or sandy pocket beaches

developed. Nowadays there are few equivalents of these systems. This could be related to the little space available between the cliff and the sea-shore due to the higher sea level. During MIS 5d sea level dropped of -15 m (Cutler et al., 2003, Dorale et al 2010) and in most of "continental" Europe climate started to deteriorate signing the end of interglacial. However, Moreno et al (2012) clearly show that the climate at western Mediterranean latitude lasted relatively warm with high frequency wet/dry pulses until at the end of the MIS 5a (ca 75 ka). In Sardinia, as expected, the climate was relatively warm and during the MIS 5c (100-90 ka) sea level raised of about ~1.5 m above the present level. During this new high stand paleogeography strongly modified because of the major space and sediment available between the cliff and the shoreline. This space allowed developing wide sandy or mixed sand and gravel beach systems. These were prograding beach ridges (mostly pocket beaches) fed either by ephemeral (or small) rivers (S'Abba Drucche) (Fig.12) or by material eroded from the close bounding cliffs (Alghero-El Trò) (Fig.25). The MIS 5c beach systems can be compared, at least in part, with those developed after the Holocene optimum (8000 y BP) and still present all around Sardinia (Pascucci et al., 2013). A modern analogue of the beach system recognized at S'Abba Drucche (Fig.12) is the small pocket beach not yet much anthropized of Porto Alabe (10 km south of S'Abba Drucche, Fig.14b).

During the following MIS 5b climate started to deteriorate and sea level fall of about --20m or more below the present (Cutler et al., 2003, Dorale et al 2010)

The following MIS5a is normally associated to a sea level rise and as observed by Dorale et al (2010) was +1 m above the present sea level. However, along Sardinia coast evidences of this event have not been found.

The transition between MIS 5 and MIS 4 (ca 75 ka) is marked by a rapid sea-level fall of about -70 m (below the present sea level) (Waelbroeck et al., 2002) (Fig. 34). Sardinian coastal lines regressed of some kilometers from the present and a wide coastal plain, in the space before occupied by the shelf, developed. Average sea-temperature dropped of about 8°C, from the temperature estimated for MIS 5c and the climate significantly deteriorated passing from the previous warm sub-humid to humid conditions (Kindler et al., 1997) to successively move toward to cold and semiarid (Moreno et al., 2012). Humid climate allowed the deposition of colluvials

and/or the formation of paleosols. Over these deposits dune or debris flow, marking the new semiarid conditions, developed. Dunes mainly developed in small valleys backed by low relief; debris flows in wider valley systems backed by relatively high hills. They can be considered as a dry-system debris flow developed because of ephemeral but intense rainstorms occured in arid region (Nanson & Gibling, 2003).

Debris flow can deeply incise and mobilize thick amount of soils formed during warm periods (Hampton & Horton, 2007; Cannon et al., 2008; Morton et al., 2008). This may be the case of the reddish material characterizing the MIS 4 deposits cropping out along the northern coast of Sardinia.

References

A. Ginés, J. Ginés, L. Gómez-Pujol, B.P. Onac & J.J. Fornós (2012). Mallorca: A Mediterranean Benchmark for Quaternary Studies. Monografies de la Societat d'Història Natural de les Balears, 18

Aitken, M.J. (1985) Thermoluminescence Dating. Academic Press, London, 267 pp.

Aitken, M.J. (1998). An Introduction to Optical Dating. Oxford University Press, Oxford.

Andreucci S., Panzeri L., Martini I.P., Maspero F., Martini M., Pascucci V., 2013. Evolution and architecture of a West Mediterranean Upper Pleistocene to Holocene coastal apron-fan system. Sedimentology. doi: 10.1111/sed.12058

Andreucci, S., Bateman, M.D., Zucca, C., Kapur, S., Aks it, _I., Dunajko, A. and Pascucci, V. (2012) Evidence of Saharan dust in upper Pleistocene reworked palaeosols of northwest Sardinia, Italy: palaeoenvironmental implications. Sedimentology, 59, 917–938.

Andreucci, S., Clemmensen, L.B., Murray, A. and Pascucci.V, (2010) Middle to late Pleistocene coastal deposits of Alghero, northwest Sardinia (Italy): chronology and evolution. Quatern. Int., 222, 3–16.

Andreucci, S., Pascucci, V., Murray, A., Clemmensen, L.B., 2009. Late Pleistocene coastal evolution of San Giovanni di Sinis, west Sardinia (Western Mediterranean). Sedimentary Geology 216, 104–116.

Antonioli, F., Anzidei, M., Lambeck, K., Auriemma, R., Gaddi, D., Furlani, S., Orrù, P., Solinas, E., Gaspari, A., Karinja, S., Kovacic c, V., Surace, L., 2007. Sea level change

during the Holocene in Sardinia and in the North-eastern Adriatic (CentralMediterranean sea) from archaeological and geomorphological data. Quaternary Science Reviews 26, 2463e2486

Antonioli, F., Ferranti, L. and Lo Schiavo, F. (1994) The submerged neolithic burials of the Grotta Verde at Capo Caccia (Sardinia, Italy). Implication for the Holocene sea-level rise. Mem. Descr. Carta Geol. d'Ital., 52, 329–336.

Arnold, L.J., Roberts, R.G., 2009. Stochastic modelling of multi-grain equivalent dose (De) distributions: Implications for OSL dating of sediment mixtures. Quaternary Geochronology 4, 204-230.

APAT, Agenzia per la Protezione dell'Ambiente per i servizi Tecnici (2005) Atlante delle coste: moto ondoso a largo delle coste italiane. Dipartimento Tutela delle acque interne e marine, Servizio difesa delle coste. Istituto poligrafico e zecca dello stato, Roma.http://www.apat.gov.it/site/itIT/Servizi_per_l'Ambiente/Stato_delle_coste/Atlante_delle_coste.

B.J Brennan. 1997 Symulation of the gamma radiation field in "lumpy" environments. Radiation measurements. Vol.27 n° 2, pp 299-305.

Banerjee, D., Murray, A.S., Bøtter-Jensen, L. and Lang, A. (2001) Equivalent dose estimation using a single aliquot of polymineral fine grains. Radiation Measurements, 33, 73–94.

Bateman, M.D., Boulter, C.H., Carr, A.S., Frederick, C.D., Peter, D. and Wilder, M. (2007) Detecting post-depositional sediment disturbance in sandy deposits using optical luminescence. Quatern. Geochronol., 2, 57–64.

Bateman, M.D., Frederick, C.D., Jaiswal, M.K. and Singhvi, A.K. (2003) Investigations into the potential effects of pedoturbation on luminescence dating. Quatern. Sci. Rev., 22,1169–1176.

Belluomini, G., Malatesta, A., Branca, M., Spano, G., 1985. Amino-acid racemization dating of Sardinian raised marine deposits. Bollettino della Società Geologica Italiana, 104, 223-228.

Blikra, L.H. and Nemec, W. (1998) Postglacial colluvium in western Norway: depositional processes, facies and paleoclimatic record. Sedimentology, 45, 909–959.

Bell, W.T. (1979) Attenuation factors to absorbed dose in quartz inclusions for thermoluminescence dating. Ancient TL, 8, 2–13.

Bluck, B.J. (1967) Sedimentation of beach gravels: examples from South Wales. J. Sed. Petrol., 37, 128–156.

Buylaert, J.P., Jain, M., Murray, A.S., Thomsen, K.J., Thiel, C., Sohbati, R., 2012. A robust feldspar luminescence dating method for Middle and Late Pleistocene sediments. Boreas 41, 435e451.

Buylaert, J.P., Murray, A.S., Huot, S., 2008. Optical dating of an Eemian site in northern Russia using K-feldspar. Radiation Measurements 43, 715e720

Buylaert, J.P., Thiel, C., Murray, A.S., Vandenberghe, D.A.G., Yi, S., Lu, H., 2011b. IRSL and post-IR IRSL residual doses recorded in modern dust samples from the Chinese Loess Plateau. Geochronometria 38, 432e440.

C. Waelbroecka, L. Labeyriea,b, E. Michela, J.C. Duplessya, J.F. McManusc, K. Lambeckd, E. Balbona, M. Labracheriee. (2002) Sea-level and deep water temperature changes derived from benthic foraminifera isotopic records. Quaternary Science Reviews 21 (2002) 295–305

Carmignani, L., Barca, S., Oggiano, G., Pertusati, P.C., Salvadori, I., Conti, P., Eltrudis, A., Funedda, A., Pasci, S., 2001. Geologia della Sardegna: note illustrative della Carta Geologica della Sardegna a scala 1:200.000. In: Memorie descrittive Carta Geolologica Italiana, vol. 60. Istituto poligrafico e zecca dello stato, Roma.

Carmignani, L., Decandia, F.A., Fantozzi, P.L., Lazzarotto, A., Liotta, D., Oggiano, G., 1995. Relationship between the tertiary structural evolution of the Sadinia- Corsica-Provençal domain and northern Apennines. Terra Nova 7, 128–137.

Casula, G., Cherchi, A., Montadert, L., Murru, M., Sarria, E., 2001. The Cenozoic grabens system of Sardinia: geodynamic evolution from new seismic and field data. Marine and Petroleum Geology, 18, 863– 888

Catuneanu, O. (2006) Principles of Sequence Stratigraphy. Elsevier, Amsterdam, 376 pp. ISBN 978-0-444-51568-1

Clifton, H.E. (1973) Pebble segregation and bed lenticularity in wave-worked versus alluvial gravel. Sedimentology, 20, 173–187.

Coltorti, M., Melis, E. and Patta, D. (2010) Geomorphology, stratigraphy and facies analysis of some Late Pleistocene and Holocene key deposits along the coast of Sardinia (Italy). Quatern. Int., 222, 16–30.

Cossu, A.V.L., Gazale, V., (1997). Osservazioni ecologiche sulla distribuzione di Lithophyllum lichenoides Philippi (Corallinales, Rhodophyta) nelle isole della Sardegna settentrionale. Bollettino della Società sarda di Scienze Naturali, 31,101-119.

Cunningham A.C., Wallinga J. (2010) Selection of integration time intervals for quartz OSL decay curves.Quaternary Geochronology. Vol.5, Iss.6, pp 657–666

Delitala, A.M.S., Cesari, D., Chessa, P.A. and Ward, M.N. (2000) Precipitation over Sardinia (Italy) during the 1946- 1993 rainy seasons and associated large-scale climate variations. Int. J. Climatol., 20, 519–541.

Denby P.M., Bøtter-Jensen L., Murray A.S. and Moska P. (2006) Application of pulsed OSL to the separation of the luminescence components from a mixed quartz/feldspar sample. Radiation Measurements 41, 774-779. [177]

De Muro S., Orrù P., 1998. Il contributo delle beach-rock nello studio della risalita del mare olocenico. Le beach-rock post-glaciali della Sardegna Nord-Orientale. Il Quaternario, 11, 19-39.

Donda, F., Gordini, E., Rebesco, M., Pascuci, V., Fontolan, G., Lazzari, P., Mosetti, R., 2008. Shallow water sea-floor morphologies around Asinara Island (NW Sardinia, Italy). Continental Shelf Research 28, 2550–2564.

Dorale, J. A., Onac B. P, Fornós J. J., Ginés J., l Ginés A., Tuccimei p.,. Peate D. W, (2010) Sea-Level Highstand 81,000 Years Ago in Mallorca. Science. Vol. 327 no. 5967 pp. 860-863

Duller, G.A.T., 2008. Single-grain optical dating of Quaternary sediments: why aliquot size matters in luminescence dating. Boreas 37, 589-612.

Duller, G.A.T., Bøtter-Jensen, L., Murray, A.S., 2000. Optical dating of single sand-sized grains of quartz: sources of variability. Radiation Measurements 32, 453-457.

Emiliani, C., 1957. Temperature and age analysis of deepsea cores. Science 125:383–385.

Fanelli, F., Palombo, M.R., Pillola, G.L., Ibba, A., 2007. Tracks and tracksways of ‘‘Praemegaceros’’ cazioti (Depe´ ret, 1897) (Artiodactyla, Cervidae) in Pleistocene

coastal deposits from Sardinia (western Mediterranean, Italy). Bollettino della Societa Paleontologica Italiana 46, 45–54.

Ferranti, L., Antonioli, F., Mauz, B., Amorosi, A., Dai Pra, G., Mastronuzzi, G.,Monaco, C., Orru` , P., Pappalardo, M., Radtke, U., Renda, P., Romano, P., Sanso`, P., Verrubbi, V., 2006. Markers of the last interglacial sea-level high stand along the coast of Italy: tectonic implications. Quaternary International 146, 30–54.

Fornos, J., Clemmensen, L.B., Gomez-Pujol, L. and Murray, A.S. (2009) Late Pleistocene carbonate aeolianite deposits on Mallorca, western Mediterranean: a luminescence chronology. Quatern. Sci. Rev., 28, 2697–2709.

Fucks M., Lang A. (2001) OSL dating of coarse-grain fluvial quartz using single aliquots protoocols on sediment from NE Peloponnese, Greece. Quatern. Sci. Rev., 20, 783–788.

Funedda, A., Oggiano, G. and Pascucci, V. (2003) I depositi Miocenici della Sardegna settentrionale: il bacino del Logudoro. In: Atti del Convegno GEOSED 2003 (Ed. V. Pascucci), pp. 381–414. Abstract book, Alghero, Italia.

Funedda, A., Oggiano, G., Pascucci, V., 2003. I depositi Miocenici della Sardegna settentrionale: il bacino del Logudoro. In: Atti del Convegno GEOSED 2003 Alghero, Sassari, Italia, pp. 381–414.

Galbraith RF, Roberts RG, Laslett GM, Yoshida H and Olley JM, 1999. Optical dating of single and multiple grains of quartz from jinmi-um rock shelter, northern Australia, part 1, Experimental design and statistical models. Archaeometry 41(2): 339-364

GalBraith, R.F., 1988 . Grafical display of estimates having differing standrd errors, Technometrics, 30, 271-281

Ginesu, S., Derudas, A., Enzo, S., Secchi, F. and Sias, S. (2009) The post-Tyrrhenian evolution in Sardinia: evidence from the Ebidozzi paleovallley (Argentiera, North-western Sardinia, Italy). Geogr. Fis. Dinam. Quat., 32, 23–30.

Hart, B.S. and Plint, A.G. (1995) Gravelly shoreface and beachface deposits. In: Sedimentary Facies Analysis (Ed. A.G. Plint). IAS, Spec. Publ., 22, 75–99.

Huntley, D.J. and Baril, M.R. (1997) The K content of the K-feldspars being measured in optical dating or in thermoluminescence dating. Ancient TL, 15, 11–13.

Huntley, D.J. and Lamothe, M. (2001) Ubiquity of anomalous fading in K-feldspars, and the measurement and correction for it in optical dating. Can. J. Earth Sci., 38, 1093–1106

Jacobs, Z. (2008): Luminescence chronologies for coastal and marine sediments. Boreas, Vol, 37, pp. 508–535.Thomsen K.J., Jain M., Murray A.S., Denby P.M., Roy

Jain, M., Ankjærgaard, C., 2011. Towards a non-fading signal in feldspar: insight into charge transport and tunnelling from time-resolved optically stimulated luminescence. Radiation Measurements 46, 292e309.

Jennings, R. and Shulmeister, J. (2002) A field based classification scheme for gravel beaches. Mar. Geol., 186, 211–228

Kindler, P., Davaud, E. and Strasser, A. (1997) Tyrrhenian coastal deposits from Sardinia (Italy): a petrographic record of high sea levels and shifting climate belts during the last interglacial (isotopic substage 5e). Palaeogeogr. Palaeoclimatol. Palaeoecol., 133, 1–25.

Kirk, R.M. (1980) Mixed sand and gravel beaches: morphology, processes and sediments. Prog. Phys. Geogr., 4, 189–210.

Laborel, J., & Laborel-Deguen, F. (1994). Biological indicators of relative sea-level variations and of co-seismic displacements in the Mediterranean region. Journal of Coastal Research, 395-415.

Lang, A., Lindauer, S., Kuhn, R. and Wagner, G.A. (1996) Procedures used for optically and infrared stimulated luminescence dating of sediments in Heidelberg. Ancient TL, 14, 7–11.

Lecca L., Carboni S., 2007. The Tyrrhenian section of San Giovanni di Sinis (Sardinia): Stratigraphic record of an irregular single high stand. Rivista di Paleontologia e Stratigrafia, 113, 509-523.

Madsen, A.T. and Murray, A.S. (2009) Optically stimulated luminescence dating of young sediments: a review. Geomorphology, 109, 3–16.

Martrat, B., Grimalt, J.O., Lopez-Martinez, C., Cacho, I., Sierro, F.J., Abel Flores, J., Zahn, R., Canals, M., Curtis, J.H. and Hodell, D.A. (2004) Abrupt temperature changes in the Western Mediterranean over the past 250,000 years. Science, 306, 1762–1765.

Manca E, Pascucci V., Deluca M., Cossu A., Andreucci S. (2013) Shoreline evolution related to coastal development of a managed beach in Alghero, Sardinia, Italy. Ocean & Coastal Management in press (2013).

Ministero dell'ambiente e della tutela del territorio e del mare, Museo friulano di storia naturale. Comune di Udine. Italian Habitats. Marine bioconstruction. 2009

Moreno, A., Gonzàlez-Sampèriz, P., Morellòn, M., Valero- Garcès, B.L. and Fletcher, W.J. (2012) Northern Iberian abrupt climate change dynamics during the last glacial cycle: a view from lacustrine sediments. Quatern. Sci. Rev., 36, 139–153.

Murray A.S., Schmidt E.D, Stevens T., Buylaert J.-P ,. Marković S.B, Tsukamoto S., Frechen M. (2013) Dating Middle Pleistocene loess from Stari Slankamen (Vojvodina, Serbia)-Limitations imposed by the saturation behaviour of an elevated temperature IRSL signal. Catena (in press)

Murray, A. S., Wintle, A. G., 2000. Luminescence dating of quartz using an improved singlealiquot regenerative-dose protocol. Radiation Measurements 32, 57-73.

Muto, T. and Steel, R.J. (2000) The accommodation concept in sequence stratigraphy: some dimensional problems and possible redefinition. Sed. Geol., 130, 1–10.

N.and Bøtter-Jensen L. (2008) Minimizingfeldspar OSL contamination in quartz UV-OSL using pulsed blue stimulation. Radiation Measurements 43, 752-757.

Nathan, R.P. and Mauz, B. (2008) On the dose-rate estimate of carbonate-rich sediments for trapped charge dating. Radiation Measurements, 43, 14–25.

Neal, A., Pontee, N.I., Pye, K. and Richards, J. (2002) Internal structure of mixed-sand-and-gravel beach deposits revealed using ground-penetrating radar. Sedimentology, 49, 789–804.

Pascucci V, Martini I. P; Endres A. (2008). Facies and ground-penetrating radar characteristics of coarse-grained beach deposits of the uppermost Pleistocene glacial Lake Algonquin, Ontario, Canada. Sedimentology Vol. 56, pp 529–545.

Pascucci V., Sechi D., Andreucci S. (2013). Middle Pleistocene to Holocene coastal evolution of NW Sardinia (Mediterranean Sea, Italy). (Submitted under reviewing)

Pecorini G. (1954) - Le dune fossili della Nurra di Alghero. Rendiconti Accademia dei Lincei, 16, 735-741.

Pecorini G. (1963) - Contributo alla stratigrafia post-miocenica della Nurra di Alghero. Rendiconti Facoltà Scienze Università

Cagliari, 33, 11.

Posamentier H.W., Walker R.G. (2006) Facies model rivisisited. SEPM (Society for Sedimentary Geology)

Postma, G. and Nemec, W. (1990) Regressive and transgressive sequences in raised Holocene gravelly beach, southwestern Crete. Sedimentology, 37, 907–920.

Prescott, J.R. and Hutton, J.T. (1994) Cosmic ray contribution to dose rates for luminescence and ESR dating: large depths and long-term time variations. Radiat.

Meas., 23, 497–500.

Richard. C Selley (200) Applied Sedimentology (Second Edition). Academic press

Roberts, R.G., Galbraith, R.F., Yoshida, H., Laslett, G. and Olley, J.M. (2000) Distinguishing dose populations in sediment mixtures: a test of single-grain optical dating procedures using mixtures of laboratory-dosed quartz. Radiation Measurements, 32, 459–465.

Rose, J., Meng, X. and Watson, C. (1999) Paleoclimate and paleoenvironmental responses in the western Mediterranean over the last 140 ka: evidence from Mallorca, Spain. J. Geol. Soc., 156, 435–448.

Siddall, M., Chappell, J., & Potter, E. K. (2007). 7. Eustatic sea level during past interglacials. Developments in Quaternary Sciences, 7, 75-92.

Siddall, M., Rohling, E.J., Almogi-Labin, A., Hemleben, Ch., Meischner, D., Schmelzer, I., Smeed, D.A. (2003). Sealevel fluctuations during the last glacial cycle. Nature 423, 853–858.

Tuccimei, P., Fornós, J., Ginés, A., Ginés, J., Gràcia, F., Mucedda, M., 2007. Sea level change at Capo Caccia (NW Sardinia) and Mallorca (Balearic Islands) duringoxygen isotope substage 5e, based on Th/U datings of phreatic overgrowths on speleothems. In: Pons, G.X., Vicens, D. (Eds.), Geomorfologia Litoral i Quaternari. Homenatge a Joan Cuerda Barcelo. Monografies de la Societat d'Historia Natural de les Balears, vol. 14, pp. 121e136.

Tuccimei, P., Onac, B.P, Dorale, J.A, Gines, J., Fornòs, J.J., Gines, A., Spada, G., Ruggeri G., Muccedda M., 2012. Decoding last interglacial sea-level variations in the western Mediterranenan using speleothem encrustations from coastal caves in Mallorca and Sardinia: A field data- model comparision. Quaternary International 262, 56-64.

Ulzega, A., Hearty, P.J., 1986. Geomorphology, stratigraphy and geochronology of Late Quaternary marine deposits in Sardinia. Zietschrift fur Geomorphologie, Suppl. Bd. 62, 119e129.

Vermeesch, P., 2009, RadialPlotter: a Java application for fission track, luminescence and other radial plots, Radiation Measurements, 44, 4, 409-410

Vigliotti, L., & Langenheim, V. E. (1995). When did Sardinia stop rotating? New palaeomagnetic results. Terra Nova, 7(4), 424-435.

Wintle, A. G., 2008b. Luminescence dating: where it has been and where it is going. Boreas 37, 471-482.

Zucca C., Sechi D. ,Andreucci S, Shaddad S., Madrau S. Previtali F., Pascucci V., Kapur S. Pedogenic and paleoclimatic evidence from Late Quaternary (Emian) calcrete in North-western Sardinia (Italy). European journal of Soil Science. (submitted)

ACKNOWLEDGEMENTS

[English]

The way has been long, but here we are for the thanks moment. I have to say that these three years were tough and intense and gone so fast. So many things happened and many are the people who I met and who have enriched me.

There are so many people that deserve a thank you but in particular, I would like thank my supervisor Vincenzo, which has been and always will be an essential guide and a scientific and life reference point. My co- tutor Stefano for his great patience, for the moments of joy and the great discussions.

The guys of the Nordic Laboratory for Luminescence Dating: in particular Jan- Pieter and Christine for their continue help and support and for making me feel at home even in faraway Denmark. Andrew source of eternal scientific wisdom and inspiration. Mark Bateman for the nice discussions and his valuable lessons . And finally I want to thank all those people who took part in this adventure and have been involved.

Italiano:

La strada è stata lunga ma eccoci arrivati ai ringraziamenti. Devo dire che questi tre anni sono duri, intensi e veloci. Tante cose sono successe e altrettante sono le persone che ho conosciuto e che mi hanno arricchito. Sono tante le persone che meritano un ringraziamento ma in particolare voglio ringraziare il mio tutor Vincenzo che è stato e sempre sarà una guida fondamentale e punto di riferimento sia scientifico che di vita.

Il mio co-tutor Stefano per la sua grande pazienza, per i momenti di allegria e per le discussioni accese che sempre fanno bene.

I ragazzi del Nordic Laboratory for Luminescence Dating: in particolare Jan-Pieter and Christine per il loro continuo aiuto e supporto e per avermi fatto sentire a casa anche nella lontana Danimarca. Andrew fonte di eterna saggezza scientifica di ispirazione. Mark Bateman per le belle discussioni e i suoi preziosi insegnamenti. Ed infine voglio

ringraziare tutti coloro che hanno partecipato a questa avventura e ne hanno fatto parte.